University of Kentucky Master's Theses   Graduate School

2007

CATALYTIC GROWTH OF STRUCTURED CARBON via THE DECOMPOSITION OF HALOGENATED REACTANTS OVER SUPPORTED NICKEL

Laxmi Deepshika Cherukuri
University of Kentucky, helloshika@gmail.com

ABSTRACT OF THESIS

CATALYTIC GROWTH OF STRUCTURED CARBON *via* THE DECOMPOSITION
OF HALOGENATED REACTANTS OVER SUPPORTED NICKEL

The synthesis of highly ordered carbonaceous materials, including carbon nanofibers, has been the subject of a disparate and burgeoning literature over the past decade. Growth of carbon nanotubes via an atypical catalytic route, the decomposition of halogenated reactants as chlorobenzene (CB) over 10% (w/w) Ni/SiO_2 is investigated. The C (carbon) yield and structural order are a function of reaction time and temperature. Greater degree of structural order and C yield is observed from CB relative to benzene, suggesting Cl/catalyst interaction(s) and metal site restructuring. Evaluation of the effect of H_2 on C growth from CB reveals that C yield is sensitive to % (v/v) H_2 with selectivity maxima at 40% (v/v) H_2. Further, C yield is significantly influenced by the nature of the heteroatom substituent on the benzene ring; presence of strong electron withdrawing groups favors C yield and weak electron withdrawing or donating groups favors competing side reactions. The effect of the strong electron withdrawing group, Cl, varies with the chemical structure of the carbon source. Presence of Cl promotes C yield in the case of aromatic and straight chained (aliphatic) compounds whereas it promotes formation of benzene in the case of cyclic (aliphatic) compounds. Results are interpreted in term of substituent/ catalyst interaction and the mechanism of solid C formation. Further, effect of % (v/v) H_2 on C growth characteristics varies significantly with the precursor. The C growth characteristics are strongly dependent on the nature of the support used, as demonstrated for the following supports: SiO_2, Ta_2O_5, Al_2O_3, NaY, activated carbon and graphite at 10% (w/w) Ni loading. Ni/SiO_2 results in maximum C yield. Variation in Ni loading significantly influences the C yield; higher loading favors greater C yield. C grown on Ni/NaY was found to be relatively more structured to C obtained on the other supports. EDX analysis of the carbon product was used to assess the possibility of Cl intercalation and it reveals presence of 0.4 at% Cl on carbon grown on Ni/Al_2O_3.
Keywords: Carbon nanotubes, CVD, Chlorobenzene, H_2, Ni/SiO_2, Halo-organics, Aliphatic compounds, Support effects

Laxmi Deepshika Cherukuri
August 2nd, 2007

CATALYTIC GROWTH OF STRUCTURED CARBON VIA THE
DECOMPOSITION OF HALOGENATED REACTANTS OVER SUPPORTED
NICKEL

By

Laxmi Deepshika Cherukuri

<u>Dr. Barbara Knutson</u>
Director of Thesis

<u>Dr. Barbara Knutson</u>
Director of Graduate Studies

<u>August 2nd, 2007</u>
Date

RULES FOR THE USE OF THESES

Unpublished theses submitted for the Master's degree and deposited in the University of Kentucky Library are as a rule open for inspection, but are to be used only with due regard to the rights of the authors. Bibliographical references may be noted, but quotations or summaries of parts may be published only with the permission of the author, and with the usual scholarly acknowledgments.

Extensive copying or publication of the thesis in whole or in part also requires the consent of the Dean of the Graduate School of the University of Kentucky.

A library that borrows this thesis for use by its patrons is expected to secure the signature of each user.

<u>Name</u>   <u>Date</u>

THESIS

Laxmi Deepshika Cherukuri

The Graduate School

University of Kentucky

2007

4

CATALYTIC GROWTH OF STRUCTURED CARBON via THE DECOMPOSITION
OF HALOGENATED REACTANTS OVER SUPPORTED NICKEL

THESIS

A thesis submitted in partial fulfillment of the
requirements for the degree of Master of Science in the
College of Engineering
at the University of Kentucky

By

Laxmi Deepshika Cherukuri
Lexington, Kentucky

Director: Dr Barbara Knutson, Professor of Chemical Engineering
Lexington, Kentucky
2007

MASTER'S THESIS RELEASE

I authorize the University of Kentucky
Libraries to reproduce this thesis in
whole or in part for purposes of research.

Signed: Laxmi Deepshika Chetukuri

Date: August 2nd, 2007

ACKNOWLEDGEMENTS

The following thesis, while an individual work, benefited from the insights and direction of several individuals. Dr. Mark A. Keane, my advisor, exemplifies the hard work and dedication, which I strive to emulate. I would like to sincerely acknowledge the mentorship and support he has extended throughout the course of my M.S. I would like to thank my Thesis Chair, Dr. Barbara Knutson for her timely advice and support towards completion of my thesis. I also wish to convey my sincere thanks and appreciation to Dr. Stephen Rankin and Dr. Fuqian Yang, for accepting to be on my committee. Further, I wish to extend my sincere appreciation to Bruce Cole whose constant support and timely assistance eased my stay at UK.

I feel most indebted to my parents, particularly my mother, whose constant motivation and support was instrumental in completion of my Master's. My father and brother stood by me whenever I needed them the most. I wish to express my sincere thanks to my best friend, Anil Kumar Thota, whose constant assistance and support eased the pathway to bring my Master's to a closure.

This appreciation would be incomplete without mentioning my roommates, lab mates and friends for making my stay at UK memorable. My experiences with each one of them have molded my personality to better face challenges on both personal and professional level.

TABLE OF CONTENTS

LIST OF FIGURES

LIST OF FILES

LIST OF TABLES

Chapter 1: Introduction

The discovery of structured carbonaceous materials (fullerene, buckyballs, nanotubes, and nanofibers) has been accompanied by a flurry of research activity dealing with structured carbon synthesis [1-4]. The focus of this work has been on novel carbon materials with nanometer dimensions, largely driven by their unique chemical and physical properties. The past decade has witnessed significant research efforts directed towards the development of efficient and high yield nanostructured carbon growth methodologies [5-7] with ultimate applications in gas storage [8-12], electrical devices, and catalyst supports [13-16].

1.1 Definition and Classification of Structured Carbon

Carbon is the most versatile element in terms of the variety of materials it can form. Three possible hybridizations are associated with carbon: sp, sp^2 and sp^3 as opposed to Si and Ge (other group IV elements), which exhibit primarily sp^3 hybridization. Various bonding states are connected with specific structural arrangements, such that sp bonding gives rise to chain structures, sp^2 bonding to planar structures and sp^3 bonding to tetrahedral structures.

C exists in various forms. Diamond, the hardest known material has no free electrons and hence serves as an electric insulator. Graphite, on the other hand, exhibits excellent thermal and electrical conductivity. In addition to the diamond and graphite bulk phases, carbon atoms can be arranged into small clusters, fullerenes, carbon nanofibers and carbon nanotubes. Carbon nanotubes and nanofibers are graphitic structures with high aspect ratio, with the diameters ranging from 0.4 – 500 nm and lengths from several micrometers to millimeters [17]. An ideal nanotube can be considered as a "hexagonal network of carbon atoms that has been "rolled up" to make

1

a seamless hollow cylinder" [18]. These hollow cylinders can be tens of micrometers long with diameters as small as 0.7 nm. The terminations of these nanotubes are often called caps or end caps. Each cap contains six pentagons and an appropriate number placement of hexagons that are selected to fit perfectly to the long cylindrical section [18]. Nanotubes are further classified into Single Walled Nanotubes (SWNTs) and Multiwalled Nanotubes (MWNTs).

The SWNTs bear a cylindrical shell of an atom thickness as the fundamental structural unit. Typically, SWNTs exist in bundles, consisting of a few to several tens of individual SWNTs. SWNTs characteristically have a diameter to up to 2 nm with lengths extending to several micrometers. SWNTs form the building blocks of MWNTs that contain multiple coaxial cylinders of ever-increasing diameter about a common axis. A central "hollow" core is typically observed in MWNTs, where spacing between the layers on each side of the core is close to that of the interlayer distance in graphite (~0.34nm) [17].

Carbon nanofibers, the focus of this study, are generally classified as graphitic structures, characterized by a series of ordered parallel graphene layers arranged in specific conformations with an interlayer distance of *ca.* 0.34 nm. An exceptional feature of these structures is the availability of large number of edge sites which are readily available for chemical or physical interaction. These ordered structures further exhibit high surface areas (up to 700 m^2/g), where the totality of the surface is chemically active [19].

The distinction between carbon nanotubes and nanofibers as presented in the recent literature is far from clear. Carbon nanofibers have larger surface area, are more

thermally stable and have a wider diameter than carbon nanotubes. The larger surface is attributed to the availability of edge sites whereas nanotubes are closed on both sides. Furthermore, SWNTs and/or MWNTs expose only carbon basal planes and do not offer intercalation accessibility or provide for facile functionalization. In contrast, carbon nanofibers expose carbon atoms on or the edges of lamella with regular periodicity [20].

The full potential of these nanostructures in various applications can only be fully realized if their synthesis is optimized and well controlled. The work in this thesis is directed at developing such a viable carbon growth process.

1.2 Synthesis Methods

Structured carbon can be grown by various methods, the most common being:

1. Arc discharge;

2. Laser ablation;

3. Catalytic (chemical) vapor deposition.

1.2.1 Arc Discharge and Laser Ablation Methods [21- 26]

In the arc discharge method (see Figure 1.1) carbon atoms are evaporated by the plasma of inert gas ignited by high currents through the opposing carbon anode and cathode. Typical synthesis involves usage of carbon rod electrodes (where the diameter of the anode is smaller than the cathode) separated by *ca.*1 mm with a voltage of 20 – 25 V and a dc electric current of 50-150 A across them. The arc is usually operated at high pressures of the order 500 Torr inert gas with a flow rates of the order 5-15 $cm^3\,s^{-1}$ for cooling purposes; the carbon deposit forms on the negative electrode. The anode decreases in length as carbonaceous material (of various morphologies) is formed and deposited on the cathode. Products generated in regions nearer to the high temperature-

evaporating end have a higher degree of graphitization. Typically, nanofibers appear over the lower temperature area whereas nanotubes are found at higher temperature area [27, 28]. A metal catalyst is essential to produce SWNTs; its absence generates MWNTs. A narrow distribution of diameter of SWNTs can be obtained by using metals such as Co, Fe or Ni [21, 22], which are incorporated in the anode. Doping the anode with catalyst particles has been found to yield carbon nanofibers that bear some or all of the catalytic metal [23].

In the laser ablation method, laser pulses are impacted on a graphite target containing metal catalysts (usually less than 1 w/w% Ni, Co, or Fe) placed in the middle of a long quartz tube, contained in a furnace that regulates the temperature typically at *ca.* 1473 K (see Figure 1.2). The pulsed laser evaporates C from the graphite target surface to yield a smooth, uniform face for vaporization. The carbonaceous deposit is swept by the flowing gas from the higher temperature zone and deposited on a water-cooled collector [18, 24].

Both arc discharge and laser ablation are highly energy demanding methodologies and are hardware intensive. Furthermore, they are batch processes reactions with short reaction times and the amount of carbonaceous material that can be produced is very limited. Moreover, nanotubes/nanofibers have to be produced separately (*i.e.* not directly on substrates) which necessitates a costly, multi-stepped and involved purification [25, 26].

1.2.2 Catalytic (Chemical) Vapor Deposition (CVD) [29-35]

CVD is quite distinct when compared with arc discharge and laser ablation in that it employs much lower temperatures (700-1400K) and longer reaction times

resulting in greater product yields. Further, nanotubes/nanofibers grown *via* CVD can be used directly without further purification unless the catalyst particle is required to be removed, methods for which are now established [29]. A basic schematic for a CVD unit is shown in Figure 1.3. Growth of structured C via CVD involves two major steps (1) thermal treatment/activation of the catalyst in a tube furnace and (2) contact with flowing hydrocarbon gas in the presence of carrier gas (typically H_2 or inert gas). Materials grown from the catalyst are collected upon cooling the system to room temperature. The most commonly accepted model for growth of structured C *via* CVD involves decomposition of the hydrocarbon gas on the free metal surface to generate carbon atoms with concomitant desorption of H_2. The carbon atoms dissolve and diffuse through the bulk of the metal to ultimately precipitate as structured C on the other side of the catalyst particle. The active catalyst species used typically are transition metal nanoparticles dispersed on a support material as silica or alumina [30, 31]. Several studies [32] indicate that while certain crystallographic orientations of the catalyst particle favor reactant decomposition, a different set of faces promote precipitation to structured C [34]. Further, it has been shown that the nature of structured C formed is significantly dependant on the hydrocarbon/hydrogen reactant mixture [33]. Thus, the morphological characteristics, degree of crystallinity and orientation of the precipitated graphite crystallites (with respect to the fiber axis) can be controlled through a judicious choice of reaction parameters as metal catalyst particle, hydrocarbon/hydrogen reactant mixture ratio and reaction conditions. Furthermore, the properties of structured C can be modified to the requisite through introduction of selected groups between the layers, a process known as intercalation, to generate carbon nanotubes/nanofibers with unique

electrical and chemical properties, thus opening numerous avenues in fabrication of novel materials [35]. On the whole, the catalytic route imposes a greater deal of control on the carbon structural characteristics while scale-up is far more feasible.

1.3 Applications

Carbon nanotubes/nanofibers have been investigated for a wide range of applications such as electronic devices [36-40], storage media [9, 11, 41-43], reinforcement materials [44, 45] and catalysts supports [46]. Their high aspect ratio and electrical conductivity makes them highly desirable for applications as field emission tips in X-ray tubes [47], field emission displays [37-40, 48, 49] and electron sources for microscopy and lithography [36]. Carbon nanotubes are highly sensitive to adsorbed gases/molecules [50, 51]. This property can be advantageously used in the manufacturing of biological or chemical sensors for detection of poisonous/dangerous gases. As the electrical characteristics of the nanotubes respond to mechanical deformation in structure, they can be used as electrochemical sensors [52-56] also. Nanofibers have been investigated for applications as storage devices since ions/molecules can intercalate through the available edge sites e.g. for lithium batteries or hydrogen storage [9, 11, 41-43]. In a further development these nanostructures have been proposed as catalyst supports [46].

1.4 Research Objectives and Thesis Outline

Halogenated organics have long been recognized as toxic compounds adversely affecting the public health and ecology. Disposal of the halogenated organic waste is now recognized as a serious environmental problem. Catalytic hydrodehalogenation represents a nondestructive, low-energy treatment wherein known hazardous

6

compounds are transformed into recyclable products with negligible associated toxic emissions. As part of an ongoing environmental catalysis program in our lab wherein gas phase hydrodehalogenation of chlorobenzene (CB) over modified Ni/SiO_2 at 553 K was explored, sudden deactivation of the catalyst accompanied by unexpected carbon growth was recorded. Characterization of the product revealed that the carbon formed was structured. This low - temperature carbon production (approximately 150 K lower than "conventional'' synthesis) was linked to the incorporation of a halogen and alkali metal component during catalyst pretreatment and reaction. Presence of K and Cl (and/or Br) on the catalyst surface were considered to provide a chemically modified pathway to an ordered carbon nanostructure in the presence of hydrogen under relatively mild conditions. The principal objective of this study is to assess the feasibility of growth of structured C from environmentally hazardous halo organics (e.g. CB) over "unmodified" supported Ni and to develop a highly efficient method to maximize C yield by adjustment of reaction parameters on supported Ni. Conversion of environmentally hazardous halo-organics to structured C, materials that have shown promise for a wide range of applications (discussed in detail earlier in this chapter) is definitely attractive from both environmental and commercial facet.

In Chapter 2, growth of structured carbon via catalytic decomposition of CB over 10% (w/w) Ni/SiO_2 is considered. The reaction of CB with H_2 in the temperature range 823–973 K also generated benzene via hydrodechlorination and a volatile component that results from catalytic hydrocracking/hydrogenolysis. The characteristics of the carbonaceous product are determined through a combination of high resolution transmission electron microscopy (HRTEM) and Temperature Programmed Oxidation

(TPO). The response of carbon yield and structural order to varying reaction time (up to 4 h on-stream) and temperature are presented and discussed. Under identical reaction conditions, the CB feed delivers appreciably higher carbon yields than that recorded for the decomposition of benzene while the carbon growth in the former case is significantly more ordered. These findings are discussed in terms of Cl/catalyst interaction(s) and metal site restructuring.

In Chapter 3, the effect of varying % (v/v) H_2 on the growth of structured carbon via CVD of CB over 10% (w/w) Ni/SiO_2 at 873 K over a time period of one hour is reported. Growth of structured carbon from aromatic (benzene), cyclic aliphatic (cyclohexane, cyclohexene) and straight-chained aliphatic precursors is reported. The effect on carbon growth characteristics due to presence of electron withdrawing and/or donating group(s) is explored. Benzene was the common by-product observed in all the reactions. While aromatic compounds containing strong electron withdrawing substituents delivered C yield greater than benzene, those containing weak electron withdrawing and/electron donating substituents deliver no measurable C yield. The presence of Cl while, enhanced formation of benzene from cyclic compounds favored C yield from straight chained compounds. Dependence of C yield on the nature of the heteroatom substituent is discussed in terms of reactant/catalyst interaction(s). The role of H_2 content in the feed is also considered. The structural characteristics of the carbonaceous product are determined through a combination BET surface area and TPO. C (solid) obtained from benzene containing strong electron withdrawing substituents was found to be relatively more structured than C obtained from all the other precursors taken into consideration here.

In Chapter 4, the effect of support on yield and structure of carbon generated via CVD of CB in H_2 over (10% w/w) Ni supported on silica (SiO_2), tantalum oxide (Ta_2O_5), alumina (Al_2O_3), zeolite (NaY), activated carbon (AC) and graphite (G) at 873 K has been assessed. The activated catalysts were characterized by BET surface area, H_2 chemisorption and Temperature Programmed Reduction (TPR). Under identical conditions, Ni/SiO_2 delivered substantially greater carbon yield. Furthermore, the response of carbon yield and structural order to varying loading has been reported in the case of Ni/SiO_2 and Ni/Al_2O_3. Decrease in loading has been found to result in a decrease in C yield. The results are discussed in terms of particle size, crystallographic orientation of the Ni sites and metal-support interaction. The carbonaceous product was characterized using BET surface area, TPO and TEM. Carbon grown on Ni/NaY has been found to be most structured. Chlorine contents up to 0.4 atom% were detected in the carbon product obtained on Ni/Al_2O_3.

The thesis ends with concluding remarks and suggestions for future work.

1.5 Figures
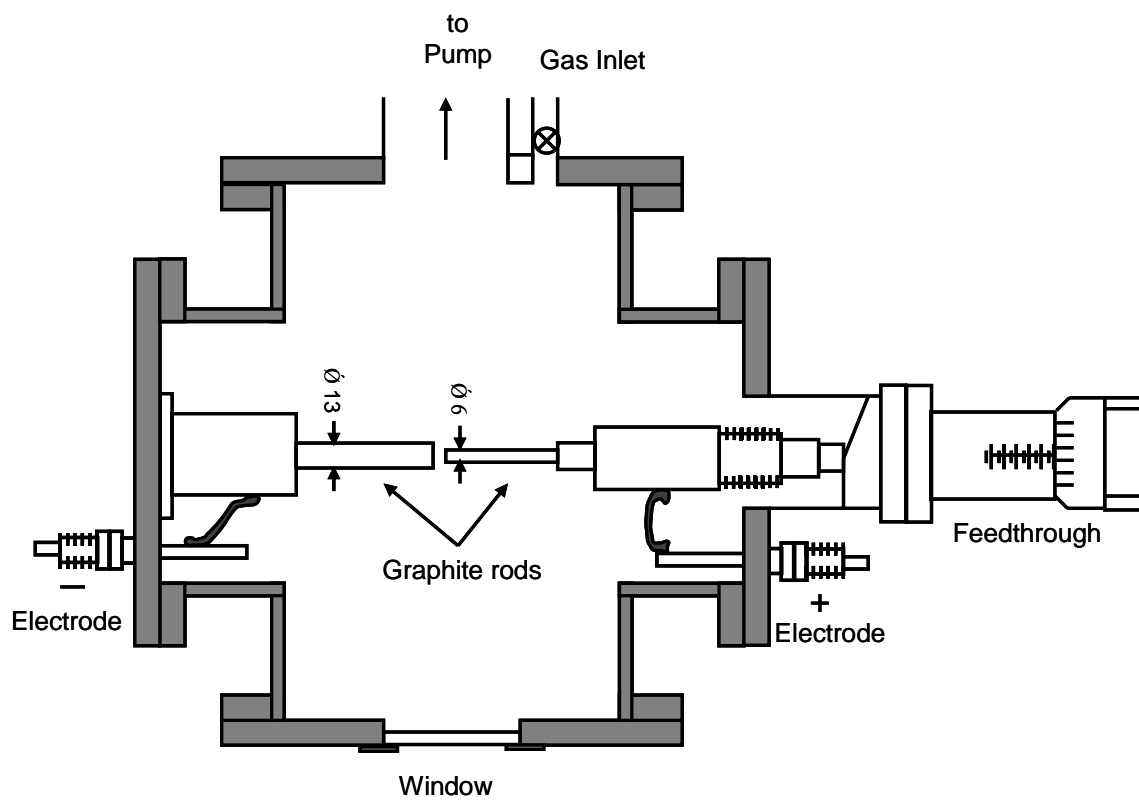
Figure 1.1: Cross-sectional of carbon arc generator that can be used to synthesize carbon nanotubes (redrawn from reference [21]).
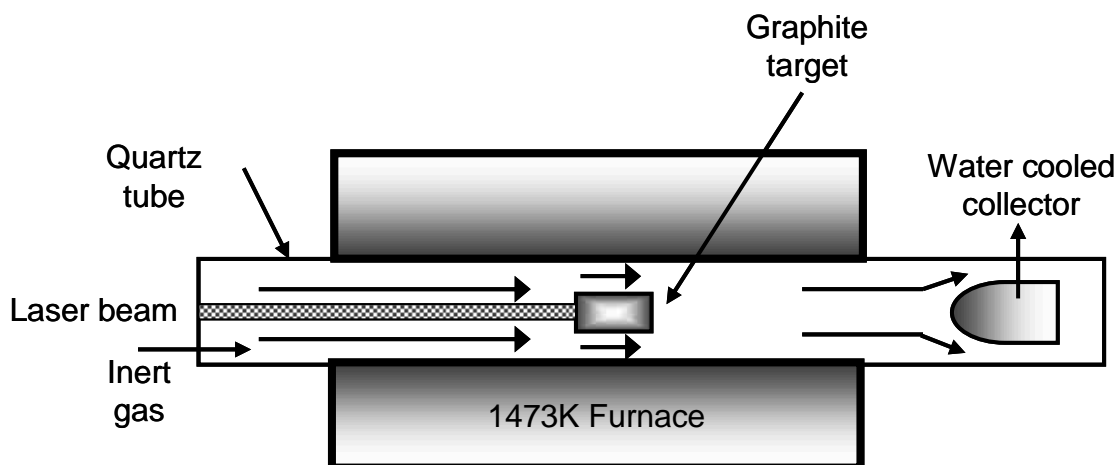
Figure 1.2: Single – walled nanotubes produced in a quartz tube heated to 1473 K by the laser vaporization method, using a graphite target and a cooled collector for nanotubes (redrawn from reference [17]).
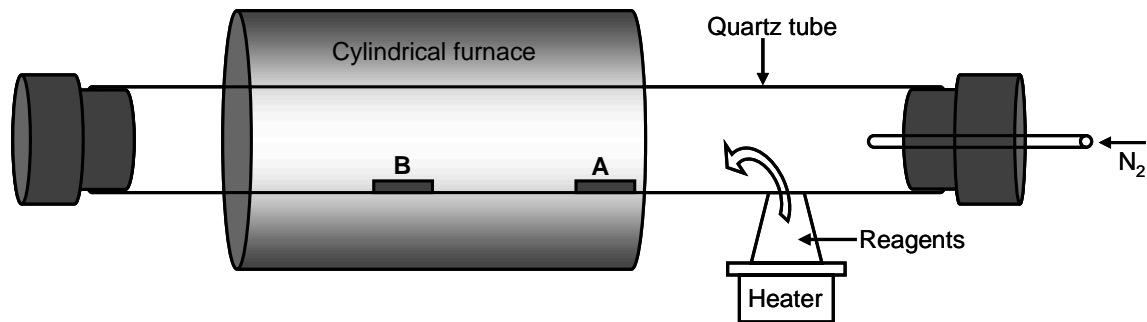
Figure 1.3: Schematic diagram of growth carbon nanostructures on uncoated silicon and glass substrates, obtained by evaporating either a solid carbon precursor such as camphor or a liquid one such as cyclohexanol (redrawn from reference [57]).

Chapter 2: Catalytic growth of structured carbon via the decomposition of Chlorobenzene over Ni/SiO2*

2.1 Introduction

The synthesis of highly ordered carbonaceous materials has been the subject of a disparate and burgeoning literature over the past decade. Ordered carbon structures have been detected in benzene, acetylene and ethylene flames [1, 2] but flame synthesis is not viewed as a viable preparative strategy. The direct synthesis of graphitic carbon (nanotubes/nanofibers) is now well established by arc discharge [3-5] and plasma decomposition [6, 7] but such methodologies also yield polyhedron carbon particles (low aspect ratio) and an appreciable amorphous carbon component [6, 8]. The latter necessitates an additional involved, cumbersome and costly purification stage in order to extract the desired high aspect ratio product. In any case, these methodologies are highly energy-demanding, hardware-intensive, batch processes, and the amount of carbon that can be produced is limited. As a means of addressing these drawbacks, there have been several attempts, in parallel, to synthesize carbon nanotubes/nanofibers through catalytic vapor deposition [3, 9]. On the whole, the catalytic route imposes a greater deal of control on the carbon structural characteristics while scale-up is far more feasible. Carbon growth over nickel, the subject of this study, has been reported for both unsupported [10-15] and supported [16-26] catalyst systems and over Ni/Fe [27, 28] and Ni/Cu [29] bimetallics. Structured carbon has been generated from a catalytic decomposition of CO [13, 18, 30] and hydrocarbons such as methane [12, 16, 18, 19, 23-26], 1- butene [14], 1,3-butadiene [14, 27], acetylene [31, 32], ethylene [14, 15, 18, 20-22, 25] and n-hexane [33]. Hydrogen is not an essential component in these systems

but its presence has been shown to be beneficial, not only in initiating the decomposition of the carbon-containing gas [34] but also as a means of minimizing amorphous carbon formation [28]. In this Chapter, we report for the first time the controlled growth of carbon nanofibers via the catalytic decomposition of CB and also consider carbon formation from a benzene feed. The transformation of an aromatic feedstock into a structured carbon product has not been studied to any great extent. The earliest report of carbon fiber (with lengths of up to 35 cm) production from the thermal decomposition of benzene in a H_2 atmosphere is provided by Koyama [35] but the details of the growth procedure were not given. Endo *et al*. [36, 37] have recorded a pyrolytic growth of structured carbon by a catalyzed carbonization of benzene using ultra fine iron particles at temperatures in excess of 1273 K. Nath *et al*. [32] obtained ''copious quantities of aligned carbon nanotube bundles'' as a result of pyridine pyrolysis at 1173 K over Fe/SiO_2. Lu *et al*. [38] generated carbon nanotubes as a result of a detonation (shock wave of 20–40 MPa at 693 K) of m-dinitrobenzene in the presence of Co while Shao *et al*. [39] have reported carbon nanotube synthesis from benzene at 753 K and 15 MPa in the presence of Ni/Fe powder. However, it is instructive to note that Hernadi *et al*. [40] observed no significant carbon growth from the reaction of toluene over Co/SiO_2 in the temperature range 973–1173 K but did observe an appreciable carbon yield from acetylene, propylene, ethylene, acetone and pentane. The results published to date are insufficient to allow any general conclusions regarding optimum carbon growth conditions or even an identification of critical catalyst/process variables, a task which is certainly impractical given the incomplete procedural descriptions that have been provided. The decomposition of CB certainly

14

represents an atypical route to ordered carbon. The momentum for the work described in this Chapter was provided by an earlier study where we observed an unexpected carbon growth from a modified Ni/SiO_2 during gas phase hydrodehalogenation at 553 K [41, 42]. This low-temperature carbon production (ca. 423 K lower than ''conventional'' syntheses) was linked to the incorporation of a halogen and alkali metal component during catalyst pretreatment and reaction. The presence of K and Cl (and/or Br) on the catalyst surface was considered to provide a chemically modified pathway to an ordered carbon nanostructure. This effect is not without precedent in that Albers *et al*. [43] noted the appearance of carbon filaments on Pt/Al_2O_3 and Pd/SiO_2 (at T <473 K) during the synthesis of hydrogen cyanide and attributed this to the presence of Fe and Cl impurities while the involvement of Na and K was also invoked. We assess herein, for the first time, the effects of reaction temperature and time on the growth of carbon over Ni/SiO_2 from a C_6H_5Cl/H_2 feed, characterize the nature of the carbon product and evaluate benzene as feed under identical reaction conditions.

2.2 Experimental Procedure

2.2.1 Catalyst Preparation/Activation and Reaction

The Ni/SiO_2 catalyst was prepared by a standard incipient wetness technique where the silica support (Aldrich fumed silica, surface area > 200 m^2 g^{-1}) was impregnated with a 2-butanolic solution of Ni $(NO_3)_2$ to yield a 10 %(w/w) Ni loading. The Ni content of the catalyst was determined by inductively coupled plasma optical emission spectrometry (ICP-OES, Vista-PRO, Varian, Inc.) from the diluted extract of aqua regia. The catalyst precursor was sieved (ATM fine test sieves) into a batch of 100 μm average particle diameter, loaded into a fixed-bed tubular quartz reactor (i.d: 1.25 cm)

and activated by heating at 10 $Kmin^{-1}$ in 60 cm^3 min^{-1} (Humonics Model 520 flow meter) dry H_2 (99.999%) to the ultimate reaction temperature (823–973 K), which was maintained for 12 h. The decomposition reactions were conducted in situ (after catalyst activation) with a co-current flow of the aromatic feed in H_2. A layer of quartz wool above the catalyst bed ensured that the reactants were vaporized and reached reaction temperature before contacting the catalyst. The reaction temperature (±1K) was monitored continuously by means of a thermocouple inserted in the catalyst bed. A Model 100 (kd Scientific) microprocessor-controlled infusion pump was used to deliver the aromatic feed, via a glass/ Teflon air-tight syringe and Teflon line at a fixed calibrated flow rate, which was carried through the catalyst bed in a stream of dry H_2. The inlet hourly C/Ni mole ratio was maintained at 69.4 with a gas hourly space velocity of (GHSV) of 4 x 10^3. The decomposition of benzene was studied at the same inlet C/Ni ratio and GHSV. In a series of blank tests, passage of both reactants in a stream of H_2 through the empty reactor, at 698 K, i.e. in the absence of catalyst, did not result in any detectable conversion. Moreover, introduction of the aromatic in a flow of He did not generate any measurable carbon growth from the activated (reduced in H_2) catalyst; H_2 is a crucial reactant component in this system. The reactor effluent was frozen in a liquid nitrogen trap for subsequent analysis which was made using a Perkin-Elmer Auto System XL chromatograph equipped with a split/splitless injector and a flame ionization detector, employing a DB-1 50 m x 0.20 mm i.d., 0.33 μm capillary column (J&W Scientific). Overall analytic repeatability was better than ±5%. Carbon balance was monitored based on known carbon inlet, gravimetric yield of solid carbon and chromatographic analysis of the reactor effluent using 2-octanol as internal

16

standard. The reaction was monitored for 4 h on-stream with no significant back-pressure/flow fluctuations. Each catalytic run was repeated up to six times (with a minimum of three repetitions) and the catalytic data quoted in this paper represent average values. The solid carbon gravimetric yield was reproducible to within ±10%.

2.2.2 Catalyst/Carbon Growth Characterization

The BET surface areas and TPO characteristics were determined using the commercial CHEM-BET 3000 (Quantachrome Instrument) unit. After outgas at 523 K for 30 min, at least two cycles of N_2 adsorption–desorption in the flow mode were employed to determine total surface area using the standard single-point BET method. TPO profiles of the catalytically generated carbon were obtained from thoroughly washed, demineralized (in HNO_3) samples to avoid any contribution due to a catalyzed gasification of carbon by residual Ni [44]. A known weight of the demineralized sample was heated from room temperature to 1273 K at 8 K min^{-1} in a 5% (v/v) O_2/N_2 mixture with on-line Thermal Conductivity Detector (TCD) analysis of the exhaust gas. These profiles were assessed against those generated for model activated carbon and graphite samples (Sigma-Aldrich). The structural characteristics of the activated catalyst and the carbon growth were probed by high-resolution transmission electron microscopy (HRTEM) using a JEOL-2010 TEM/STEM equipped with energy-dispersive X-ray (EDX) detector (Oxford Instruments) operated at an accelerating voltage of 200 kV. A transient EDX mapping (2 nm s^{-1}) was conducted over the length of individual carbon nanofibers. Specimens for TEM analysis were prepared by ultrasonic dispersion in n-butanol where a drop of the resultant suspension was evaporated on a holey carbon support grid.

2.3 Results and Discussion

2.3.1 Process Parameters

The reaction of C_6H_5Cl with H_2 over Ni/SiO_2 generated, as principal products, benzene via catalytic hydrodechlorination and a solid carbon deposit via C_6H_5Cl decomposition. Hydrodechlorination to benzene yields HCl as the only inorganic product with no evidence of Cl_2 formation [45, 46]. Carbon balance measurements revealed the formation of volatile product(s) that were not isolated in the liquid nitrogen trap. Such volatiles can be formed through additional hydrogenolysis/hydrocracking reactions and did not account for more than ca. 20 mol% conversion of the feed. Work is going on to establish the composition of this volatile product component in order to develop a detailed reaction scheme. The emphasis of is, however, firmly placed on the growth of carbon nanofibers from C_6H_5Cl rather than a detailed consideration of the catalytic features associated with any side reactions.

The solid carbon yield (Y_c) as a function of time-on-stream is illustrated in Figure 2.1 for a representative reaction temperature. There is a clear induction period (up to ca. 0.5 h), wherein there is limited carbon growth and this is followed by a period of continuous carbon deposition up to 4 h on-stream. Transient effects in catalytic carbon growth have received scant attention in the literature but there is evidence of a decrease in carbon deposition rate with extended reaction times [21, 47] that can be linked to a poisoning of the active metal particle due to encapsulation by carbon [29] while an induction period with regard to carbon growth has been mooted by some authors [13, 48]. The carbon efficiency, i.e. fraction of carbon in the total inlet feed that is converted to a solid carbon product, was observed to pass through a maximum (at ca. 2 h), as shown in Figure 2.1. The initial time-lag and time-related optimum in efficiency

is significant and must be linked to some surface-active site reconstruction as a result of C_6H_5Cl interaction(s). The commonly accepted model [11, 49, 50] for carbon growth from a metal catalyst involves reactant decomposition on the top surface of a metal particle followed by a diffusion of carbon atoms into the metal with precipitation at other facets of the particle to yield the graphitic fiber. The growth proceeds further through dissolution and diffusion of carbon. It has been shown that certain crystallographic orientation(s) of Ni favor(s) reactant decomposition while a different set of faces serves to promote the precipitation of a graphitic carbon product [10, 51]. Graphitic fibrous growth has been linked to the formation of a metal carbide species [18, 48, 52] and Ni_3C has been proposed as the nucleation species [15, 48, 53]. The involvement of metal carbide, i.e. metastable with respect to the metal and graphite, still remains a matter of supposition. The observed growth of carbon nanofibers can be considered to result from a stable but fluid supersaturated solution of carbon in the metal rather than an explicit carbide assignation. The rate determining step is the dissolution and diffusion of carbon through the metal particle where the driving force for diffusion has been ascribed to either a temperature [11, 49] or a concentration [19, 50, 51] gradient. In terms of a concentration gradient process, the carbon concentration in the metal must be greater than that at the metal/graphite interface in order to drive the diffusion forward. Carbon species at the metal/gas interface are known to exhibit a higher solubility than carbon originating from graphite [18, 50]. The induction period shown in Figure 2.1 must then coincide with a restructuring of the surface Ni, creating exposed faces that present an atomic arrangement favoring dissociative/destructive chemisorption with concomitant carbon diffusion/precipitation. Indeed, we have shown

elsewhere that C_6H_5Cl–Ni/SiO$_2$ interactions induce significant reconstruction/faceting of supported Ni particles [41, 46].

We set an upper limit of 1 h for the reaction time as a suitable point of comparison when probing the effect of varying reaction temperature and the nature of the aromatic feed.

A 1-h period of carbon growth yields a highly reproducible and representative product with no associated temperature or pressure/flow fluctuations. The effect of temperature on carbon yield (Y_C) is illustrated in Figure 2.2; at T = 823 K, there was negligible carbon growth. Carbon yield increased with increasing temperature to pass through a maximum at ca. 923 K. Such a temperature related maximum has been noted elsewhere [21, 22, 27, 54-56] and the optimum T appear to be strongly dependent on the nature of the catalyst and the feedstock. With an increase in reaction temperature carbon generation from C_6H_5Cl was increasingly favored over benzene production as can be assessed from the product benzene to carbon ratios (benzene/C) plotted in Figure 2.2; at T > 873 K, decomposition was preferred over hydrodechlorination. The carbon yields that have been reported in the literature are highly dependent upon reaction conditions and the type of catalyst used. The use of unsupported mono- or bimetallic transition metal catalysts has been reported to lead to high yields, i.e. in excess of 200 g_C g_{metal}^{-1} [57]. Avdeeva et al. [56] and Ermakova et al. [17, 57] obtained carbon yields of up to 384 g_C g_{Ni}^{-1}, 161 $g_C g_{Ni}^{-1}$ and 45 g_C g_{Fe}^{-1} from coprecipitated silica, alumina and Fe/SiO$_2$ over the temperature range 573 –973 K. Nagy and co-workers [2, 40], in examining the growth of filamentous carbon from zeolite and silica substrates, recorded yields of up to 65 g_C g_{metal}^{-1} from 2.5% (w/w) Co and Fe loaded samples. Similarly, Anderson and

Rodriguez [47] using a series of silica-supported bimetallic Fe: Ni catalysts, reported a maximum yield of 21 $g_C g_{metal}^{-1}$ at 873 K from a CO/H_2 reactant mixture. We have reported [20-22] carbon yields in the range 2–125 $g_C\ g_{Ni}^{-1}$ for the decomposition of ethylene (723–873 K) over a range of promoted and non-promoted supported Ni catalysts. The carbon yields generated in this study fall within the range of values cited above.

The level of carbon growth (under identical reaction conditions) from a C_6H_6, feed is compared with that generated from C_6H_5Cl in Table 2.1 on the basis of carbon yield (Y_C) and carbon efficiency. The degree of carbon deposition was appreciably greater from the CB feed, and carbon efficiency far exceeded that generated for benzene, particularly at 923 K. Given the equivalency of the growth conditions, the enhancement of carbon yield must be associated with the Cl component in the CB feed. This result is not without precedent in that Cullis *et al*. [58], as far back as 1959, observed a difference in carbon deposition from methane when compared with a chloromethane feed. Moreover, in catalytic reforming the level of (unwanted) carbon deposition has been directly related to the Cl content of the catalysts [59, 60]. It was shown elsewhere that Ni/SiO_2 bears a significant reversibly and irreversibly held HC1 component during CB hydrodechlorination [46, 61]. The presence of a sufficient residual halogen component on the catalyst can induce electronic perturbations through a reduction in d-electron density of the surface Ni metal that should serve to strengthen the interaction with incoming reactant [62, 63], weakening the C-C bonds in the adsorbed aromatic, favoring decomposition. Published evidence suggests that the ''irreversibly'' held halogen component [46] is built into the surface sub layers of the

Ni particles and this incorporation of Cl into the metal sites, allied to the faceting/restructuring may serve to facilitate carbon diffusion and precipitation, elevating the overall decomposition/carbon growth efficiency.

2.3.2 Catalyst/Carbon Characterization

Surface area measurements provide a means of distinguishing between a carbon nanofiber as opposed to a nanotube product. The nanofiber has a greater availability of edge sites while the nanotube is characterized by a large exposed exterior basal plane with a typical surface area of ca. 25 m^2 g^{-1}, significantly lower than that associated with carbon fibers [27, 64, 65]. The BET surface areas of the activated Ni/SiO$_2$, model graphite and activated carbon and representative catalytically generated carbon are given in Table 2.2. It can be seen that the surface areas associated with the carbon growth is intermediate between the high surface area model amorphous carbon and low surface area graphite and is greater than that associated with nanotube growth. There is no obvious surface area dependency on growth time and/or temperature.

A representative low magnification TEM image of the activated Ni/SiO$_2$, illustrating the surface morphology/dispersion of the metal phase, is shown in Figure 2.3. Selected area electron diffraction (SAED) confirmed that the supported Ni was present in the metallic form and not as an oxide. The nature of the carbon nanofiber growth that was common to both C_6H_5Cl and C_6H_6 feed is illustrated by the TEM images shown in Figure 2.4. The fibrous nature of the carbon is immediately evident and the images shown in Figure 2.4 are characteristic of the carbon growth observed at every reaction time and temperature that was considered. There is a general consensus in the literature [49, 66] that the diameter of the nanotube/ nanofiber is governed by the

dimensions of the seed metal particle while the length depends largely on the duration

of reaction. The majority of the Ni particles in the activated catalysts spanned the size

range 10–20 nm while the carbon fibers exhibited (from TEM analysis) diameters of up

to 40 nm. There are then definite instances of carbon growth where the fiber width

exceeds the initial Ni particle diameter and this is indicative of Ni particle sintering

during the CB/benzene decomposition reaction. Similar metal sintering has been

reported during carbon growth from a CO/H_2 feed over Fe/Ni [47] and from CH_4 [67]

and C_2H_6 [21, 22] decomposition over Ni/SiO_2. The occurrence of a central hollow core

in the growing fiber, clearly shown in Figure 2.4(b), has been attributed to a

deformation or faceting of the supported metal particle that alters the relative rate of

carbon diffusion and fiber nucleation [49, 68]. A TEM image of a representative

isolated nanofiber is shown in Figure 2.5 wherein an entrapped Ni particle is visible at

the fiber tip. Where the metal interaction with the support is relatively weak, as in the

case of Ni-impregnated SiO_2 [69], the pressure exerted on the metal/support interface

due to graphite formation is of sufficient magnitude to extract the metal particle from

the support. Once the Ni particle is detached from the SiO_2 substrate, a fresh surface is

exposed to the incoming feed and growth continues with the Ni particle located on the

fiber tip. It can be seen that the entrapped Ni particle has adopted a decidedly facetted

geometry that was not apparent in the freshly activated sample, indirect evidence of a

restructuring (and sintering) that accompanied carbon growth. The structural integrity of

the carbon nanofibers can be assessed from the TEM images presented in Figure 2.5

and Figure 2.6 where the lattice structure is in evidence. The inter-platelet spacing is ca.

0.3 nm, diagnostic of graphitic species. It should be noted that the TEM images

correspond to samples taken directly from the reactor and the presence of an amorphous carbon layer visible on the fiber edges is an artifact of the cooling stage (upon completion of the catalytic step).

The application of TPO facilitates a distinction between structured and non-structured (amorphous) carbon in that the temperature at which gasification of graphitic carbon is induced is notably higher [70, 71]. The TPO profiles of carbon grown from C_6H_5Cl decomposition (873 K) over Ni/SiO$_2$ at varying reaction times are presented in Figure 2.7 and can be assessed against the TPO characteristics of model amorphous and graphitic carbon. On the basis of the TPO response, carbon grown from Ni/SiO$_2$ possesses a degree of order but is by no means as structured as graphite. The oxidation profiles associated with catalytic carbon growth are broad, a feature that is diagnostic of a range of carbon structures with both an amorphous and a graphitic component. Over the 4-h period of carbon growth there does not appear to be any significant variation in the structural characteristics of the carbon product. The TPO profiles of carbon grown (over a common 1-h period) at different reaction temperatures are given in Figure 2.8; CB served as reactant in each case. While there were no noticeable differences in the TPO profiles for the carbon generated over the temperature range 873–923 K, the carbon grown at 973 K contained an appreciably greater amorphous component. The latter can be ascribed to a contribution due to a thermal (pyrolitic) cracking which yields a less graphitic product [18].

This study has, however, revealed that the structure of carbon generated from the decomposition of benzene differs from that delivered by the CB feed, as shown in Figure 2.9. The TPO profile for the carbon generated from benzene possesses two

24

peaks, indicative of two stages of oxidation, the low-temperature broader peak corresponding to that associated with the model activated carbon and a sharper peak at a higher temperature that is indicative of a more structured component. On the whole, the carbon product from CB exhibits a greater degree of structural order; the higher BET surface area recorded for the benzene generated carbon (Table 2.2) also points to such structural differences. The degree of crystalline order of the carbon product is controlled by various factors including the wetting properties of the metal with graphite and the crystallographic orientation of the metal faces that are in contact with the carbon deposit [11, 27, 72]. If the metal atoms at the face where the carbon is deposited are arranged in such a manner that they are consistent with those of the basal plane structure of graphite then the carbon that dissolves in and diffuses through the particle will be precipitated as an ordered structure. Conversely, if there is little or no match between the atomic arrangements of the depositing face and graphite, a more disordered carbon will be generated. It appears that the surface restructuring due to Cl/catalyst interactions has facilitated the precipitation of a more ordered structure. In a related study, Zheng *et al*. [73] noted that a chlorination treatment of titanium carbide can induce a ''local re-bonding'' of each carbon and so impose structural order.

One intended outcome of this work was an assessment of the viability of incorporating Cl (from the feed) into the carbon growth. An intimate association of surface Cl with the active metal center may facilitate an inclusion of electron-withdrawing species into the growing carbon, which should certainly impact on the electronic properties of the carbon product. Such a direct introduction of Cl would circumvent the problematic intercalation step that is the established method used to

introduce halogens/alkali metals into carbon but which suffers the decided drawback of a rapid exfoliation [74]. It has been shown elsewhere that an intercalation of halogens into graphitic materials produces at least an order of magnitude increase in electrical conductivity [75-77]. The surface composition of individual carbon nanofibers was determined by EDX mapping and a representative analysis is given in Figure 2.10. The dark field image is presented in Figure 2.10(a) wherein the length of the isolated nanofiber that was analyzed is shown; the averaged EDX spectrum over this nanofiber segment is given in Figure 2.10(b). This particular nanofiber bore a Ni particle at the tip which accounts for the appreciable Ni content shown in Figure 2.10(c). Mapping along the fiber length (beginning at the tip) revealed a lower Ni content while the C counts remained essentially constant. Evidence of Ni particle entities dispersed along the length of carbon fibers grown during ethylene decomposition has been provided elsewhere [78]. It is to be expected that the diffusion of carbon through the nickel lattice will induce a displacement of Ni atoms with defect formation and fragmentation. There was, however, negligible Cl or Si along the length of the fibers; any Cl that is formed (as HC1) must desorb from the catalyst surface without incorporation in the carbon growth.

2.4 Conclusions

A catalytic decomposition of C_6H_5Cl over 10% (w/w) Ni/SiO_2 represents a viable route to structured (<40 nm in diameter) carbon nanofibers where reaction at 923 K delivered a carbon yield of 40 g_C g_{Ni}^{-1} and an associated carbon efficiency of 0.47. The carbon yield from a C_6H_5Cl feed is appreciably greater than that obtained from C_6H_6 while the former delivers a more ordered (graphitic) product, effects that we attribute to charge

transfer/Ni site restructuring due to Cl/catalyst interaction(s). Time-on-stream behavior has revealed a distinct induction period (over the first 0.5 h) wherein carbon production is negligible and this is followed by a period of continual carbon growth up to 4 h on-stream with no significant variation in structural characteristics. Reaction at temperatures in excess of 923 K resulted in lower carbon yields and a greater relative amorphous carbon content which is ascribed to the onset of a thermal (non-catalytic) decomposition of the feed. The pressure exerted on the metal/support interface due to the carbon growth is of sufficient magnitude to extract metal particles from the silica support with the result that individual Ni particles are typically found at the nanofiber tips while there is evidence of an incorporation of Ni fragments dispersed along the growing nanofibers; there was no evidence of any Cl inclusion in the carbon growth.

2.5 Tables and Figures

Table 2.1: Carbon yield (Y_C) and efficiency associated with the catalytic decomposition of benzene and a CB feed over Ni/SiO_2: $\Delta t = 1$ h

T (K)	$Y_C g_C g_{Ni}^{-1}$		Carbon efficiency	
	Benzene Feed	CB Feed	Benzene Feed	CB
873	11	24	0.13	0.29
898	<1	34	<0.1	0.40
923	Trace	40	0.01	0.47

Table 2.2: BET surface areas of the activated catalyst, model carbon samples and selected catalytically grown carbon

Sample/carbon growth conditions	Surface area $(m^2 g^{-1})$
Activated catalyst	190
Amorphous carbon	676
Graphite	7
Catalytically grown carbon	
Benzene feed, $\Delta t = 1h$, T=873 K	229
CB feed, $\Delta t = 1h$, T=873 K	194
CB feed, $\Delta t = 2h$, T=873 K	177
CB feed, $\Delta t = 4h$, T=873 K	179
CB feed, $\Delta t = 1h$, T=883 K	197
CB feed, $\Delta t = 1h$, T=898 K	178
CB feed, $\Delta t = 1h$, T=923 K	191
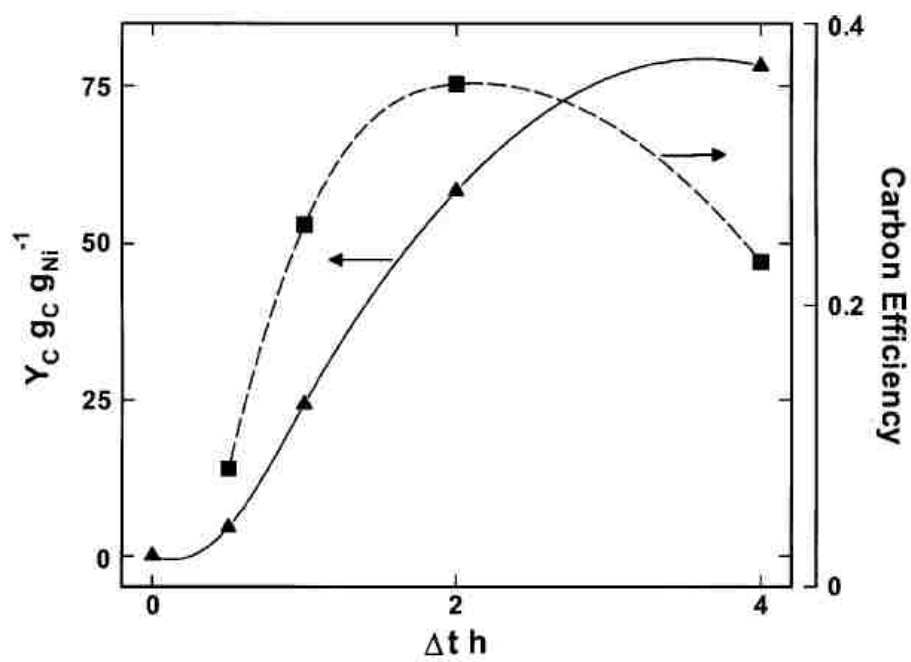
Figure 2.1: Carbon yield (▲, expressed per gram Ni) and carbon efficiency (■) as a function of time-on-stream: T = 873 K.
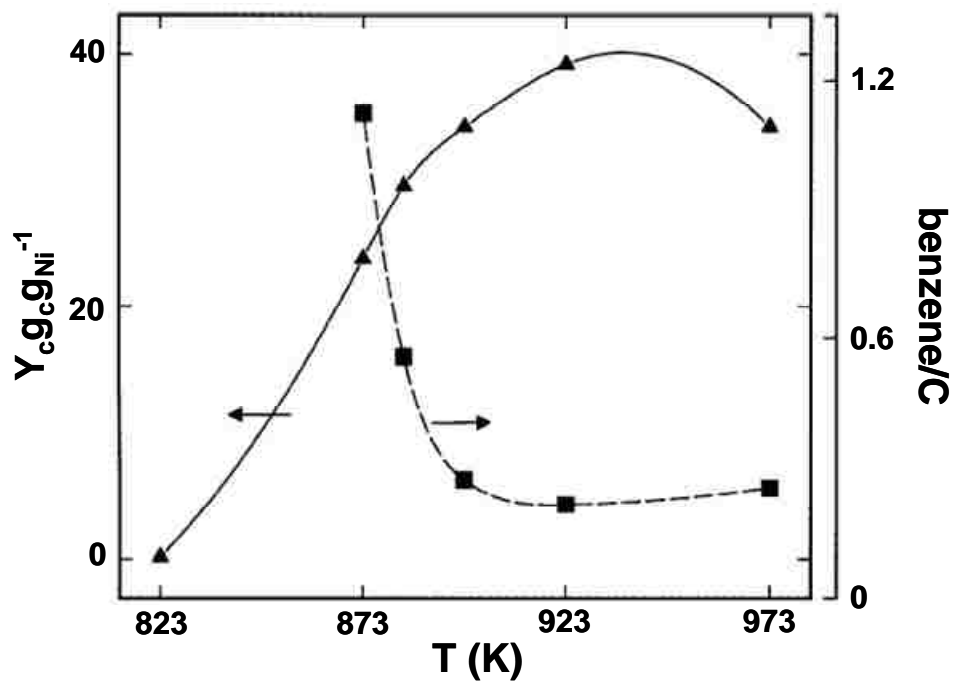
Figure 2.2: Carbon yield (▲, expressed per gram Ni) and the product ratio of carbon in the form of benzene to solid carbon (benzene/C, ■) as a function of reaction temperature: $\Delta t = 1$ h.
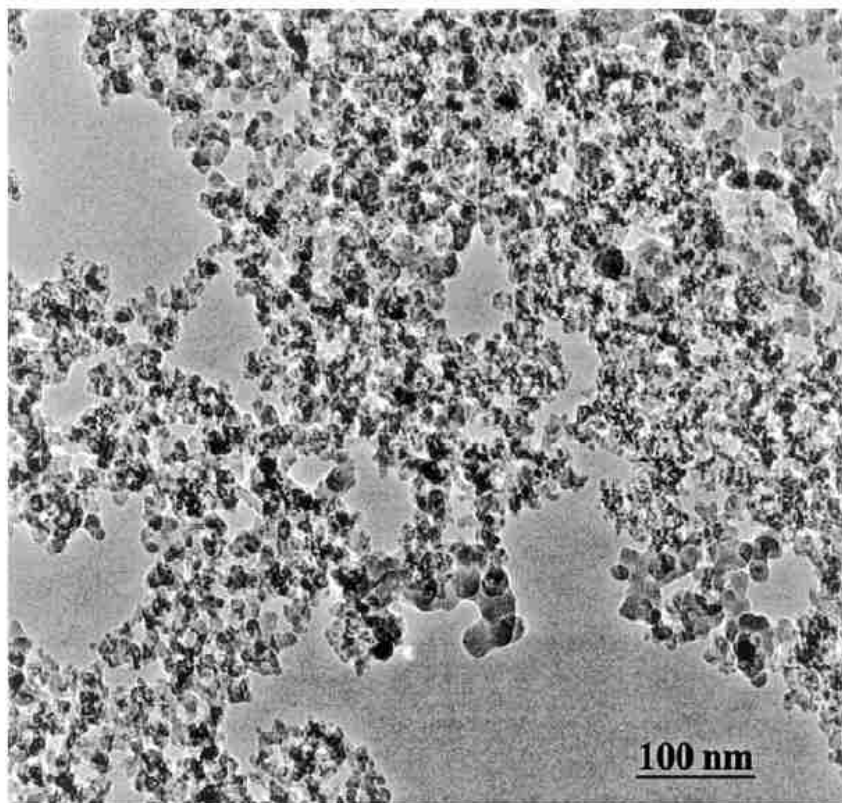
Figure 2.3: Representative low-magnification TEM image of freshly activated Ni/SiO$_2$.
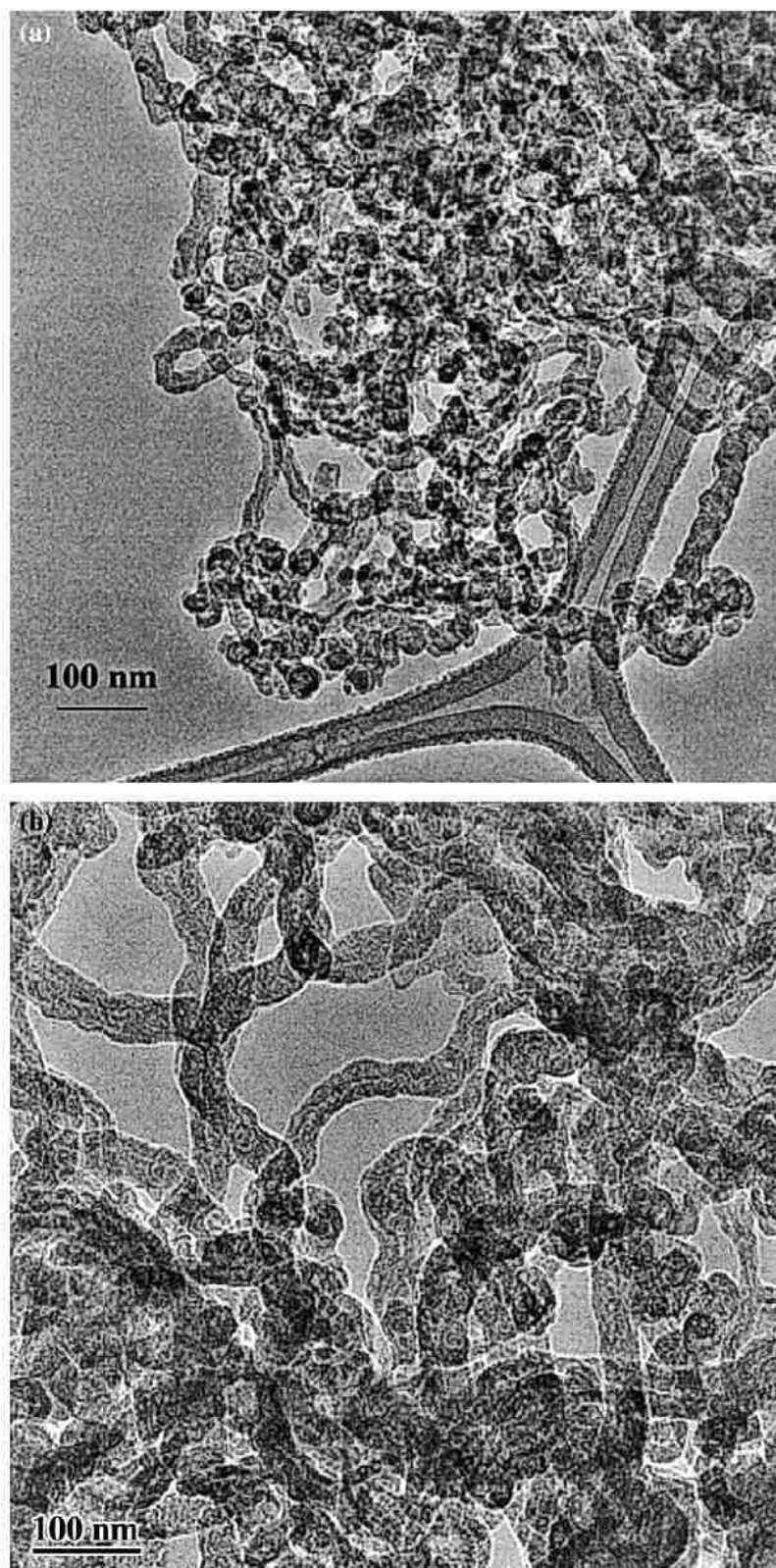
Figure 2.4: Representative low-magnification TEM image of the carbon nanofibers generated from the decomposition of CB over Ni/SiO$_2$.
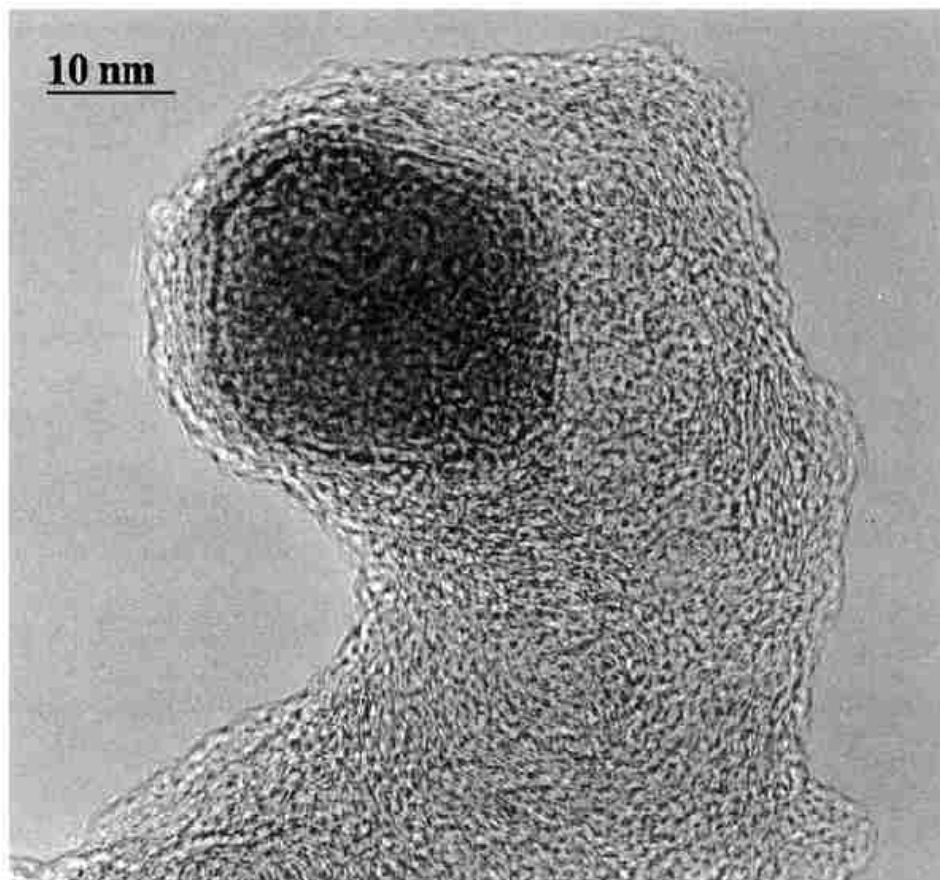
Figure 2.5: Representative TEM image of an isolated carbon nanofiber bearing a Ni particle at the fiber tip.
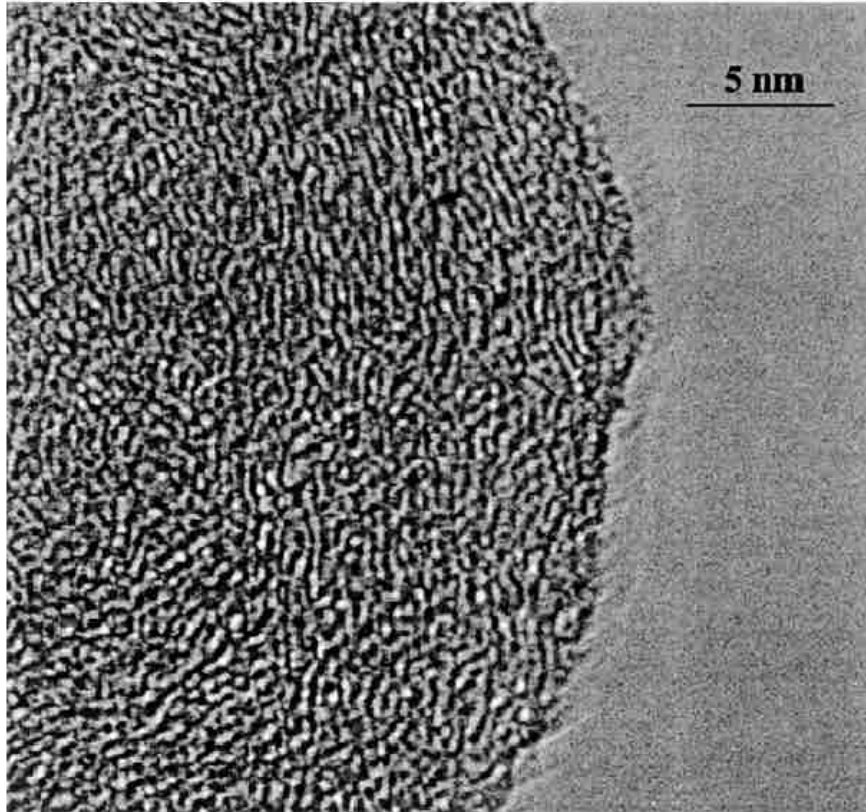
Figure 2.6: Representative HRTEM image of an isolated carbon nanofiber.
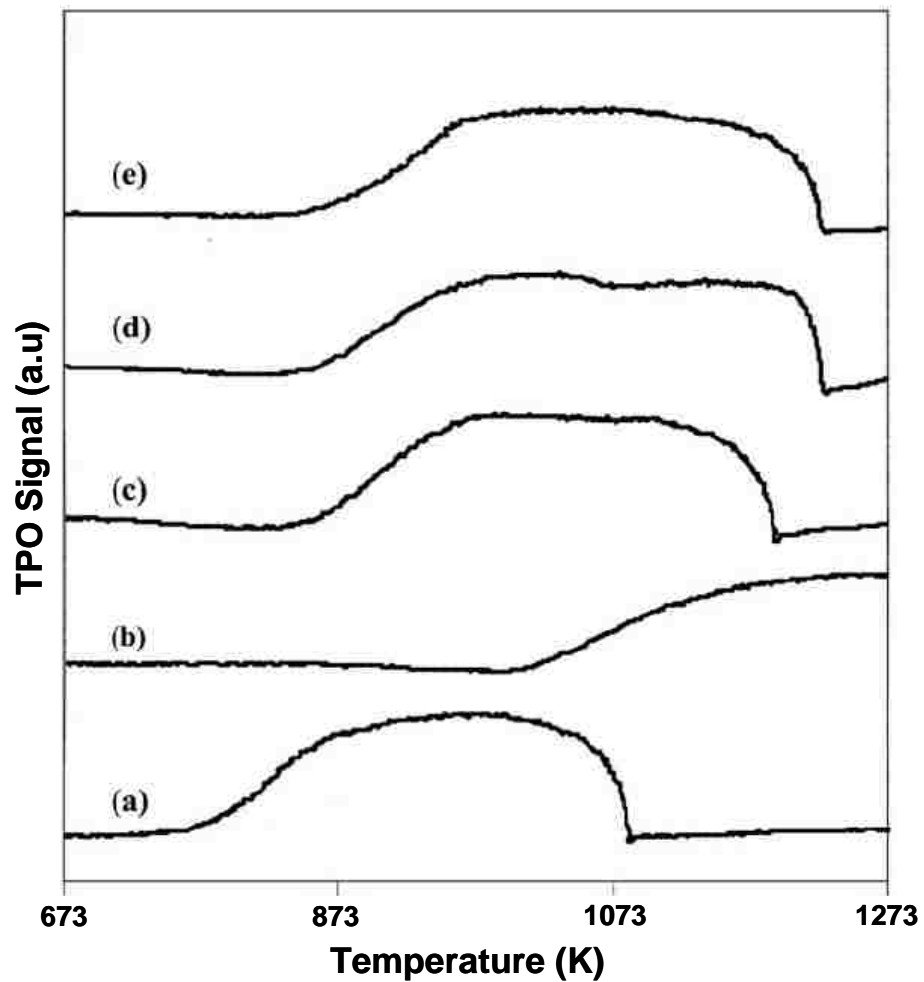
Figure 2.7: TPO profiles for (a) model amorphous carbon, (b) model graphite and carbon generated from the decomposition of CB over Ni/SiO$_2$ at 873 K where (c) $\Delta t = 1$ h, (d) $\Delta t = 2$ h and (e) $\Delta t = 4$ h.
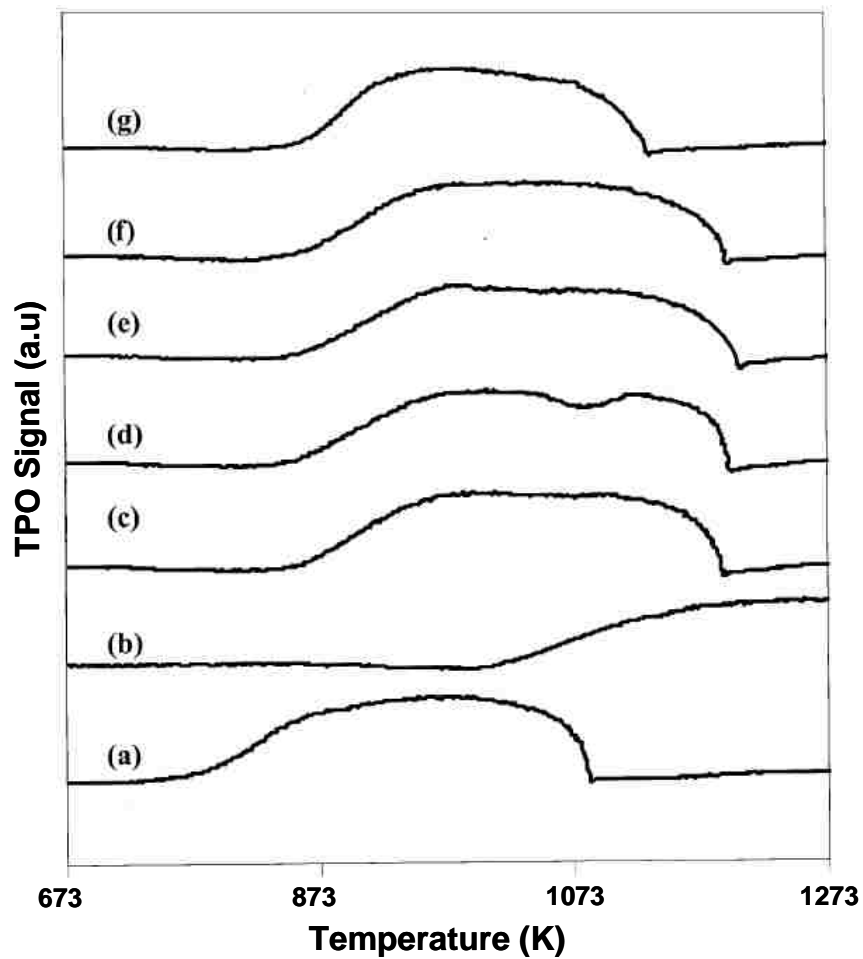
Figure 2.8: TPO profiles for (a) model amorphous carbon, (b) model graphite and carbon generated from the decomposition of CB over Ni/SiO_2 at $\Delta t = 1$ h where (c) T = 873 K, (d) T = 883 K, (e) T = 898 K, (f) T = 923 K and (g) T = 973 K.
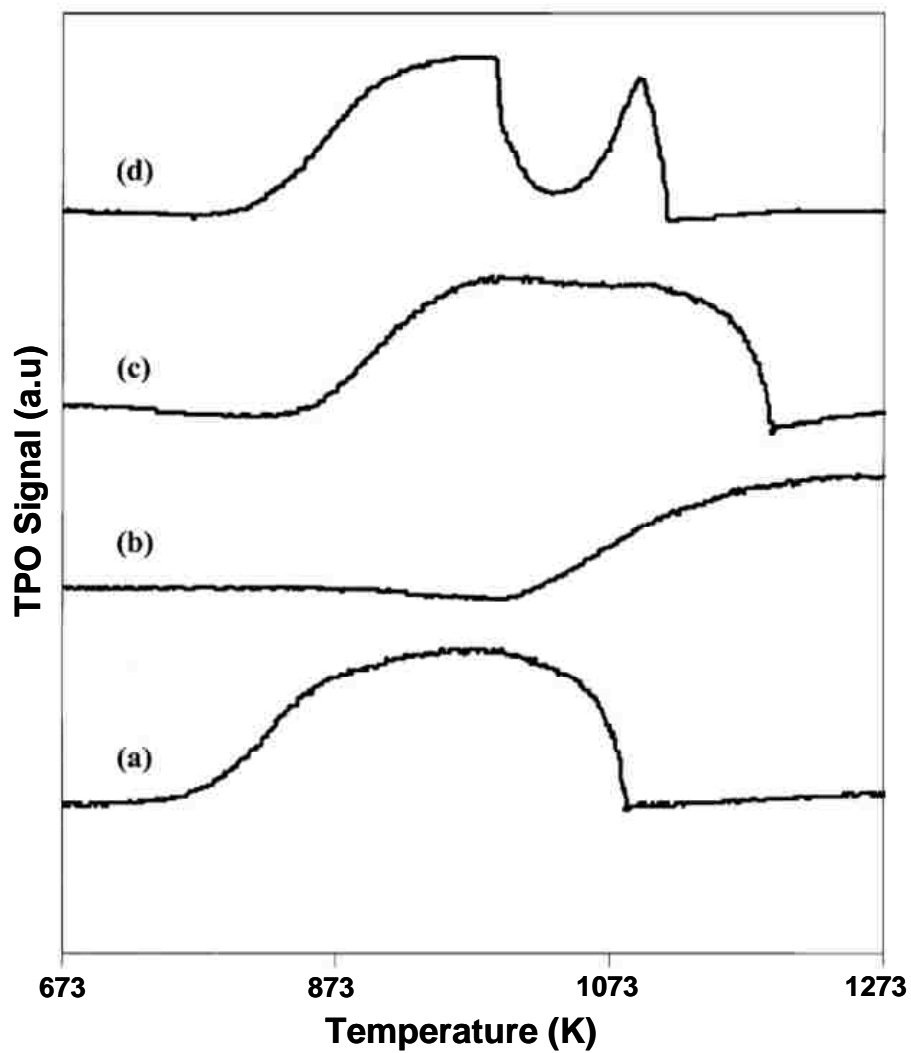
Figure 2.9: TPO profiles for (a) model amorphous carbon, (b) model graphite and carbon generated from the catalytic decomposition (T = 873 K, Δt = 1 h) of (c) CB and (d) benzene.
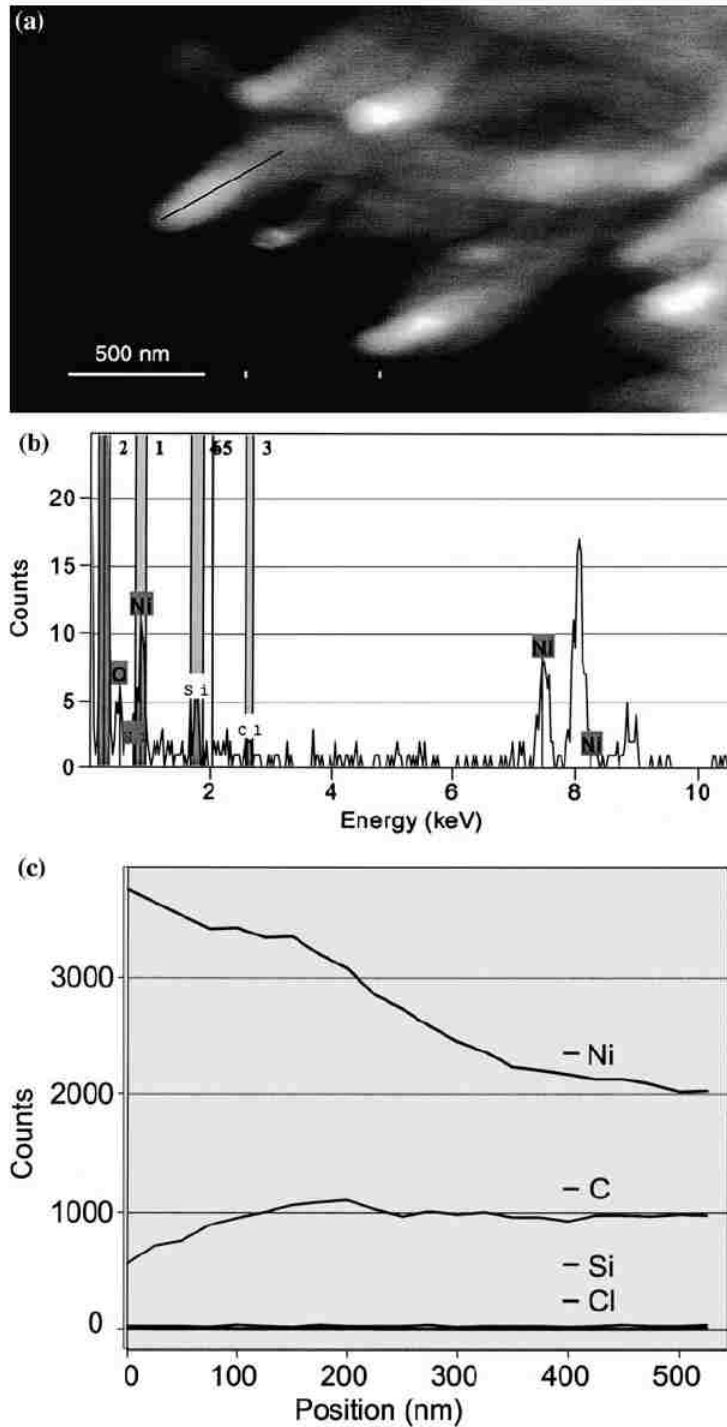
Figure 2.10: STEM/EDX elemental maps of an individual carbon nanofiber generated from the decomposition of CB over Ni/SiO$_2$ showing (a) STEM annular dark field image of the catalyst exhibiting growth of a number of individual carbon nanofibers with the 500 nm segment of nanofiber that was mapped, (b) EDX spectrum over the entire 500 nm carbon nanofiber mapping and (c) elemental map (Ni, C, Cl and Si) showing distribution along the length of the nanofiber beginning at the tip.

38

Chapter 3: Role of Carbon Precursor in Determining Solid Carbon Yield and Structure

3.1 Introduction

Carbon growth over Ni, has been recorded for bulk Ni [1, 2] and Ni supported on Al_2O_3 [3], SiO_2 [3-6], Ta_2O_5 [7], TiO_2 [3], activated carbon (AC) [3], graphite (G) [3] and MgO [8] and over Ni/Fe [9] and Ni/Cu [2] powders. Moreover, growth of structured carbon from such carbon sources as CO [10], acetonitrile [11], methane [12, 13], 1-butene [14], butadiene [15], acetylene [16], ethylene [9, 14, 17-19], 1,3-butadiene [9, 20], ethylene di-amine [21], n-hexane [22], pentane [23], cyclohexane [24] as well as aromatic compounds such as benzene [25-30], toluene [28, 30] and xylene [30, 31] has been recorded and characterized. Differences in the quantity and quality of the carbon product obtained with variation in carbon precursor has been noted in several studies [32-34]. Li *et al* [35] compared the growth of structured carbon from precursors such as hexane, cyclohexane, benzene, anthracene and naphthalene using Fe/MgO over the temperature range 823 − 1073 K in an Ar atmosphere and reported that conjugated sp^2 structures (benzene, anthracene and naphthalene) favor formation of "high quality" SWNTs whereas aliphatic compounds (hexane and cyclohexane) generate MWNTs and flake-like impurities, suggesting a dependence of product structure on structure of carbon precursor used. However, no quantitative analysis in terms of C yield or solid C formation was provided [35].

The impetus for the work described herein was provided by an earlier study (Chapter 2) where we observed substantial growth of structured carbon *via* decomposition of CB and benzene in H_2 atmosphere over 10% (w/w) Ni/SiO_2 at 873 K. Introduction of aromatics (benzene and CB) in a flow of He did not generate any

measurable carbon growth from the activated (reduced in H_2) catalyst indicating that H_2 was a crucial reactant component in this system. However, the role of H_2 was not conclusively established. Greater C yield obtained from CB than benzene was discussed in terms of substituent (Cl)/catalyst interaction(s) and metal site restructuring (Chapter 2). In this study, the role of H_2 on CB decomposition and C yield is explored by considering the effect of % (v/v) H_2 using He as the dillutant. Furthermore, in order to gain a better understanding of substituent/catalyst interaction on C growth characteristics, the effect of electron withdrawing (F, Br and I) and electron donating (-CH_3) groups on benzene ring is evaluated using such reactants as fluorobenzene (FB), bromobenzene (BB) iodobenzene (IB) and toluene respectively. A detailed study of the growth of structured carbon from reactants bearing different electron withdrawing and donating substituent groups has not, to the best of our knowledge, been published. Moreover, carbon yield/conversion/selectivity from 1, 3 - dichlorobenzene (DCB), 3-chlorobromobenzene (3-CBB) and xylene is considered to assess the effect on carbon growth due to presence of a second electron withdrawing/donating substituent. To understand the role of Br clearly, physical mixture of CB and BB in the ratio of 1:1 (CB + BB) has been used. Carbon growth response from 3-chlorotoluene (CT) was investigated to concretely understand the role of Cl substituent in aromatic compounds. Cyclohexane, cyclohexene and hexane were examined to evaluate C growth characteristics in aliphatic compounds. Furthermore, cyclohexyl chloride and chlorohexane (CH) have been considered to study the possible generic effect due to the Cl substituent on cyclic and straight chained compounds, respectively. The results are evaluated in conjunction with those obtained for benzene and CB and recorded in

Chapter 2. Finally, the effect of %(v/v) H_2 on C yield is explored by subjecting all the reactants considered to the optimum %(v/v) H_2 established for C growth from CB.

3.2 Experimental Procedure

The Ni/SiO$_2$ catalyst was prepared by standard incipient wetness technique where the silica support (Aldrich fumed silica, surface area = 200m^2 g^{-1}) was impregnated with 2-butanolic solution of Ni (NO$_3$)$_2$ to yield a 10% (w/w) Ni loading. The Ni content of the catalyst was determined by inductively coupled plasma - optical emission spectrometry (ICP-OES, Vista PRO, Varian Inc) from the diluted extract of aqua regia. The catalyst precursor was sieved into a batch of 100 μm average diameter, loaded into a fixed bed tubular quartz reactor (i.d. = 1.25 cm) and activated by heating at 10 K min^{-1} in a stream of dry H_2 to the reaction temperature (873 K) and maintained at that temperature for at least 12 h. Gas flow rates to the reactor were regulated by mass flow controllers (MKS instruments), and the total gas flow rate in all experiments was maintained constant at 60 cm^3 min^{-1}. A Model 100 (kd scientific) microprocessor – controlled infusion pump was used to deliver the feed at a fixed calibrated rate *via* a glass/teflon airtight syringe and teflon line. The inlet hourly of C/Ni molar ratio was maintained at 69.4 with a constant GHSV of 4 × 10^3. The reaction temperature was monitored continuously by means of a thermocouple inserted in the catalyst bed. A layer of quartz wool was placed in a preheating zone above the catalyst bed to ensure that the reactants were vaporized and reached the reaction temperature before contacting the catalyst. The reactant effluent was frozen in a liquid nitrogen trap for subsequent analysis which was made using the Perkin - Elmer Auto system XL Chromatograph equipped with a split/split less flame ionization detector employing DB - 1 50 m x 0.20

mm i.d., 0.33 μm capillary column (J& W Scientific): overall analytic repeatability of the effluent products was within $\pm 5\%$. The gravimetric yield of carbon was determined from the catalyst bed mass differential pre- and post-reaction. The reactants/carbon sources used were benzene (99.9%), toluene (99.9%), xylene (99.9%), FB (99.9%), CB (99.9%), BB (99.9%), IB (99.9%), CT (99.9%), DCB (99.9%), 3-CBB (99.9%), cyclohexane (99.9%), cyclohexene (99.9%), cyclohexylchloride (99.9%), hexane (99.9%) and CH (95.9%). Based on the known carbon inlet, gravimetric yield of solid carbon and chromatographic analysis of reactor fluent, carbon balance was calculated using 2-octanol/toluene as internal standard. Carbon balance measurements revealed formation of volatiles that were not isolated in the liquid trap, which result from additional hydrogenolysis/hydrocracking reactions and accounted for up to approximately ca. 57 mol l% conversion of the feed. Each catalytic run was repeated up to six times (with a minimum of 3 repetitions) and the catalytic data quoted in this paper represent average values. The solid carbon gravimetric yield was reproducible to within $\pm 10\%$. In the absence of the catalyst, passage through an empty reactor, did not result in any measurable carbon growth.

The BET surface areas and TPO characteristics of the carbonaceous product were determined using the commercial CHEMBET 3000 (Quantachrome Instrument) unit. After outgas at 523 K for 30 min, at least two cycles of nitrogen adsorption – desorption in the flow mode were employed to determine total surface area using the standard single-point BET method. TPO profiles of the catalytically generated carbon were obtained from thoroughly washed, demineralized (in HNO_3) samples to avoid any contribution due to the catalyzed gasification of carbon by residual Ni [80]. A known

mass of the demineralized sample was heated from room temperature to 1273 K at 8 K min^{-1} in a 5% (v/v) O_2/He mixture with online TCD analysis of the exhaust gas. These profiles were assessed against those generated for model activated carbon and graphite samples (Sigma-Aldrich).

3.3 Results and Discussion

3.3.1 Carbon Growth: Influence of Hydrogen Content

There is ample evidence in literature to show that growth of structured carbon is influenced by the nature of the carrier gas, which has included N_2 [32, 37-41], He [37-39, 41], Ar [37-39, 41], H_2 [11, 32, 33, 35, 41-43] and NH_3 [32, 40]. Hydrogen has been identified as a critical component in the growth of structured C and is proposed to initiate hydrocarbon decomposition [9, 16, 44-55] while influencing the structure of the carbon product [56, 57]. Owens *et al* [33] have shown that H_2 is essential for C growth which is borne out in Figure 3.1, wherein limited conversion (Figure 3.1(A)) and zero C yield (Figure 3.1(B)) were observed in the absence of H_2. Reaction of CB generated benzene as the sole condensable byproduct. Reaction selectivity to C was certainly sensitive to H_2 content with an apparent selectivity maximum (within experimental error) at 40% (v/v) H_2 (Figure 3.1(C)). Further increase resulted in decrease of C yield. Such a %(v/v) H_2 related maximum has been noted elsewhere [33, 52, 58] and the optimum %(v/v) H_2 was reported to be strongly dependent on the nature of the catalyst and the feedstock. Carbon generation from CB was increasingly favored over benzene production up to 40% (v/v) H_2 as can be assessed from the product carbon to benzene ratios (C/benzene) plotted in Figure 3.1(D); decomposition was preferred over hydrodechlorination. Thereafter decline in C/benzene with further increase was noted.

Increase in the hydrogen content may have resulted in reconstruction of the metal particles where carbon production was less favored, a result shown elsewhere too [7, 19, 34].

3.3.2 Carbon Growth: Influence of Carbon Precursor/Reactant

Reaction of monohaloarenes (as FB, CB, BB and IB) generated benzene as the sole condensable liquid byproduct (see Table 3.1). The C-X (X= F, Cl, Br and I) bond dissociation energy values quoted in Table 3.2 [59] indicate that C-X bond cleavage among monohaloarenes should follow the order: IB > BB > CB > FB, a trend that has been found to hold good in the case of liquid phase dehalogenation of alkyl halides [32, 40], aliphatic halides [41] and dehalogenation of haloarenes [60, 61]. However, on the basis of selectivity to benzene, the observed dehalogenation trend is: IB > CB > BB > FB (see Table 3.1). Assessment of the level of C growth from benzene feed with that from monohaloarenes on the basis of C efficiency and C yield points out (from Table 3.1) that, while the degree of carbon deposition from FB and CB (under identical conditions) is substantially greater than that from benzene (with that from CB > FB), BB and IB are not sources of solid C. Though the (overall) conversion of BB and IB is greater/equivalent to benzene, no C yield was observed from either of the reactants (BB and IB). Given the equivalency of growth conditions, the enhancement/reduction in carbon yield must be associated with the nature of the halogen substituent. The results indicate that while the presence strong electronegative halogen substituents (F and Cl) on the aromatic ring favors C production, weakly electronegative substituents (as in Br and I) favor side reactions such as dehalogenation (to benzene) and decomposition (to volatiles) (Table 3.1).

It has been established previously [62, 63] that Ni/SiO$_2$ bears a significantly

surface HX (X=Cl, Br) during haloarene (CB and BB) hydrodehalogenation, where the

irreversibly held halogen component is built into the surface sub layers of the Ni

particles. In our previous communication (Chapter 2), enhanced decomposition of CB

relative to benzene was attributed to the presence of a residual Cl component on the

catalyst which induces electronic perturbations through reduction in d-electron density

of the surface Ni metal causing strengthening of the interaction with incoming reactant,

weakening the C-C bonds in the adsorbed aromatic favoring reactant decomposition.

We have further published (Chapter 2) evidence to suggest that the ''irreversibly'' held

halogen component allied to the faceting/restructuring may serve to facilitate carbon

diffusion and precipitation elevating the overall carbon growth. A plausible reason for

the varying reactivity and C yield observed among monohaloarenes in this study could

be that while interaction of the catalyst with strong electronegative compounds as in F

and Cl in the held HX (X = F, Cl) causes restructuring of the catalyst by creating

exposed faces favoring dissociative/destructive chemisorption with concomitant carbon

diffusion/precipitation causing substantial C yield, interaction with weak

electronegative substituents as Br and I (in HBr / HI) does not result in structural

changes to the supported metal and the more facile dehalogenation is promoted. It is

very important to note here that based on our previous studies [64, 65] and present

experimental data results, while reconstruction of the catalyst is proposed as a cause of

the observed variation, there is no demonstrable evidence (except in the case of CB

(Chapter 2)) for this effect. Such evidence should be the subject for future work.

The effect of a second electron withdrawing group was considered by examining the transformation of DCB and 3-CBB. Overall conversion of DCB was significantly less than that associated with CB. Furthermore, lower C yield was recorded from DCB than CB. The presence of a second electron withdrawing group apparently has an overall deactivating effect, resulting in a lower conversion of DCB compared with CB, a result shown elsewhere [64]. This lower conversion of DCB, perhaps translates into relatively lower C yield (than CB). Benzene and CB were the condensable byproducts obtained on hydrodechlorination of DCB. Selectivity to benzene was significantly less than that from CB indicating a stepwise hydrodechlorination. It is interesting to note that, increase in Cl content (in DCB relative to CB) of the feed increased the hydrocracking reactions i.e. a significant increase in selectivity to volatiles. Furthermore, the combined selectivity of DCB to benzene and CB is significantly less than the selectivity to benzene using CB as reactant. Chambers *et al* [58], studying the effect of Cl on growth of structured C from ethylene/hydrogen mixtures on Co catalyst at 673 K, reported an increase in growth of solid C with increase in Cl_2 gas feed up to 75 ppm; thereafter a steady decline with further increase (up to 200 ppm) was noted indicating that there exists an optimum amount of Cl that enhances solid C formation. In addition, increase in methane formation with increase in Cl content (in gas feed) was recorded. The increase in solid C production was attributed to reconstruction of the catalyst induced through Cl interactions which favored (solid) C formation. In the present study, greater C yield from CB and DCB than benzene indicates that presence of Cl enhances C yield formation. However, lower C yield and higher selectivity to hydrocracking reactions in DCB relative to CB with the latter exhibiting reduced

46

(negligible) selectivity to hydrocracking reactions and greater C yield than benzene suggests: (1) there exists an optimum Cl amount (in the feed) that delivers maximum C yield, i.e. increase in feed Cl content does not necessitate a proportional increase in C yield, a result analogous to that stated in [58]; (2) variation in Cl content of the feed causes significant variations in the (%) selectivity to C (solid) and side reactions. Significant C yield observed in DCB contrary to that observed in BB and IB further establishes that presence of Cl on the aromatic ring benzene enhances C yield.

A relatively lower conversion was observed in the case of 3-CBB than CB, BB and DCB. While lower conversion of 3-CBB [62] than CB and BB can be attributed to presence of a second electron withdrawing group as in the case of DCB, lower conversion than DCB could be due to the nature of the second halogen substituent Br which has been shown in this work to reduce the overall conversion. Benzene, CB and BB were the liquid by products obtained; no C yield was recorded. Greater debromination than dechlorination was recorded contrary to what would be predicted based on the conversions of CB and BB in single component systems. To understand the role of Br clearly, CB + BB has been used as reactant. Conversion of BB exceeded that of CB where, the physical mixture did not yield any solid C. A similar trend had been reported elsewhere [62] in hydrodehalogenation of CBB and CB + BB mixture wherein, an observed enhanced debromination and BB conversion in CBB and CB + BB, respectively, was attributed to occurrence of an exchange reaction in which the debrominated intermediate is subsequently chlorinated by surface HCl. In the present set of experiments, the observed greater debromination in 3-CBB and higher BB conversion in CB + BB suggests the occurrence of a halogen exchange reaction.

47

However, greater BB conversion observed in CB + BB should not result in the observed zero/negligible C yield. At this juncture, it is proposed that reactant/catalyst interactions result in some "surface reconstruction" where dehalogenation (to benzene) and cracking (to volatiles) is preferred. A similar mechanism is proposed for 3-CBB as reactant but further work is required to establish this effect.

The role of aromatic substitution was further investigated by examining the action of toluene and xylene, i.e. methyl substitution. Reaction of toluene generated benzene as the sole condensable byproduct. Reactivity/overall conversion of xylene was negligible (<10%). Unlike benzene, both toluene and xylene did not yield C. Limited selectivity to benzene from toluene with negligible/zero C yield indicate that toluene favors decomposition to volatiles, which do not undergo any further reaction (to yield solid C). Hernadi et al [47] have reported an insignificant carbon yield from toluene over Co/SiO_2 in the temperature range of 973–1173 K which was attributed to low conversion. However, neither comparison with benzene nor possible decomposition routes were discussed. Recently Das et al [30] reported C yields from benzene, toluene and xylene to increase in the order benzene < xylene < toluene when using ferrocene as a combined carbon and catalyst (Fe) source at 948 K. No concrete explanation for the observed variation was given but a need for a detailed thermodynamic and kinetic study was expressed. In another study, Hernadi et al [66] observed lower conversion and C yield from methyl acetylene than acetylene on mono(Co or Fe) and bimetallic (Fe,Co or Ni,V) catalysts at 993 K, which they attributed to varying structural effects and hydrogen transport difficulties due to presence of the methyl group. The results in this paper indicate that the presence of methyl group(s) on the benzene ring does not

promote formation of solid C. Further study is required to concretely comment on the observed phenomenon. It is interesting to note that Cl substitution of toluene renders it more reactive than toluene (greater overall conversion). Benzene and toluene were the liquid byproducts obtained from CT while C yield was higher than that recorded for toluene. The trend with respect to toluene and CT is similar to that observed for benzene/ CB in that the presence of Cl on the ring renders the ring more reactive and a greater source of solid C. Further, greater C yield from DCB relative to CT with the latter exhibiting relatively greater selectivity to side reactions further establishes that presence of $-CH_3$ group on the ring promotes selectivity to competing reactions to C yield.

The conversion, C yield and (%) selectivities associated with cyclic compounds are shown in Table 3.1. While cyclohexane and cyclohexene are sources of solid C (though in small amounts), cyclohexyl chloride is not, a trend opposite to that observed in the case of benzene and CB (and toluene/CT), suggesting a deviation in behavior for aromatic and aliphatic feed. Benzene was the only liquid byproduct obtained. Negligible/zero C yield from cyclohexyl chloride and its comparatively greater selectivity to benzene than cyclohexane (~18 times higher) and cyclohexene (~2 times greater) suggests that the presence of Cl in cyclic compounds favors benzene formation. Gheit *et al* [67] in a recent study, reported that at temperatures of 323 - 673 K, relative to Pt/H-ZSM, HCl (3 wt%) doped Pt/H-ZSM favors formation of benzene from cyclohexene. Such an effect was attributed to increase in Pt dispersion and number of acid sites on interaction with HCl. The present study indicates that Cl associated with cyclic compounds enhances formation of benzene. Greater C yield from benzene than

the considered cyclic compounds (cyclohexane, cyclohexene and cyclohexyl chloride) with benzene as their only liquid byproduct suggests that perhaps, growth of solid C (in cyclic compounds occurs) via benzene.

In the case of straight chained compounds, a higher C yield was obtained from chlorohexane relative to hexane; see Table 3.1. Benzene was the only liquid by-product in the case of hexane whereas both hexane and benzene were detected in the effluent in the case of CH. Selectivity to benzene is negligible in the case of both hexane (<1%) and CH (<5%). Overall conversion of CH is less than hexane (by ~5%). However, substantially greater C yield is observed from CH relative to hexane. Comparison of C yields from benzene, hexane and CH indicates that in straight chained compounds, formation of benzene and solid C are mutually exclusive reactions; a trend similar to that reported for CB (Chapter 2). Formation of benzene from cyclic and straight chained compounds has been investigated over a range of unsupported and supported metal catalysts such as Pt [67-76], Pd [76] and Ni [77-80] where the commonly used supports include Al_2O_3 [79] zeolite [67, 72, 73, 76], MgAl(O) [72, 73] and $TiO_2 - ZrO_2$ [81, 82]. Pt has been identified as most efficient catalyst for dehydrogenation/dehydrocyclization of cyclic and straight chained compounds where an increase in the basicity of the support was reported to enhance formation of benzene [72, 73]. However, a support is not a requisite for dehydrocyclization/ dehydrogenation activity as bulk Pt [83, 84] has also been demonstrated as an efficient catalyst. A survey of the literature revealed that the use of Ni for dehydrogenation/dehydrocyclization is limited [78, 85, 86]. The conversion of cyclohexene, cyclohexylchloride, hexane and CH to benzene over supported Ni has, to the best of the author's knowledge, not been reported. At this

juncture, due to non-identification of volatiles, the mechanism of benzene formation from cyclic and straight chained compounds considered here is not feasible. The focus of this study is strictly on growth of structured C and not on the competing side reactions. However, the results obtained definitely point towards possible usage of Ni/SiO$_2$ for dehydrogenation/ dehydrocyclization of cyclic and straight chained compounds.

The above results demonstrate a dependence of C yield on the nature of the C precursor reactant with some variability of the role of Cl as a C deposition promoter. Carbon yields reported in literature are highly dependant on the nature of the catalyst used and reaction conditions maintained. Ermakova *et al* [6, 87] reported C yields up to 384 $g_{CG}g_{Ni}^{-1}$ and 40 $g_{CG}g_{Ni}^{-1}$ in the temperature range 573 - 973 K for the catalytic decomposition of CH$_4$ over Ni/SiO$_2$ and Fe/SiO$_2$. Takenaka *et al* [88] using CH$_4$ on Ni/SiO$_2$ at 773 K recorded C yields up to 491 $g_{CG}g_{Ni}^{-1}$. Park *et al* [44-46, 89, 90] have reported growth of structured C in the range of 2 - 125 $g_{CG}g_{Ni}^{-1}$ for ethylene decomposition using Ni supported catalysts in the temperature range 723 - 873 K. In our previous communication, we reported carbon yields up to 40 $g_{CG}g_{Ni}^{-1}$ for the decomposition of CB on Ni/SiO$_2$ in the temperature range of 823 - 973 K (Chapter 2). The carbon yields obtained in this study fall in the range of values cited above.

3.3.3 Carbon Growth: Influence of Hydrogen Content on Hydrocarbons

Carbon growth from each of the C precursors examined in this study was also measured at a 40 %(v/v) inlet H$_2$ content, *i.e.* optimum growth conditions established for CB (see Figure 3.1); the results are presented in Table 3.3. On comparison of Table 3.3 with Table 3.1, it can be observed that reactivity/overall conversion was equivalent

or lower for the monohaloarenes (CB, FB, BB and IB) on switching from 100 %(v/v) H_2 to 40% (v/v) H_2 with an equivalent/higher selectivity to benzene. A lower %(v/v) H_2 increased C yield from both FB and CB while BB and IB did not generate any measurable C (also the case for 100% (v/v) H_2). With regard to benzene, a decrease in %(v/v) H_2 resulted in significantly higher (overall) conversion/reactivity with relatively greater C yield. In the case of di-haloarenes (DCB and 3–CBB), decrease in %(v/v) H_2 content resulted in a decrease in overall conversion/reactivity but resulted in an increase in C yield from DCB. No significant variation in % selectivity to respective liquid byproducts from DCB (benzene and CB) and 3-CBB (CB, BB and benzene) was observed. Decrease in %(v/v) H_2 served to increase conversions of CB and BB in the CB+BB (mixture) a trend, in contrast to that observed in single component systems of CB and BB. No significant variation in % selectivity to benzene with variation in %(v/v) H_2 (in CB+BB) was observed. Both 3-CBB and CB + BB, did not generate any measurable (solid) C; a trend similar to that observed in 100% (v/v) H_2.

With regard to cyclic compounds, while decrease in %(v/v) H_2 generated greater C yield with a considerable decrease in (overall) conversion of cyclohexane and cyclohexyl chloride, it increased (overall) conversion with no significant difference in C yield in cyclohexene. Furthermore, a decrease in %(v/v) H_2 generated relatively greater selectivity to benzene in cyclohexyl chloride, a trend in contrast to that observed in cyclohexene. No variation in selectivity to benzene in cyclohexane with variation in %(v/v) H_2 was observed. In straight chained compounds, while decrease in %(v/v) H_2 content increased C yield and decreased (overall) conversion/reactivity, it did not cause significant variation in selectivity to liquid by products.

Limited literature is available wherein the effect of %(v/v) H_2 on growth of structured C over a range of reactants has been investigated [33, 35]. Owens *et al* observed increase in C yield with increase in the fraction of H_2 in the gas feed for both ethylene and acetylene decomposition (809 K) over Pt black catalyst where the effect was reported to be more pronounced with acetylene than ethylene [33]. Such an effect was attributed to the varying wetting characteristics of the reactants with respect to graphite resulting in a significant response to changes in %(v/v) H_2. Park *et al* [52] reported that with a Fe–Ni (2: 8) bimetallic catalyst, while the conversion of ethylene to solid C goes through a maximum at 33% H_2 at 873 K, for CO [9] over Fe: Ni [4:6/6:4] catalyst, C yield was maximum between 20 - 30% H_2 indicating that the effect of %H_2 is significantly dependant on the nature of precursor and catalyst used. Li *et al* [35], in their study of growth of structured C grown from benzene, cyclohexane and hexane, observed that the effect of H_2 varied significantly with the precursor in that, while injection of H_2 enhanced formation of SWNTs from cyclohexane, it caused severe reduction in the purity of the SWNTs generated from benzene. It was postulated that for aliphatic compounds, excess H_2 may hinder decomposition at high temperatures while, in the case of aromatic compounds, the possible catalytic hydrogenation can compete with carbon deposition. However, no quantitative analysis were provided. The results obtained in this study reveal that the effect on (overall) conversion, C yield and selectivity to side reactions (liquid byproducts and volatiles) produced with variation in %(v/v) H_2 varies with the nature of the carbon precursor, a result shown elsewhere [9, 33, 52]. C yield, the focus of this study increased with decrease in %(v/v) H_2 for the conversion of benzene, CB, FB, DCB, cyclohexane, cyclohexyl chloride, hexane and

CH. However, in the case of BB, IB, toluene, CT, xylene, 3 - CBB, CB + BB and cyclohexene, decrease in H_2 content did not affect the C yield. A conclusive explanation for this effect is beyond the scope of this study and should be the subject of future work.

3.3.4 Catalyst/Carbon Characterization

The BET surface areas of activated Ni/SiO_2, model graphite and activated carbon along with catalytically generated solid C obtained from CB at varying %(v/v) H_2 are given in Table 3.4. BET surface areas of solid carbon grown in both 100% (v/v) H_2 and optimized 40% (v/v) H_2 from various carbon sources that are substantial source of solid C are quoted in Table 3.5. The BET surface areas of the carbon grown in varying %(v/v) H_2 and from varying carbon sources fall within that of high surface area model amorphous carbon and low surface area graphite. While the BET surface areas did vary with %(v/v) H_2 and carbon source, no obvious surface area trend is observed. On comparison of BET surface areas of C grown from varying carbon sources (Table 3.5), smaller surface area of C grown from cyclohexane (in 40%(v/v) H_2) and CT (in 100% (v/v) H_2) and greater surface area of C from FB (in 100% (v/v) H_2) is observed, indicative of comparatively lesser and greater porosity of the C grown respectively. These variations could also arise due to differences in fiber diameter and possible contribution from amorphous carbon component. The BET surface areas obtained in this study are in agreement with those quoted in literature for structured carbon [91-94]

The structural order of the carbonaceous deposit, that is, amorphous and/or graphitic was determined using TPO. The TPO profiles of carbon grown in varying %(v/v) H_2 atmospheres are assessed against the profiles associated with model activated carbon and graphite in Figure 3.2; the T_{max} values of which are tabulated in Table 3.4.

The profiles fall between that of standard activated carbon and model graphite, suggesting that the C growth is structured in nature but not graphitic. Furthermore, the TPO profiles are broad indicative of a range of carbon structures with both an amorphous and a graphitic component. Several studies [33, 52] that examined the role of H_2 in determining the structure of the carbonaceous deposit reported that C grown in relatively higher concentrations of H_2 exhibited greater degree of structural order. The presence of added hydrogen was reported to induce reconstruction of the metal particle surfaces to generate set of faces that favored the precipitation of carbon in the form of graphite [33, 52]. However, in this study except for growth in 75% (v/v) H_2 where comparatively less ordered/amorphous C was generated, TPO characteristics (Table 3.4 and Figure 3.2) did not vary significantly with %(v/v) H_2. Further, the TPO profile of C deposit in 75% (v/v) H_2 is relatively narrower than others indicative of presence of a lesser range of carbonaceous products. Apparently, reconstruction of catalyst surface in 75% (v/v) H_2 is promoting growth of amorphous C.

TPO profiles of C grown from various C sources which are a significant source of solid C in both 100% (v/v) H_2 and 40% (v/v) H_2 atmosphere are shown in Figure 3.3. The TPO T_{max} values are quoted in Table 3.5. The TPO profile for carbon generated from benzene in 100% (v/v) H_2 possesses two peaks, indicative of two stages of oxidation, the low temperature broader peak corresponding to that associated with the model activated carbon and a sharper peak at a higher temperature that is indicative of a more structured component. Comparison of TPO T_{max} values of C grown from FB and CB with benzene (in both 40% (v/v) H_2 and 100% (v/v) H_2) reveals that C grown from CB and FB is relatively more structured than benzene signifying that presence of

strong electron withdrawing groups (as F and Cl) enhances formation of structured C. However, increase in the Cl content of the feed in DCB relative to CB reduced the degree the crystalline order of the C deposit. Further, the C deposit from DCB exhibits lesser degree of structural order than benzene also. Chambers *et al* [58] in their study on influence of Cl on ethylene/hydrogen mixture over Co catalysts at 673 K while, recorded an optimum Cl content for C yield, have reported an increase in the degree of crystalline order of the carbon product with increase in chlorine (from 0-200 ppm) content. Comment on the observed variation in the structure of C (solid) with variation in Cl content (of the feed) requires further analysis.

By comparison, the TPO T_{max} values of the C deposit from DCB and CT (in both 100% (v/v) H_2 and 40% (v/v) H_2) indicate that the C generated from CT is relatively more amorphous indicating that the presence of a methyl group enhances growth of amorphous C. Comparison of TPO T_{max} values of CH and hexane reveals that C grown from CH is more amorphous than that from hexane signifying that presence of Cl in straight chained compounds enhances growth of amorphous C, a result in contrast to the trend recorded in aromatic benzene and CB. Furthermore, comparison of TPO T_{max} values of C grown in both 100% (v/v) H_2 and 40% (v/v) H_2 for each carbon precursor reveals that C grown in 100% (v/v) H_2 from benzene, DCB and CH exhibits greater degree of crystalline order than that grown from the respective precursors in 40% (v/v) H_2. No significant variation with %(v/v) H_2 is observed in TPO characteristics (Table 3.5 and Table 3.3) of C grown from FB, CB and CT; usage of the term "significant" indicates variation in temperature of > 10 K. While several studies [9, 35, 52] identified variation in the structural charecteristics of the C product with H_2

concentration, only one study conducted by Li *et al* [35] (discussed in section 3.3.3) reported the varying effect of H_2 on structural charecteristics of C product with precursor. However, no detailed analysis was provided. The results obtained in this study indicate that the role of %(v/v) H_2 in determining the structural characteristics of the C product varies with carbon precursor.

By comparison, TPO charecteristics of C grown from benzene, cyclohexane and hexane in 40% (v/v) H_2 reveal no significant differences (see Table 3.5 and Figure 3.3) indicating that the obtained C product is independant of the chemical structure of the precursor/reactant used, a result that is in contrast to that recorded by Li *et al* [35]. However, it is important to note that in this study negligible amount of C yield obtained from cyclohexane and hexane in 100% (v/v) H_2 limited the characterization of the solid C obtained from these reactants in 100% (v/v) H_2. As a result it is difficult to comment explicitly on the role of the chemical structure of the reactant on the structure of C product obtained. From the results obtained in this study it is reasonable to conclude that: (1) presence of strong electron withdrawing groups (as F and Cl) enhances growth of structured C; (2) variation in Cl content of the feed causes significant differences in the structural characteristics of the C deposit; (3) presence of a methyl group enhances growth of amorphous carbon; (4) effect produced on the structure of the C (solid) due to presence of Cl (in the feed) varies in aromatic and aliphatic reactants and (5) effect of %(v/v)H_2 on C structure varies with C source.

3.4 Conclusions

H_2 has been found to be requisite for decomposition of CB over 10% (w/w) Ni/SiO_2 at 873 K. Maximum C yield was observed at a 40% (v/v) H_2 inlet carrier gas

content. C yield has been found to vary with the nature of the benzene ring substituent where FB and CB serve as substantial sources of solid C with no measurable C growth from BB and IB. Effect of Cl varied with the chemical structure of the carbon source in that the presence of Cl promoted C yield in the case of aromatic and straight chained (aliphatic) compounds whereas it promoted formation of benzene in the case of cyclic compounds. Furthermore, while the presence of Cl (in the feed) promoted growth of structured C in aromatic compounds, it favored growth of amorphous C in straight chained compounds. In addition, the effect of varying %(v/v) H_2 on C yield and structure varied with the carbon precursor.

3.5 Tables and Figures

Table 3.1: Experimental data of reactions carried out over 10% (w/w) Ni/SiO$_2$ at 873 K in 100% (v/v) H$_2$ from various carbon sources.

Carbon source	Conversion (%)	Carbon Yield ($Y_c g_c g_{Ni}^{-1}$)	Carbon Efficiency (%)	C/Bz	Selectivity to Benzene (%)	Selectivity to other Liquid by products (%)	Selectivity to side reactions (%) *
Benzene	53	11					83
Toluene	52	~		~	4		100
Xylene	6	~			~		100
FB	87	15	18	49	<1		79
CB	87	24	29	<1	41		64
DCB	75	17	26	4	9	CB 3	60
BB	76	~			31		100
IB	50	~			75		100
3Chlorobromobenzene (CBB)	54	~	~	~	8	CB BB 21 2	100
Physical mixture of chlorobenzene and bromobenzene (CB+BB)	CB BB 23 28	~	~	~	25		100
CT	69	10	10	14	1	Toluene 24	85
Cyclohexane	92	4	5	3	2		95
Cyclohexene	86	3	3	2	18		98
Cyclohexylchloride	86	~	~		35		100
Hexane	53	7	8	41	<1		87
CH	93	11	15	5	3	Hexane 14	84

*Side reactions defined as combined selectivity to liquid byproducts + volatiles

Table 3.2: Bond dissociation energy values between C-X (X= Halogens) [59].

C-X (Carbon -Halogen)	Bond Energies (kJ/mol)
C-F	536
C-Cl	397
C-Br	280
C-I	209

Table 3.3: Experimental data of reactions carried out over 10% (w/w) Ni/SiO$_2$ at 873 K in 40% (v/v) H$_2$ from various carbon sources.

Carbon source	Conversion (%)	Carbon Yield (Y$_c$g$_c$g$_{Ni}$$^{-1}$)	Carbon Efficiency (%)	C/Bz	Selectivity to Benzene (%)	Selectivity to other Liquid by products (%)	Selectivity to side reactions (%) *
Benzene	77	13	15				86
Toluene	35	~			12		100
Xylene	~	~			~		~
FB	80	30	36	296	<1		55
CB	86	31	37	<1	58		58
DCB	68	20	29	7	6	CB 6	54
BB	64	~			49		100
IB	43	~			97		100
3Chlorobromobenzene (CBB)	51	~	~	~	7	CB BB 20 3	100
Physical mixture of chlorobenzene and bromobenzene (CB+BB)	CB BB 32 32	~	~	~	16		100
CT	69	14	14	~	~	Toluene 17	80
Cyclohexane	79	11	13	6	3		83
Cyclohexene	96	3	3	<1	3		96
Cyclohexylchloride	73	4	6	<1	54		91
Hexane	77	12	14	76	<1		83
CH	93	14	18	8	3	Hexane 10	81

*Side reactions defined as combined selectivity to liquid byproducts + volatiles

Table 3.4: BET surface areas and TPO T_{max} values of solid carbon obtained from CB at 873 K under varying %(v/v) H_2 over 10% (w/w) Ni/SiO$_2$.

% (v/v) H_2	Average BET Surface Area (m^2/g)	TPO T_{max} (K)
20	206	1047
40	218	1045
50	209	1050
60	162	1048
75	209	993
100	194	1051
Activated Carbon	676	973
Activated Catalyst	190	
Graphite	7	>1273

Table 3.5: BET surface areas and TPO T_{max} values of solid C obtained from various carbon sources at 873 K in 100% (v/v) H_2 and 40% (v/v) H_2 atmospheres over 10% (w/w) Ni/SiO$_2$.

Carbon source	BET Surface (m^2/g) Area		TPO T_{max}(K)	
	100% (v/v) H_2	40% (v/v) H_2	100% (v/v) H_2	40% (v/v) H_2
Benzene	229	172	1012 (993,1103)	978
FB	274	259	1040	1045
CB	194	219	1051	1040
DCB	213	198	1005	968
CT	135	180	950	958
Cyclohexane		126	~	985
CH	255	225	968	957
Model Activated Carbon	667			973
Model Graphite	7			>1273
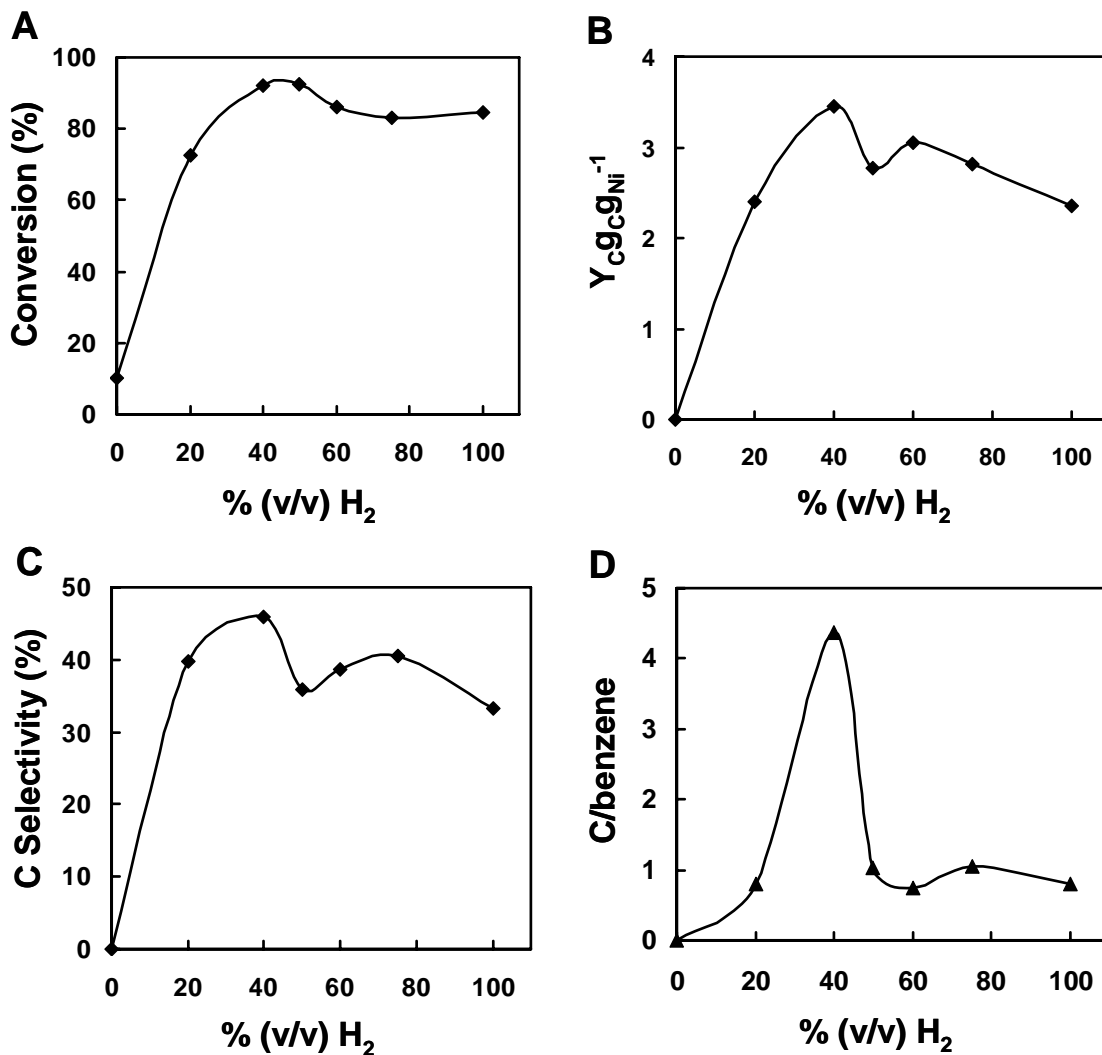
Figure 3.1: (A) Conversion (♦, expressed in %) of CB at 873 K over 10% (w/w) Ni/SiO$_2$ expressed as a function of %(v/v) H$_2$ (B): Carbon Yield (♦, expressed per gram Ni) obtained from catalytic decomposition of CB at 873 K expressed as a function of %(v/v) H$_2$ (C): selectivity to C (♦, expressed in %) of CB at 873 K expressed as a function of %(v/v) H$_2$ and (D): C/benzene (▲, expressed in ratio) of CB at 873 K expressed as a function of %(v/v) H$_2$.
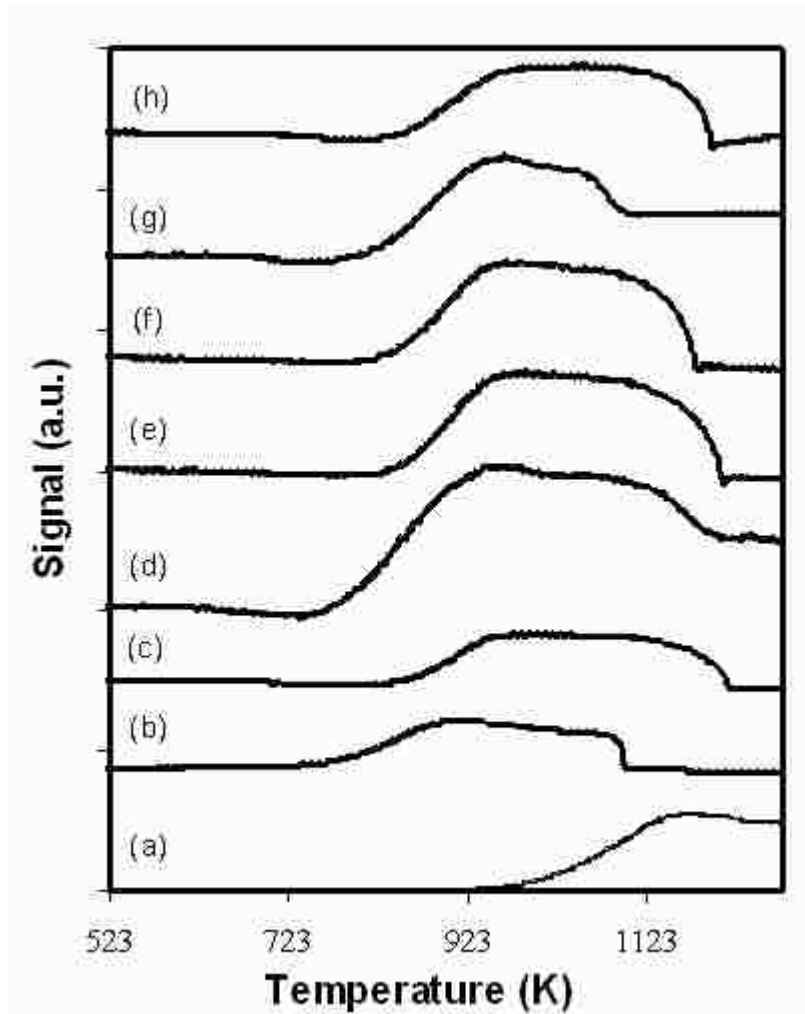
Figure 3.2: TPO profiles for (a) model graphite (b) model amorphous carbon and carbon generated from decomposition of CB over 10% (w/w) Ni/SiO_2 at 873 K at t = 1 h at %(v/v): H_2 (c) 20 (d) 40 (e) 50 (f) 60 (g) 75 (h) 100
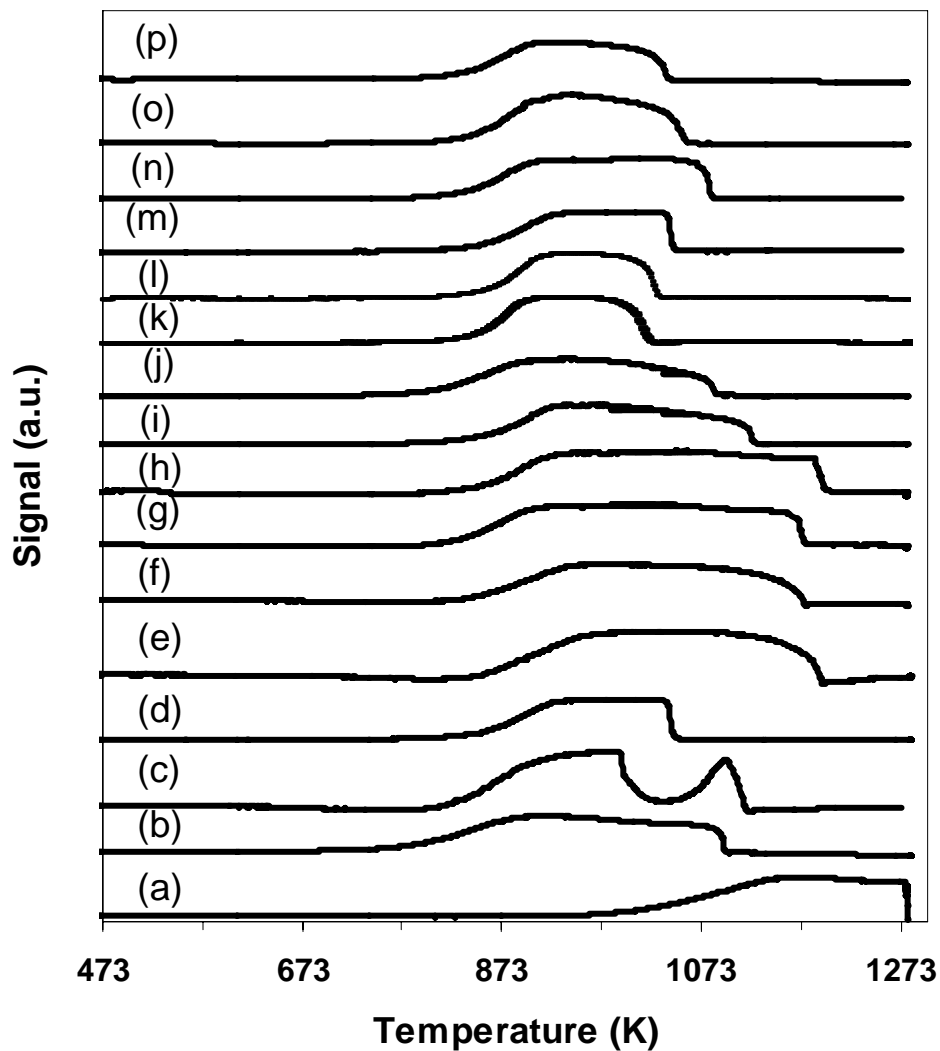
Figure 3.3: TPO profiles for (a) model graphite, (b) model amorphous carbon and carbon generated over 10% (w/w) Ni/SiO$_2$ at 873 K at t = 1h via the decomposition of (c) benzene in 100% (v/v) H$_2$ (d) benzene in 40% (v/v) H$_2$ (e) CB in 100% (v/v) H$_2$ (f) CB in 40% (v/v) H$_2$ (g) FB in 100% (v/v) H$_2$ (h) FB in 40% (v/v) H$_2$ (i) DCB in 100% (v/v) H$_2$ (j) DCB in 40% (v/v) H$_2$ (k) CT in 100% (v/v) H$_2$ (l) CT in 40% (v/v) H$_2$ (m) Cyclohexane in 40% (v/v) H$_2$ (n) Hexane in 40% (v/v) H$_2$ (o) CH in 100% (v/v) H$_2$ (p) CH in 40% (v/v) H$_2$

Chapter 4: Catalyst Support Effects in the Catalytic Growth of Structured Carbon via the Decomposition of CB over Ni

4.1 Introduction

Growth of structured C with a range of C precursors [1-23] has been investigated over a range of unsupported and supported metal catalysts such as Fe [24, 25], Co [25, 26], Ni [24-31] and Pt [32] where the commonly used supports include Al_2O_3 [25, 26, 33], SiO_2 [24-30], Ta_2O_5 [30], TiO_2 [26], activated carbon (AC) [30], graphite (G) [30] and MgO [34]. While the use of bulk metal catalysts facilitates high carbon yields (up to 300 $g_Cg_{metal}^{-1}$) [35-37], it fails to provide control over the diameter of the structured carbon product [38-40]. Use of a support to disperse a chosen metal is not only cost effective but it also serves to influence catalyst performance through electronic interactions, spillover and migration effects [34]. Furthermore, control over the size/diameter of the structured carbon product through adjustment of reaction parameters and/or catalyst (notably metal particle size) [41-43] has also been established. However, use of supported metal catalysts for C growth suffers from two major drawbacks (1) it delivers relatively lower yields (of the order 2 g_C $g_{catalyst}^{-1}$) and (2) problematic removal (or dissolution) of the metal catalyst particles without damage to the carbon product [7, 44-47]. Recently, substantially high C yields have been recorded in various studies [26-28, 48-51] when supported Ni was used as catalyst. Vander Wal *et al* [24] tested copper, iron and nickel on various substrates (as SiO_2, TiO_2, Al_2O_3, CaO, AC and graphite) and reported that Ni/TiO_2 delivered highest nanofiber yield among the twelve systems based on the "density" of the nanofiber coverage. Ermakova *et al* [27-29] and Aveeda *et al* [49, 50] have recorded carbon yields of 384 $g_{CG_{Ni}}^{-1}$ and 250 $g_{CG_{Ni}}^{-1}$, respectively (similar to that obtained from bulk metals),

using impregnated Ni/SiO_2 and Ni/Al_2O_3 with CH_4 as C precursor. More recently, Takenaka *et al* [52] using Ni/SiO_2 have recorded high carbon yields (up to $491g_C\ g_{Ni}^{-1}$) when using CH_4 as carbon source. Removal of the metal catalyst particle and dissolution of the substrate by repeated acidic solution treatment with HNO_3 or HF has also been recorded [53]. Variation in both quality [25, 26, 30, 31] and quantity [24, 27-31, 33, 52] of the carbon product due to differences in the metal catalyst [24, 25] and support [24-26, 30, 52, 54] used has been recorded. Dependence of carbon yield on metal catalyst particle size [26, 30, 31] and source/precursor gas [31, 54] has also been observed. Furthermore, there is substantial evidence to the effect that the lattice orientations/dimensions of the carbon product are governed by the electronic structure/dimensions of the catalyst metal particle [38].

The previous investigation on growth of structured C from varying C sources (Chapter 3) via catalytic decomposition over 10% (w/w) Ni/SiO_2 at 873 K revealed that C yield from CB was substantially greater than from other precursors considered. Furthermore, the C grown from CB was relatively more structured than that obtained from other precursors, with the exception of FB which exhibited structural characteristics equivalent to CB. In this chapter, the role of Ni/support interaction(s) is examined for the catalytic decomposition of CB at 873 K with a common 10% (w/w) Ni loading associated with an array of substrates such as Al_2O_3, Ta_2O_5, NaY, graphite and activated carbon (AC). Graphite [35], is a known electrical conductor having a well defined structure with high degree of crystallinity, while Al_2O_3 is a conventional refractory amorphous oxide that is known to act as an insulator. AC exhibits a high surface area with little or no metal support interaction; Ta_2O_5 is a refractory oxide

characterized by strong metal support interaction (similar to TiO_2) [39, 55]. NaY is a microporous zeolite [56], a weak acidic support [57, 58]. The results obtained are evaluated in conjunction with the results obtained from CB decomposition on 10% (w/w) Ni/SiO_2 at 873 K from our previous study (Chapter 2). Use of supports exhibiting such diverse properties should impact the yield and structure of the C product; such is the premise of this work. Also, the effect of varying Ni loading is considered for Ni/SiO_2 and Ni/Al_2O_3.

4.2 Experimental Procedure

The catalysts were prepared by incipient wetness impregnation with an aqueous solution of Ni $(NO_3)_2$, as described elsewhere [30]. Results have been discussed in terms of particle size, crystallographic orientation of the Ni sites to the incoming feed and metal-support interaction. The catalyst precursors (Ni/X; X= SiO_2, Al_2O_3, NaY, Ta_2O_5, AC and G) were sieved into batches of 100 μm (ATM fine test sieves) average particle diameter, loaded into a fixed bed tubular quartz reactor (i.d. 1.25cm) and activated by heating at 10 K min^{-1} in a stream of dry H_2 at 60 cm^3 min^{-1} to the reaction temperature of 873 K and maintained at the reaction temperature for at least 12 h. A Model 100 (KD scientific) microprocessor–controlled infusion pump was used to deliver the feed (CB) at a fixed rate *via* a glass/teflon airtight syringe and teflon line at a fixed calibrated flow rate. The flow of H_2 gas was controlled using a mass flow meter (MKS Instruments). The inlet hourly of C/Ni molar ratio was maintained at 69.4 at a gas hourly space velocity (GHSV) of 4×10^3. Addition of support to the catalyst bed for higher Ni loadings ensured constant velocity at a constant C/Ni ratio. The reaction temperature was monitored continuously by means of a thermocouple inserted in the catalyst bed. A layer of quartz wool was placed above the catalyst bed to ensure that the reactants

vaporized before contacting the catalyst. The reaction effluent was collected in a liquid nitrogen trap for subsequent analysis which was made using Perkin-Elmer Auto system XL Chromatograph equipped with a split/split less flame ionization detector employing DB - 1 50 m X 0.20 mm i.d., 0.33 μm capillary column (J& W Scientific). The gravimetric yield of carbon was determined from the catalyst bed mass differential pre- and post-reaction; carbon yield was reproducible to better than $\pm10\%$. Based on known carbon inlet, gravimetric yield of solid carbon, and chromatographic analysis of reactor fluent using 2-octanol as internal standard, carbon balance was calculated.

BET, TPR and H_2 chemisorption were carried out using the commercial CHEMBET 3000 (Quantachrome Instrument) unit employing a thermal conductivity detector. Data acquisition and manipulation was carried out using the TPR Win^{TM} package. BET surface areas were recorded with a 30% (v/v) N_2/He flow; pure N_2 (99.9%) was used as the internal standard. At least two cycles of N_2 adsorption-desorption were employed in order to determine the BET surface area of the catalyst using single point method. TPR employed a reducing mixture of 5% (v/v) H_2/N_2 with a heating rate of 10 Kmin^{-1} from room temperature to 873 K where the effluent gas was directed through a liquid nitrogen trap. The reduced samples were swept with a flow of N_2 for 1 h, cooled to room temperature and subjected to H_2 chemisorption using a pulse (50 μl) titration procedure. Hydrogen pulses were introduced until the signal area was constant, indicating surface saturation. TPO profiles of the catalytically generated carbon were obtained from thoroughly washed demineralized (in HNO_3) samples to avoid any contribution due to a catalyzed gasification of carbon by residual Ni [59]. A known weight of the demineralized sample was heated from room temperature to 1273

K at 8 Kmin^{-1} in a 5% (v/v) O$_2$/He mixture with on-line TCD analysis of the exhaust gas. The TEM analysis was conducted using a JEOL 2000 TEM microscope and JEOL 2010 TEM/STEM microscope (Oxford Instruments) operated at an accelerating voltage of 200 kV. EDX mapping was conducted at both the tip and a point along the length of individual carbon nanofibers. Specimens for TEM analysis were prepared by ultrasonic dispersion in n-butanol where a drop of the resultant suspension was evaporated on a holey carbon support grid.

4.3 Results and Discussion

4.3.1 Catalyst Characterization

BET surface areas for the catalysts considered in this study are recorded in Table 4.1. The AC support, with significant micro- and meso- porosity, is characterized by a large surface area whereas Ta$_2$O$_5$ and G support present low surface areas [30]. The BET areas for Ni/SiO$_2$ and Ni/Al$_2$O$_3$ are in agreement with values quoted in the literature [30, 44, 60-62]. NaY, a microporous zeolite support exhibited relatively lower surface area than typically suggested in literature [56, 63]. Such variations could arise due to significant differences in porosity of the support.

TPR is an effective approach to study the reducibility of supported metals. The TPR profiles of 10% w/w Ni loaded samples, shown in Figure 4.1, exhibit broad positive H$_2$ consumption peaks where the associated T$_{max}$ values span the range 620 - 770 K. Except for Ni/Al$_2$O$_3$, which exhibits distinct behavior in that the reduction profile presents two distinguishable peaks, all the catalysts at 10% (w/w) Ni loading exhibit a single H$_2$ consumption peak. The single H$_2$ consumption peak (at 623 K) associated with Ni/SiO$_2$ has two distinguishable high temperature shoulder peaks at 738

K and 853 K. Mizushima *et al.* [64] attributed the TPR T_{max} obtained at *ca.* 630 K to NiO reduction in their TPR study of impregnated Ni/SiO_2. Choi *et al* attributed reduction peaks between 600 - 700 K to reduction of NiO species supported on SiO_2 [65, 66]. Several studies [66-76] attribute the temperature peaks in the range of 723 - 973 K obtained for TPR of Ni/SiO_2 to metal-support interactions. TPR of Ni/Al_2O_3 gave two distinguishable peaks at 656 K and 808 K. TPR profiles of Ni/Al_2O_3 presenting one [77], two [78] and even four [79] reduction peaks have been reported in the literature, suggesting that the TPR response is sensitive to catalyst preparation. Temperatures below 773 K for TPR of Ni/Al_2O_3 have been attributed to reduction of NiO (to Ni) having a weak interaction with the support while that above 873 K have been attributed to Ni (in the form of $NiAl_2O_4$) having strong interaction with the support [80-82]. The TPR profile of Ni/AC characterized by a single broad consumption peak at 670 K with low and high temperature shoulders at 601 K and 858 K. Matos *et al* attributed [83] temperature peaks obtained between 598-603 K for the TPR of Ni/AC to well dispersed hydrated phases of Ni oxides generated by decomposition of the supported salts. Zhou *et al* attributed the broad consumption peak obtained in the range of 553-703 K to the presence of several reducible species [84]. The TPR T_{max} of Ni/NaY is characterized by a single peak at 763 K with two shoulders at approximately 670 K and 840 K**.** Lucas *et al* [63] attributed TPR peaks obtained at 613 K and 753 K to the reduction of NiO species that have different interactions with the Y zeolite support. Several studies [63, 85, 86] attribute reduction peaks obtained at lower temperatures (up to 780 K) to the reduction of Ni^{2+} localized in the super cage (and/or sodalite) cavities while that at high temperatures (780 - 853 K) to nickel reduction localized in hexagonal cavities. The TPR

generated in this study suggests a reduction of nickel located in both sodalite and hexagonal cavities. The TPR T_{max} values associated with the six supported Ni catalysts taken into consideration here, shown in Figure 4.2, represent decomposition of the supported nitrate precursor with a subsequent reduction of NiO to Ni^0 where the differences in the H_2 consumption profiles must result from the variations in interfacial energies between nickel and each support. Higher temperature shoulders in the case of Ni/SiO_2, Ni/Al_2O_3, Ni/G, Ni/AC and Ni/NaY does suggest some metal/support interaction that serves to stabilize the supported NiO phase [67-69, 81-83, 87, 88]. The TPR profiles of Ni/SiO_2 and Ni/Al_2O_3 with varying loading is shown in Figure 4.2 and Figure 4.3. No significant difference in the TPR profiles is observed in the case of Ni/Al_2O_3. In Ni/SiO_2, the shoulder peaks become more distinguishable with increase in loading from 1% to 10%. A slight shift to higher reduction temperatures is observed in the TPR profiles, suggesting a relatively stronger metal-support interaction at higher loadings. However, a search of literature revealed results contrary to those observed in this study. Canizares et al [89] reported variation in the TPR peak maxima with the amount of metal present in the catalyst: the higher the Ni loading, the lower the TPR peak maxima(um). Such variation with metal loading was ascribed to formation of larger metal particles at higher loadings (due to mobility of Ni atoms in closer proximity) which exhibit a more facile reduction [89]. Poncelet et al [90] reported that the reduction profiles broadened and the reduction temperature values shifted to higher temperatures with decreasing metal loading from 3% to 1% Ni supported on alumina. In order to further characterize the supported Ni metal sites, H_2 chemisorption was conducted and the H_2 uptake values are quoted in Table 4.1. At the 10% w/w Ni

loading, Ni/SiO$_2$ exhibited the highest H$_2$ uptake while Ni/Ta$_2$O$_5$ showed the least. A high uptake is consistent with smaller metal particle sizes. Decrease in metal loading resulted in substantial decrease in H$_2$ uptake in the case of both Ni/SiO$_2$ and Ni/Al$_2$O$_3$, suggesting the presence of larger Ni particles. It is, however, typically the case that lower dispersions (larger mean particle sizes) are observed at higher loadings [89-91]. The latter is attributed to a more facile metal particle growth at higher loadings [89-91]. However, Bartholomew and Pannell reported dispersions of 13 and 22% and particle sizes of 7.6 and 4.5 nm for Ni/Al$_2$O$_3$ for samples with 1 and 3% Ni respectively, on reduction at 773 K [92] i.e. decrease in metal dispersion with decrease in metal loading. Such an effect was attributed to suppression of hydrogen adsorption. The TPR and H$_2$ uptake results presented in this Chapter are by no means conclusive. However, it is reasonable to state that the nature of the support and Ni loading impacts on metal precursor reducibility and resultant metal dispersion.

4.3.2 Carbon Growth: Support Effects

Carbon yields, %C efficiencies and reaction selectivities are given in Table 4.2. Reaction of CB in H$_2$ atmosphere generated benzene via catalytic hydrodechlorination and solid C via CB decomposition. Carbon balance measurements revealed formation of volatiles that were not isolated in the liquid trap which could result via additional hydrogenolysis/hydrocracking reactions. The volatiles formed have not been identified in this study. The focus of this study is solely on the effect of varying support on carbon yield rather than a detailed study of the catalytic side reactions. Inspection of the data in Table 4.2 reveals that reaction of CB on Ni/SiO$_2$ generated highest C yield. C growth was significantly less favored when Ni was supported on either of the carbonaceous

supports. Taking the product selectivities given in Table 4.2 into consideration, it is clear that CB hydrodechlorination was by far the preferred reaction on Ni/AC with hydrocracking to volatiles predominating over Ni/G. With the exception of Ni/SiO$_2$, there were no significant differences in overall conversion for Ni supported on Al$_2$O$_3$, Ta$_2$O$_5$, NaY, AC or G supports. Carbon yields increased in the sequence: Ni/AC < Ni/G < Ni/Ta$_2$O$_5$ ~ Ni/NaY< Ni/Al$_2$O$_3$ < Ni/SiO$_2$. Reaction selectivity to C yield was also sensitive to Ni loading, as can be inferred from Table 4.3. In the case of both Ni/SiO$_2$ and Ni/Al$_2$O$_3$, lower Ni loading resulted in a decrease in C yield and increased selectivity to benzene. Several studies have been conducted to determine the role of metal loading on the growth of structured C [93, 94]. Takenaka *et al* [93] recorded a steady increase in C yield with increase in metal loading (from 1% w/w) up to 40% w/w Ni (for Ni/SiO$_2$) for the decomposition of CH$_4$ at 773 K. However, a further increase (from 40 to 90% w/w) was reported to cause reduction in C yield [93]. In another study [94], Yu *et al* recorded an increase in C yield with increase in metal loading (from 20 to 60% w/w) for CO disproportion on Fe/SiO$_2$ at 873 K. Such responses have been linked to significant variations in metal particle sizes with loading [93, 94]. The above results clearly demonstrate dependence of C yield on the nature of the Ni support and Ni loading.

In the production of solid C, CB must first undergo a destructive chemisorption to generate carbon atoms that diffuse through the metal particle with subsequent precipitation. There is a general consensus in literature [95, 96] that when the supported metal presents different exposed crystallographic planes to incoming reactant, significantly different catalytic activities can result. It has been shown that certain

crystallographic orientation(s) of Ni favor(s) reactant decomposition [97, 98] while different set of faces serves to promote the precipitation of a structured carbon product [64, 79, 99]. Ermakova *et al* claimed that hydrocarbon decomposition on nickel occurs on different edges of the nanoparticle due to anisotropy of nickel wherein the lament axis has been reported to be parallel to the Ni(111) planes [48, 97]. Several studies [97] report that Ni(110) and Ni(100) surfaces are much more active for hydrocarbon (methane) dissociation than Ni(111) [100, 101] to yield carbon fibers. It has been concluded that during C growth, a nickel particle exposes more open surfaces to the gas phase, and the (111) planes epitaxially grow graphite. Vinciguerra *et al* reported that the Ni(111) face has the appropriate symmetry and distance to overlap with the lattice of graphene sheet [102]. The orientations of a metal particle anchored on a support are different to those encountered with bulk metal and vary significantly with the nature and strength of metal – support interaction [103-105] i.e. the predominant exposed metal face is influenced by the choice of support. Direct correlation between percentage of Ni particles with either (111) or (100) orientation and rate of reaction [106], with Ni(111) favoring carbon growth/precipitation, has been reported [38, 107]. Furthermore, it has been shown elsewhere using Fe catalyst and propylene feed that the rate of carbon deposition is dependant on the metal site geometry [108]. The rate determining step thus appears to be dissolution and diffusion of carbon through the metal particle. Apart from the crystallographic orientations, strong dependence of C yield and growth rate on the catalyst metal particle size has been demonstrated in several studies [93, 109, 110]. Presence of both large and small metal particles has been reported to be unfavorable for growth of structured C and an optimum particle size

favoring C growth has been proposed [93, 94]**.** Given the number of interrelated factors that can have a bearing on growth of solid C, it is difficult to identify explicitly one catalyst property that affects C production. However, it is clear from our results that metal - support interactions are a contributing factor, impacting TPR characteristics and ultimately on the particle size of the Ni metal, all of which in turn apparently cause significant divergence in CB reaction selectivity observed in this study. The C yields recorded, for the most part, are comparable to those quoted elsewhere for supported Ni systems [30, 99, 111].

4.3.3 Carbon Growth: Structural Effects

The BET surface area of catalytically generated carbon on various substrates is given in Table 4.4. Surface areas associated with the nanofiber growth are intermediate between the high surface area of amorphous carbon (676 m^2/g) and the low surface area of graphite (7 m^2/g) and are greater than that associated with nanotube growth (25 m^2/g) [5, 11, 112]. Significant variation in the surface areas of C grown with variation in nature of support and loading used is noted (see Table 4.4). Comparison of BET surface areas of C grown on varying supports at 10% (w/w) Ni loading reveals a smaller surface area of C grown on Ni/Ta_2O_5 and greater surface area of C on Ni/NaY which can result from differences in dimensions and porosity. The tabulated BET surface areas coincide with values quoted in literature [113-116]. The results further reveal that decrease in loading in Ni/SiO_2 and Ni/Al_2O_3 caused a reduction in C surface area. The presence of an amorphous carbon component can also contribute to the overall areas. TPO was employed to evaluate the extent of carbon structural order i.e. amorphous and/or graphitic nature. As quoted in earlier chapters also, an increasing order in the

carbon structure is accompanied by an elevation of the temperature at which gasification is induced [117]. The TPO characteristics of carbon grown over an array of substrates at a constant loading (10%) are recorded in Table 4.4; the TPO characteristics for model amorphous and graphite samples are included to facilitate comparison. On the basis of these results it is apparent that while the C produced from Ni/NaY catalyst displayed the highest level of graphitic character, that grown from Ni/Al$_2$O$_3$ exhibited the least (ΔT_{max} = 138K). The oxidation profiles associated with catalytic carbon growth are broad (see Figure 4.4), a feature that is diagnostic of a range of carbon structures with both an amorphous and a graphitic component; the degree of broadness is noticeably greater for Ni/NaY. The T$_{max}$ values increased with increasing Ni loading (Table 4.4) and the TPO profiles broadened noticeably (Figure 4.5) suggesting the presence of a wider range of carbonaceous material with an overall higher degree of order [56, 118, 119]. The above observations suggest that there is a contribution of the support and Ni loading in determining the structural characteristics of the carbon product. On the whole, the solid C obtained on decomposition of CB over Ni catalyst on varying substrates and loading exhibits structural order to varying degrees.

The nature of the carbon nanofiber growth generated by all the supported Ni systems is illustrated by the TEM image shown in Figure 4.6 wherein the fibrous nature of the carbon is immediately evident. Typical diameters of structured C obtained in this study range between 10 - 40 nm. One feature common to the carbon growth observed in this study is the occurrence of Ni metal particle at the tip of the growing fiber indicating that the carbon growth occurs *via* tip growth mode corresponding to weak metal - support interaction [120] wherein the pressure buildup with the formation of graphite

layers at the metal/support interface is of sufficient magnitude to extract Ni particles from the substrate. Once the Ni particle is detached from the substrate, a fresh face is exposed to the incoming feed and growth (of structured C) continues with the Ni particle located on the fiber tip. As noted in Chapter 2, there is evidence in literature that intercalation of electron withdrawing species (eg. Cl) increases the electronic properties of the carbon product by at least an order of magnitude [121-123]. Furthermore, (as stated in Chapter 2 also), a direct introduction of Cl (via the feed) would avoid the problematic established intercalation step which suffers from the drawback of rapid exfoliation [124]. However, our investigation on the possibility of Cl incorporation directly from the feed (CB) into the carbon growth on 10% (w/w) Ni/SiO$_2$, revealed no evidence of any Cl inclusion (Chapter 2). Recently, Brichka *et al* [125] have reported a presence of 0.25 at %Cl on carbon nanotubes formed via the pyrolysis of CH$_2$Cl$_2$ on alumina membranes in the temperature range of 573 - 973 K. The possibility of a supportate effect in terms of Cl inclusion in the carbon growth was considered, employing EDX analysis of the carbon nanofiber; a typical image is shown in Figure 4.7. Ni, C and respective support material (e.g. Al and O in the case of Al$_2$O$_3$ support, shown in Figure 4.7), were detected at both the fiber tip and along the fiber length; see EDX spectra and atomic content in Figure 4.8 and Figure 4.9. Evidence of the dispersion of Ni particles along the length of carbon fiber has been observed in previous study (Chapter 2) also. It is interesting to note that while only trace amounts (< 0.06%) of Cl were detected on C from Ni/NaY and Ni/Ta$_2$O$_5$, up to 0.4 atom% were detected on C grown from Ni/Al$_2$O$_3$. The latter represents a significant Cl content and suggests that there is a support effect in terms of Cl inclusion. Such an incorporation of

Cl in the structured C growth should impact on associated chemical/electronic properties which may have potential application(s) in electronics and catalysis [121, 123].

4.4 Conclusions

Characterization of Ni catalysts on varying supports and loading using TPR and H_2 uptake revealed (1) the degree of metal - support interaction varied with the support and (2) Ni dispersion was dependent on the nature of the support. C yield recorded at a 10% w/w Ni loading increased in the order: Ni/AC < Ni/G < Ni/NaY ~ Ni/Ta$_2$O$_5$ < Ni/Al$_2$O$_3$ < Ni/SiO$_2$. Ni loaded on either of the carbonaceous substrate did not generate significant amounts of solid C. A decrease in Ni loading (for Ni/SiO$_2$ and Ni/Al$_2$O$_3$) has been found to lower C yield. These responses can be linked to metal - support interaction, particle size and crystallographic orientations of the Ni metal particles. TPO characterization revealed that C growth from Ni/NaY exhibited greater degree of structural order. TEM analysis revealed the presence of Ni metal particles at the nanofiber tip indicating C growth via tip growth mode. Cl content (up to 0.4 atom%) was detected for C grown from Ni/Al$_2$O$_3$. The results demonstrate a significant impact of the support and loading in determining the extent and nature of carbon deposition via CB decomposition on supported Ni.

4.5 Tables and Figures

Table 4.1: BET surface areas and H_2 uptake associated with the supported Ni catalysts considered in this study

Catalyst	BET Surface Area(m^2/g) of the Catalyst	H_2 Uptake (µmole/g)
10% Ni/SiO$_2$	181	17
10% Ni /Al$_2$O$_3$	147	9
10% Ni/Ta$_2$O$_5$	9	1
10% Ni/NaY	157	2
10% Ni/G	13	4
10% Ni/AC	801	9
5% Ni/SiO$_2$	255	<1
1% Ni/SiO$_2$	237	<1
5% Ni/Al$_2$O$_3$	157	<1

Table 4.2: Overall feed conversion, carbon yield (Y_C), %C Efficiency and selectivity to side products (combination of selectivity to benzene and volatiles) resulting from the catalytic decomposition of CB over the six supported 10% (w/w) Ni catalysts: $\Delta t = 1$ h.

Catalyst	Conversion (%)	Carbon Yield ($Y_c g_c g_{Ni}^{-1}$)	C Efficiency (%)	Selectivity to Benzene (%)	Selectivity to side reactions (%)
10% Ni/Ta$_2$O$_5$	77	13	15	19	80
10% Ni/NaY	77	13	15	22	81
10% Ni /G	76	4	5	14	94
10% Ni /AC	78	~	~	67	100
10% Ni/SiO$_2$	87	24	29	41	74
10% Ni /Al$_2$O$_3$	75	16	18	27	76

Table 4.3: Overall feed conversion, carbon yield (Y_C), %C Efficiency and selectivity to side products (combination of selectivity to benzene and volatiles) resulting from decomposition of CB over Ni/SiO$_2$ and Ni/Al$_2$O$_3$ with different Ni loadings: $\Delta t = 1$ h.

Catalyst	Conversion (%)	Carbon Yield ($Y_cg_cg_{Ni}^{-1}$)	C Efficiency (%)	Selectivity to Benzene (%)	Selectivity to side reactions (%)
10% Ni/SiO$_2$*	97	11	13	58	87
5% Ni/SiO$_2$	99	3	16	92	84
1% Ni/SiO$_2$	99	<1	1	60	99
10% Ni/Al$_2$O$_3$	75	16	18	27	76
5% Ni/Al$_2$O$_3$	75	5	10	78	86

10% Ni/SiO$_2$* is the 10% Ni/SiO$_2$ catalyst to which silica has been added to maintain a constant GHSV and constant C/Ni for varying Ni loading.

Table 4.4: BET surface areas of the solid carbon product obtained via catalytic decomposition of CB over supported Ni catalysts.

Catalyst	BET Surface Area (m^2/g) of the C grown on the catalyst	TPO T_{max}(K)
10% Ni/SiO$_2$	191	1051
10%Ni /Al$_2$O$_3$	171	953
10% Ni/Ta$_2$O$_5$	154	968
10% Ni/NaY	236	1091
10% Ni/SiO$_2$*	194	1003
5% Ni/SiO$_2$	164	973
5%Ni /Al$_2$O$_3$	164	918
Activated C	676	973
Model Graphitic Carbon	7	1283

10% Ni/SiO$_2$* is the 10% Ni/SiO$_2$ catalyst to which silica has been added to maintain a constant GHSV and constant C/Ni for varying Ni loading.
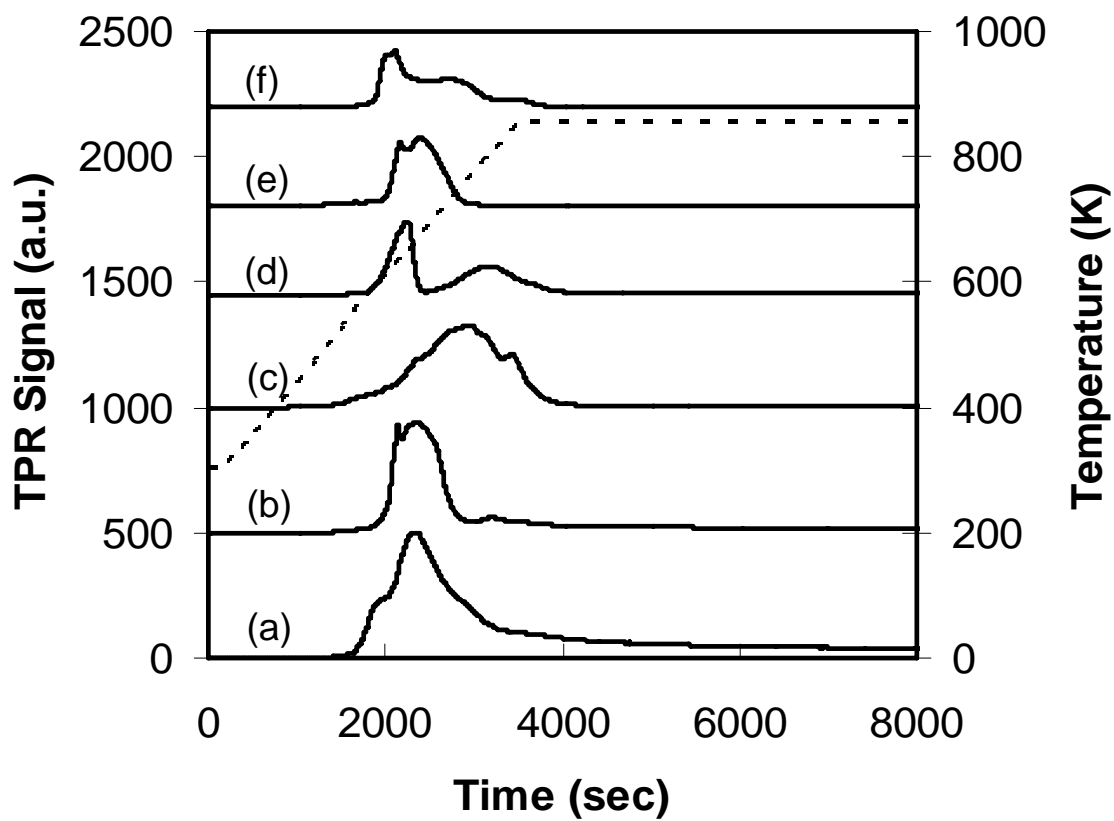
Figure 4.1: TPR profiles of (a) 10% (w/w) Ni/AC (b) 10% (w/w) Ni/G (c) 10% (w/w) Ni/NaY (d) 10% (w/w) Ni/Al$_2$O$_3$ (e) 10% (w/w) Ni/Ta$_2$O$_5$ and (f) 10% (w/w) Ni/SiO$_2$ catalysts.
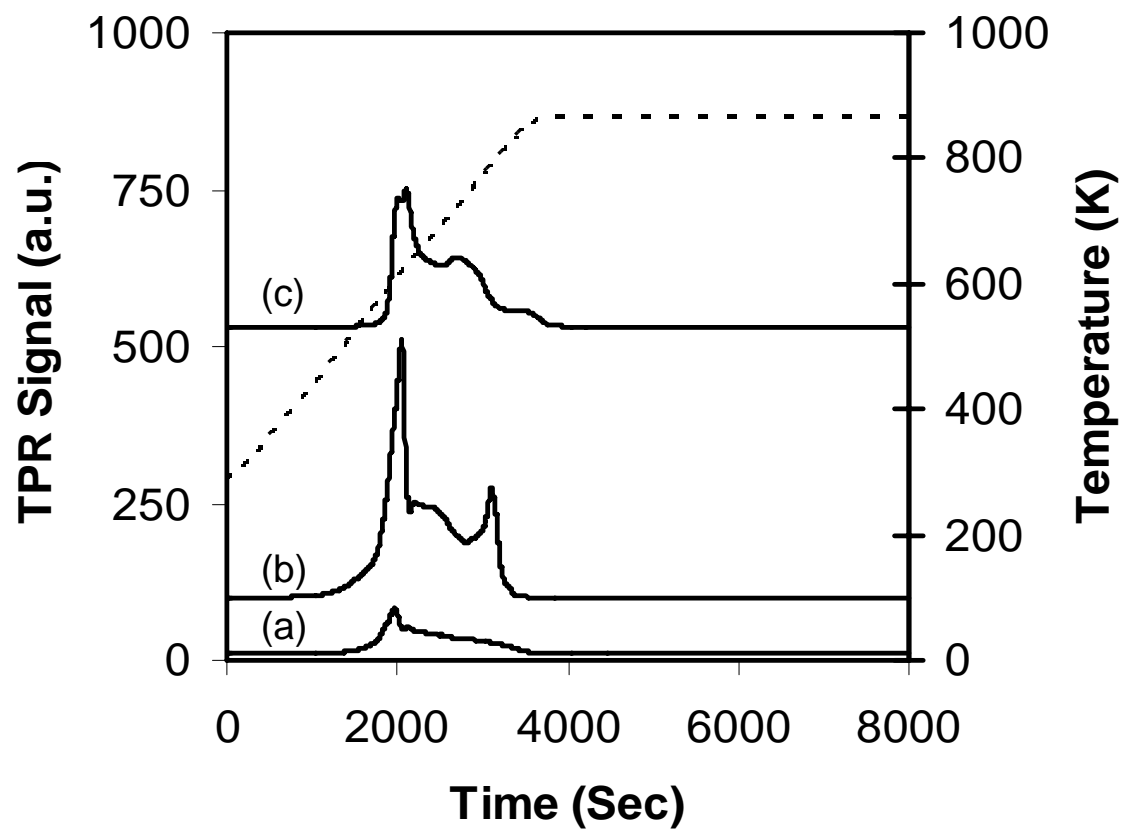
Figure 4.2: TPR profiles of (a) 1% (w/w) Ni/SiO$_2$ (b) 5% (w/w) Ni/SiO$_2$ and (c) 10% (w/w) Ni/SiO$_2$
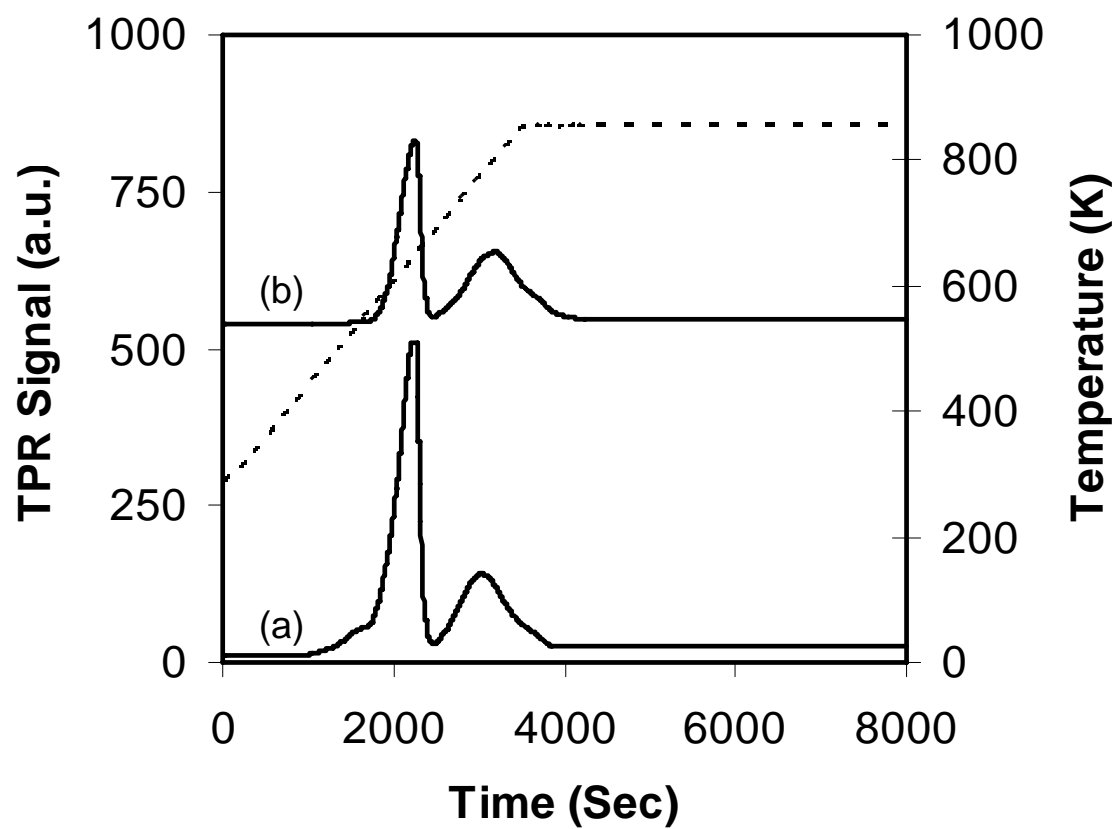
Figure 4.3: TPR profiles of (a) 10% (w/w) Ni/Al$_2$O$_3$ and (b) 5% (w/w) Ni/Al$_2$O$_3$ at 873 K.

Figure 4.4: TPO profiles for (a) model amorphous carbon, (b) model graphite and carbon generated from decomposition of CB in H_2 atmosphere at 873K at $\Delta t = 1h$ over (c) 10% (w/w) Ni/NaY (d) 10% (w/w) Ni/Al_2O_3 (e) 10% (w/w) Ni/Ta_2O_5 and (f) 10% (w/w)Ni/SiO_2

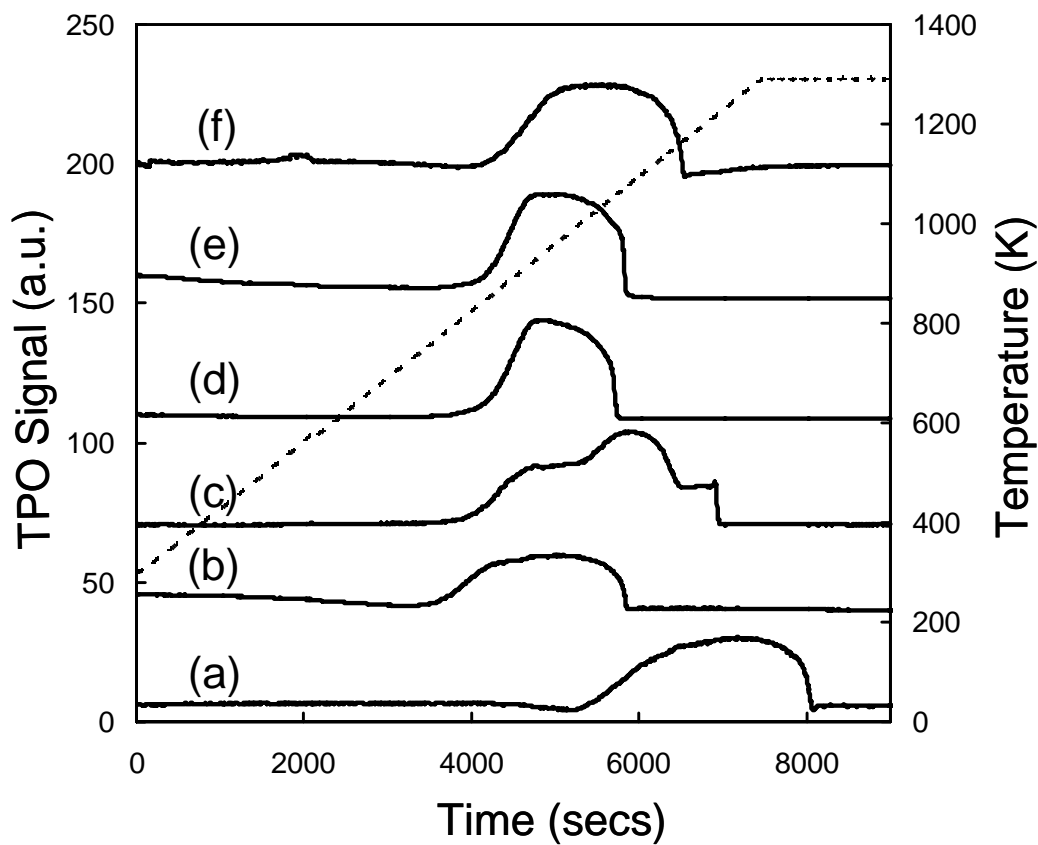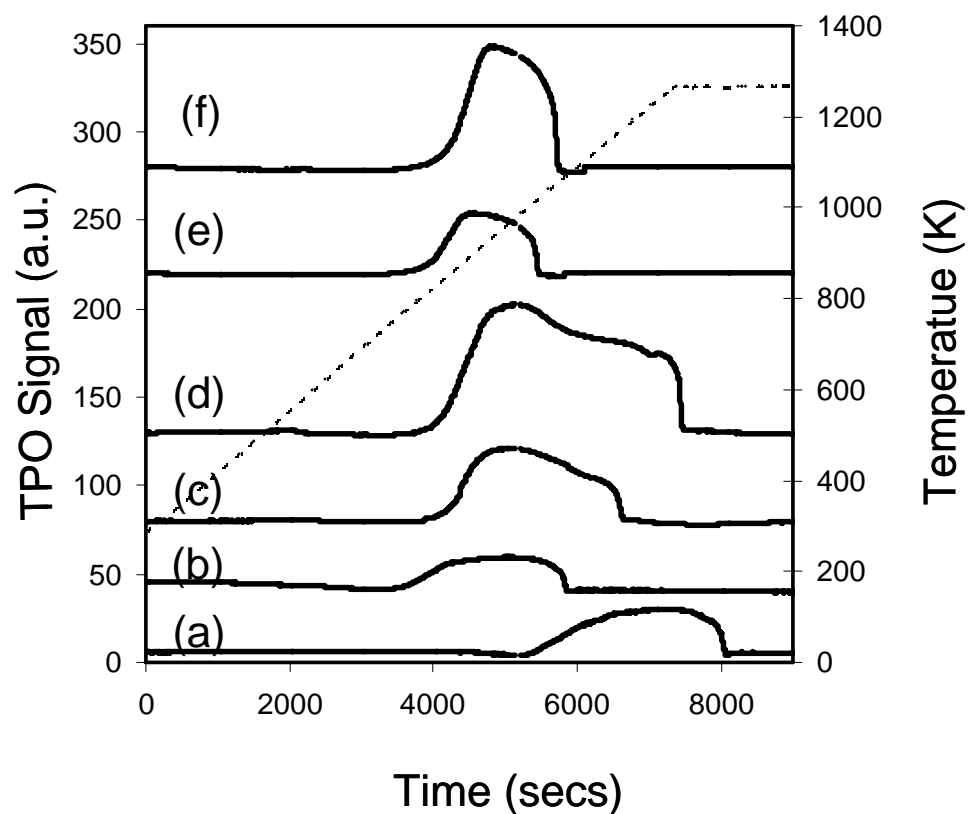Figure 4.5: TPO profiles for (a) model amorphous, carbon (b) model graphite and carbon generated from decomposition of CB in H_2 atmosphere at 873 K at Δt = 1h over (c) 5% (w/w) Ni/SiO_2 (d) 10% (w/w) Ni/SiO_2* (e) 5% (w/w) Ni/Al_2O_3 (f) 10% (w/w) Ni/Al_2O_3. (10% Ni/SiO_2* is the 10% Ni/SiO_2 catalyst to which silica has been added to maintain a constant GHSV and constant C/Ni for varying Ni loading)
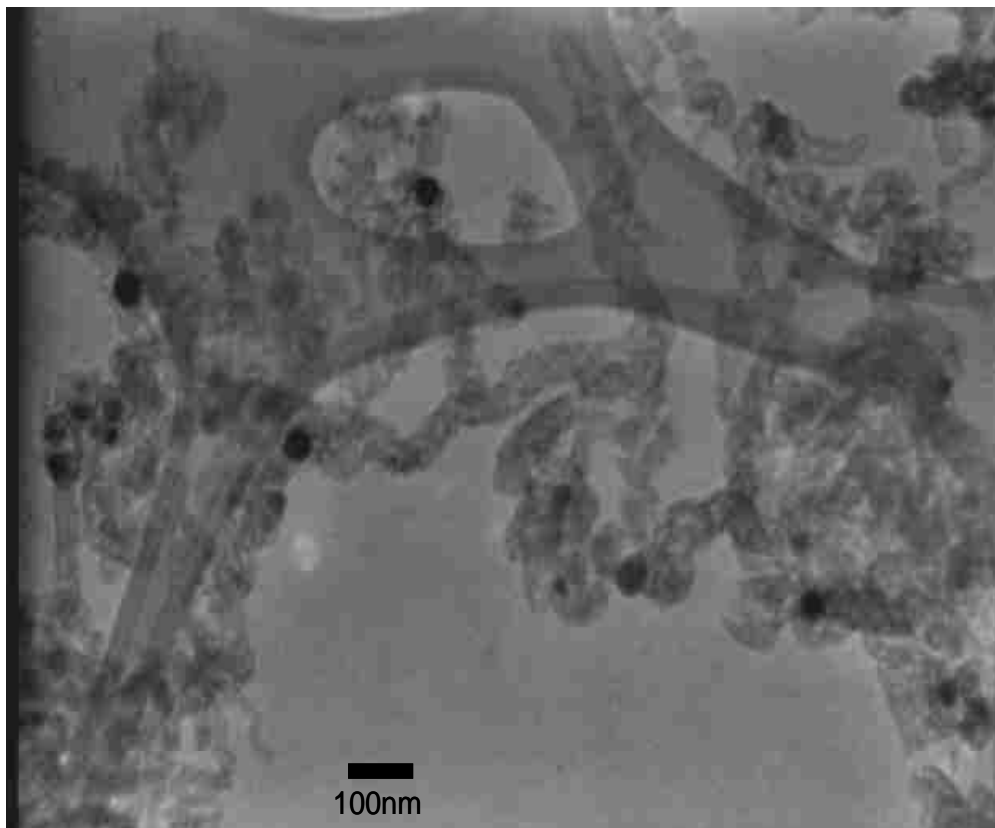
Figure 4.6: Representative TEM image of the carbon nanofibers showing structural features of carbon grown from 10% (w/w) Ni/Ta$_2$O$_5$: T = 873 K, Δt = 1 h. Note: this image typifies the carbon growth from all the supported Ni catalysts taken into consideration in this study.
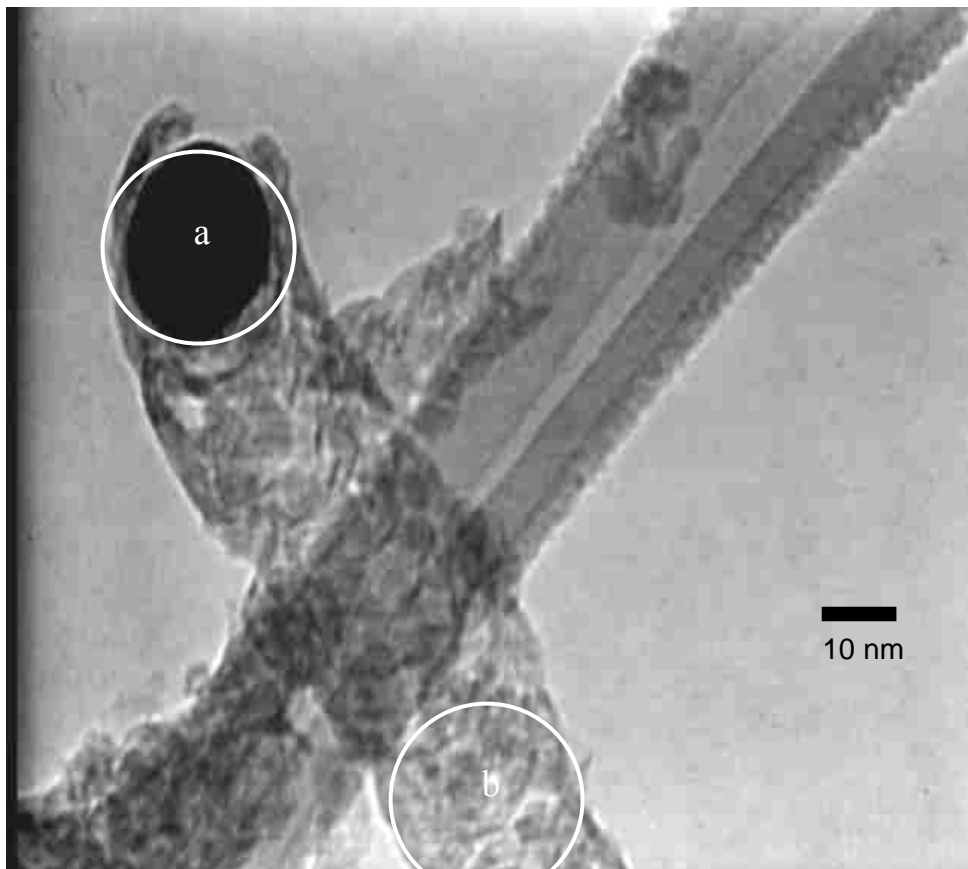
Figure 4.7: Representative TEM image of an individual carbon nanofiber grown from 10% (w/w) Ni/Al_2O_3: T = 873 K after 1h on-stream. Note: Area marked (a and b) indicate area which has been mapped for EDX spectra: see figures 4.8 and 4.9
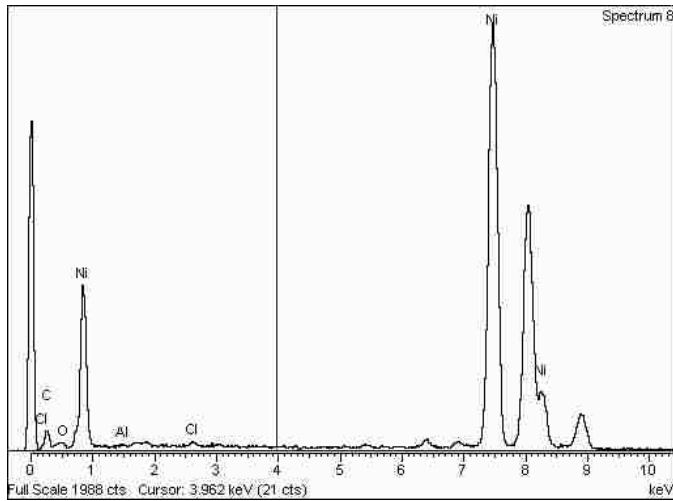
Element	Atomic %
C K	16.88
O K	1.98
Al K	0.19
Cl K	0.66
Ni K	80.30
Totals	100

Figure 4.8: EDX spectrum for the marked area (a in figure 4.7) and the associated atom% values of the elements detected
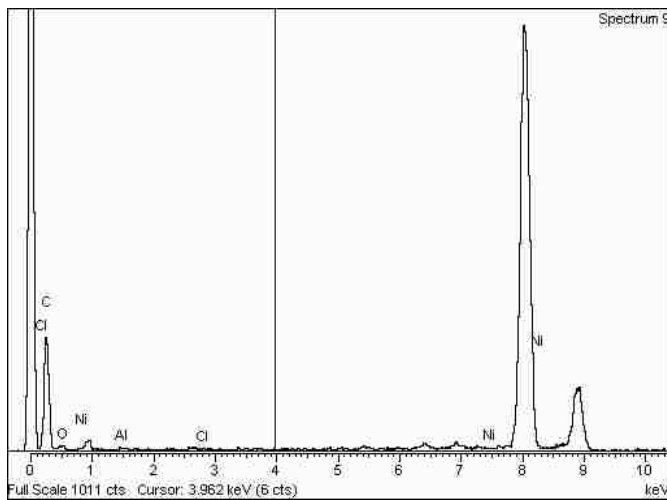
Element	Atomic%
C K	97.93
O K	1.73
Al K	0.30
Cl K	0.37
Totals	100

Figure 4.9: EDX spectrum for the marked area (b in figure 4.7) and the associated atom% values of the elements detected.

Conclusions and Future Work

In this thesis, growth of structured C via CVD of environmentally hazardous compounds such as CB, over supported Ni has been systematically investigated. The critical findings of this work are outlined below with suggested guidelines for future research.

In Chapter 2, growth of structured C by CVD of CB, over (10% w/w) Ni/SiO_2, with H_2 in the temperature ranges $823 - 973$ K was explored. Response of carbon yield and structural order to varying reaction time and temperature were presented and discussed. Under identical reaction conditions, CB delivered appreciably higher carbon yields than that recorded from decomposition of benzene while the carbon growth in the former case was significantly more ordered. The results have been interpreted in terms of charge transfer/Ni site restructuring due to Cl/catalyst interaction(s). Though, recorded C yield data from CB and benzene indicates formation of benzene and growth of solid C from CB to be exclusive reactions, identification of the volatiles should be able to further establish this effect.

In Chapter 3, examination of effect of %(v/v) H_2 on the growth of structured carbon via CVD of CB over 10% (w/w) Ni/SiO_2 at 873 K revealed H_2 to be a requisite for decomposition of CB. Maximum C yield was observed at a 40% (v/v) H_2 inlet carrier gas content. C yield has been found to vary with the nature of the benzene ring substituent where FB and CB serve as substantial sources of solid C with no measurable C growth from BB and IB. 3-CBB and physical mixture of CB + BB did not yield solid C. Observed enhanced debromination and BB conversion in CBB and CB + BB, respectively, were attributed to occurrence of an exchange reaction in which the debrominated intermediate is subsequently chlorinated by surface HCl. Presence of −

CH$_3$ group on benzene ring was observed to reduce C yield. However, no concrete reason was put forth for the observed variation. Effect of Cl varied with the chemical structure of the carbon source in that the presence of Cl promoted C yield in the case of aromatic and straight chained (aliphatic) compounds whereas it promoted formation of benzene in the case of cyclic compounds. Furthermore, while the presence of Cl (in the feed) promoted growth of structured C in aromatic compounds, it favored growth of amorphous C in straight chained compounds. In addition, the effect of varying%(v/v) H$_2$ on C yield and structure varied with the carbon precursor. The above observed variations were attributed either to (1) plausible reconstruction of the catalyst on interaction with the substituents or (2) mechanism of the solid C formation. Detailed TEM analysis of the post-reaction catalyst/product exploring the structural variations of the Ni catalyst particles in conjunction with identification of the volatiles should be able to identify the causal factors explicitly.

In Chapter 4, the effect of support and loading on yield and structure of (solid) carbon was assessed. Characterization of reduced catalysts (using BET surface area, H$_2$ chemisorption, and TPR techniques) revealed the degree of metal–support interaction to be dependant on both support and loading. C yield recorded at a 10% w/w Ni loading increased in the order: Ni/AC < Ni/G < Ni/NaY ~ Ni/Ta$_2$O$_5$ < Ni/Al$_2$O$_3$ < Ni/SiO$_2$. Ni loaded on either of the carbonaceous substrate did not generate significant amounts of (solid) C. Decrease in loading was observed to decrease the C yield. The results were discussed in terms of particle size, crystallographic orientation of the Ni sites and metal-support interaction. The carbonaceous product was characterized using BET surface area, TPO and TEM. C grown on 10% (w/w) Ni/NaY was found to be more structured

than others. Amounts of Cl up to 0.4 at% were detected on C grown on 10% (w/w) Ni/Al_2O_3. Detailed TEM analysis of activated catalyst on each support aimed to document the Ni catalyst particle size and particle-size distributions (pre-reaction) on each support in conjunction with post-reaction TEM analysis intended to record diameter of the structured C should be able to establish an unambiguous relationship between the catalyst particle-size and diameter of the structured C obtained in this study. Such study should also be able to further elucidate on the plausible effect of the crystallographic planes suggested in this study.

Appendix

Following are the internal calibration graphs obtained for some of the reactants considered. The reactant considered is used as heading of the graph

A = Area obtained
W = Weight used
i = Internal standard considered (octanol/toluene)
r = Reactant

Benzene

$y = 0.6874x$
$R^2 = 1$

Toluene

$y = 0.698x$
$R^2 = 0.9999$

FB

$y = 0.6907x$
$R^2 = 0.9998$

CB

$y = 0.9585x$
$R^2 = 0.9998$

BB

y = 1.3787x
R² = 0.9998

CT

y = 0.9704x
R² = 0.9999

3-CBB

y = 1.7594x
R² = 1

CH

y = 1.0204x
R² = 0.9999

Cyclohexane

y = 1.0763x
R² = 0.9998

Cyclohexene

y = 0.7288x
R² = 0.9999
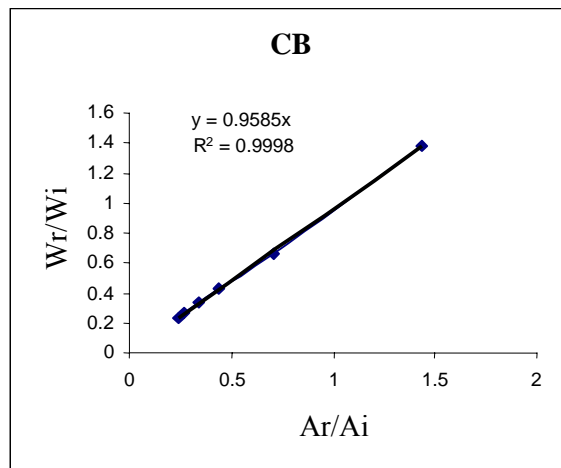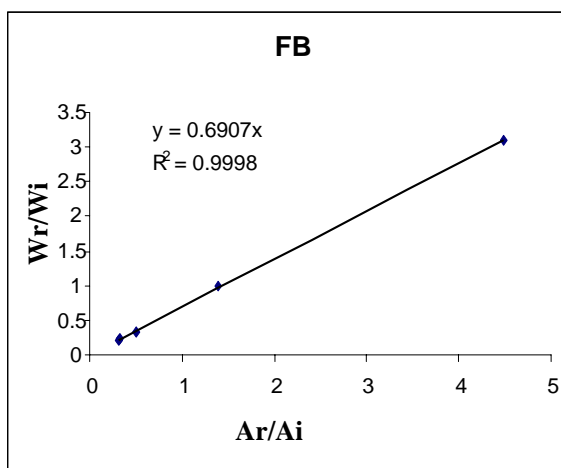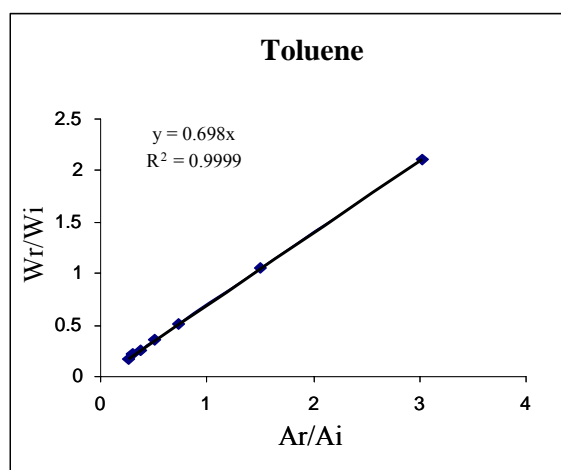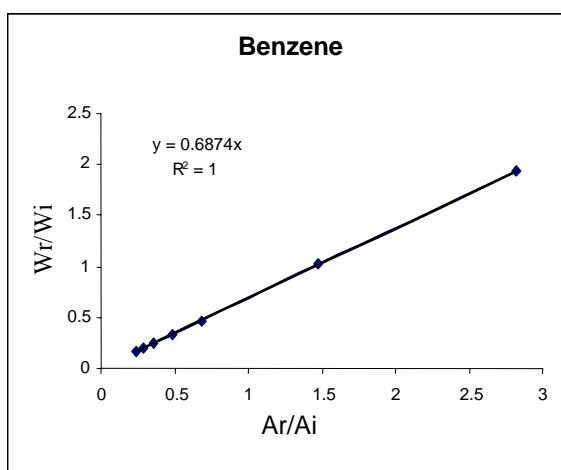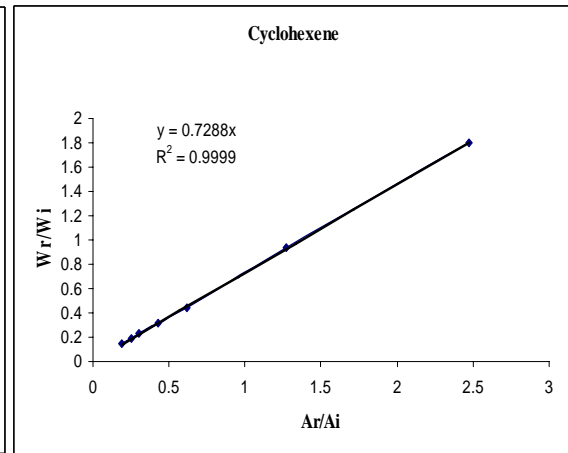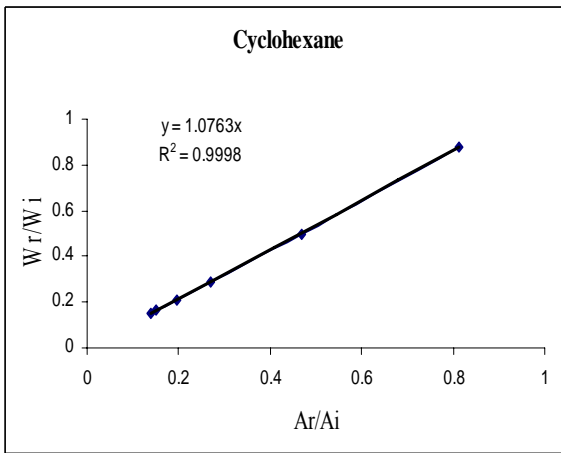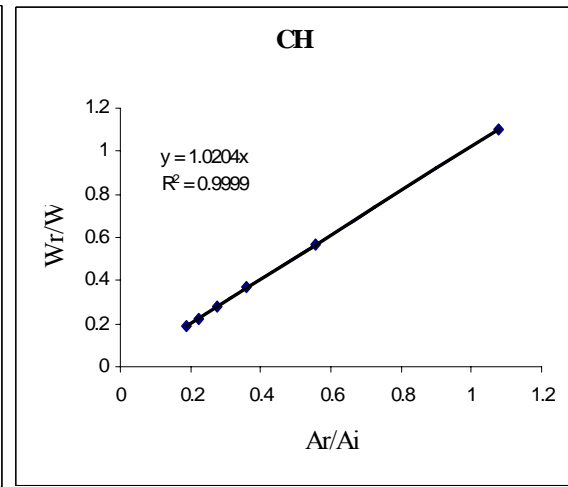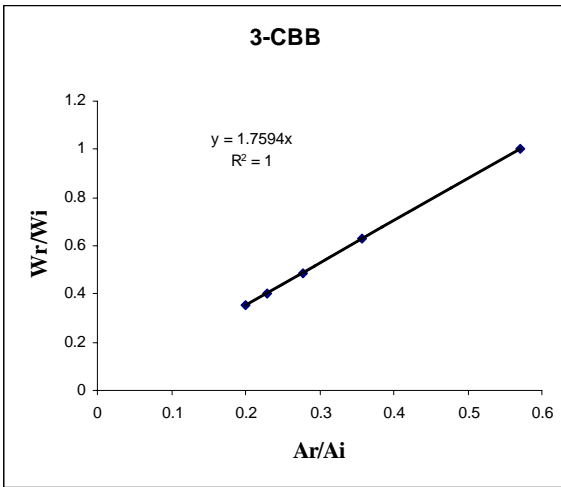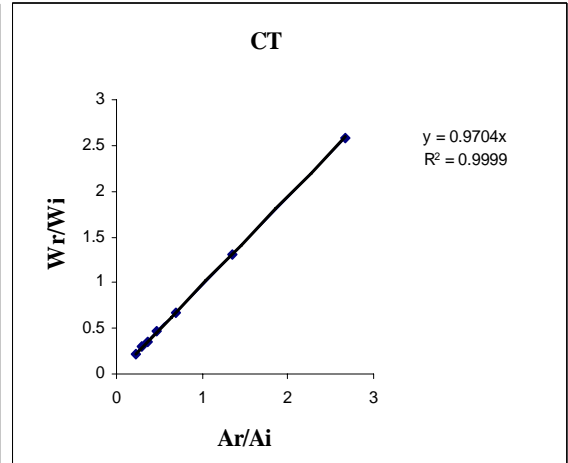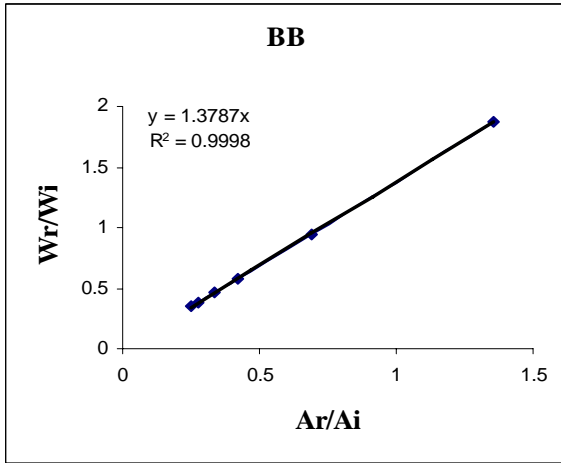
References

Chapter 1

[1]   V. P. Dravid, X. Lin, Y. Wang, X. K. Wang, A. Yee, J. B. Ketterson, and R. P. H. Chang, Science 259 (1993) 1601-1604.
[2]   S. Iijima, Nature 354 (1991) 56-58.
[3]   C. N. R. Rao, B. C. Satishkumar, A. Govindaraj, and M. Nath, Chemphyschem 2 (2001) 78-105.
[4]   S. W. Liu, X. H. Tang, L. X. Yin, Y. Koltypin, and A. Gedanken, Journal of Materials Chemistry 10 (2000) 1271-1272.
[5]   P. M. Ajayan, Chemical Reviews 99 (1999) 1787-1799.
[6]   N. Hatta and K. Murata, Chemical Physics Letters 217 (1994) 398-402.
[7]   T. W. Ebbesen and P. M. Ajayan, Nature 358 (1992) 220-222.
[8]   P. A. Gordon and P. B. Saeger, Industrial & Engineering Chemistry Research 38 (1999) 4647-4655.
[9]   A. C. Dillon, K. M. Jones, T. A. Bekkedahl, C. H. Kiang, D. S. Bethune, and M. J. Heben, Nature 386 (1997) 377-379.
[10]   P. Chen, X. Wu, J. Lin, and K. L. Tan, Science 285 (1999) 91-93.
[11]   C. Park, P. E. Anderson, A. Chambers, C. D. Tan, R. Hidalgo, and N. M. Rodriguez, Journal of Physical Chemistry B 103 (1999) 10572-10581.
[12]   F. Salman, C. Park, and R. T. K. Baker, Catalysis Today 53 (1999) 385-394.
[13]   B. Coq, J. M. Planeix, and V. Brotons, Applied Catalysis a-General 173 (1998) 175-183.
[14]   J. Ma, N. M. Rodriguez, M. A. Vannice, and R. T. K. Baker, Journal of Catalysis 183 (1999) 32-44.
[15]   L. Singoredjo, M. Slagt, J. van Wees, F. Kapteijn, and J. A. Moulijn, Catalysis Today 7 (1990) 157-165.
[16]   W. K. Maser, P. Bernier, J. M. Lambert, O. Stephan, P. M. Ajayan, C. Colliex, V. Brotons, J. M. Planeix, B. Coq, P. Molinie, and S. Lefrant, Synthetic Metals 81 (1996) 243-250.
[17]   K. B. K. Teo, C. Singh, M. Chhowalla, and W. I. Milne, Encyclopedia of Nanocience and Nanotechnology 1 (2004) 665-686.
[18]   G. Dresselhaus, M. S. Dresselhaus, and P. Avouris, Carbon Nanotubes: Synthesis, Structure, Properties and Applications, Springer, New York, 2001.
[19]   http://www.wtec.org/loyola/nano/US.Review/09_03.htm.
[20]   R. L. Vander Wal and L. J. Hall, Chemical Physics Letters 349 (2001) 178-184.
[21]   D. S. Bethune, C. H. Kiang, M. S. Devries, G. Gorman, R. Savoy, J. Vazquez, and R. Beyers, Nature 363 (1993) 605-607.
[22]   H. J. Huang, H. Kajiura, Y. Murakami, and M. T. Ata, Carbon 41 (2003) 615-618.
[23]   F. Weisbuch, V. N. Tokarev, S. Lazare, C. Belin, and J. L. Bruneel, Thin Solid Films 453-54 (2004) 394-398.
[24]   B. I. Yakobson and R. E. Smalley, American Scientist 85 (1997) 324-337.

[25]   G. S. Duesberg, J. Muster, H. J. Byrne, S. Roth, and M. Burghard, Applied Physics a-Materials Science & Processing 69 (1999) 269-274.

[26]   A. G. Rinzler, J. Liu, H. Dai, P. Nikolaev, C. B. Huffman, F. J. Rodriguez-Macias, P. J. Boul, A. H. Lu, D. Heymann, D. T. Colbert, R. S. Lee, J. E. Fischer, A. M. Rao, P. C. Eklund, and R. E. Smalley, Applied Physics a-Materials Science & Processing 67 (1998) 29-37.

[27]   S. D. Luo, D. C. Huang, Y. H. Huang, X. Y. Dou, and X. W. Zhao, Carbon 43 (2005) 109-115.

[28]   S. Iijima and T. Ichihashi, Nature 363 (1993) 603-605.

[29]   P. Serp, M. Corrias, and P. Kalck, Applied Catalysis a-General 253 (2003) 337-358.

[30]   M. A. Ermakova and D. Y. Ermakov, Catalysis Today 77 (2002) 225-235.

[31]   X. Z. Jiang, S. A. Stevenson, and J. A. Dumesic, Journal of Catalysis 91 (1985) 11-24.

[32]   J. Nakamura, H. Hirano, M. S. Xie, I. Matsuo, T. Yamada, and K. Tanaka, Surface Science 222 (1989) L809-L817.

[33]   L. Delzeit, I. McAninch, B. A. Cruden, D. Hash, B. Chen, J. Han, and M. Meyyappan, Journal of Applied Physics 91 (2002) 6027-6033.

[34]   R. T. Yang and J. P. Chen, Journal of Catalysis 115 (1989) 52-64.

[35]   F. J. Salzano and S. Aronson, The Journal of Chemical Physics 45 (1966) 2221-2227.

[36]   N. de Jonge, Y. Lamy, K. Schoots, and T. H. Oosterkamp, Nature 420 (2002) 393-395.

[37]   W. B. Choi, Y. W. Jin, H. Y. Kim, S. J. Lee, M. J. Yun, J. H. Kang, Y. S. Choi, N. S. Park, N. S. Lee, and J. M. Kim, Applied Physics Letters 78 (2001) 1547-1549.

[38]   D. S. Chung, S. H. Park, H. W. Lee, J. H. Choi, S. N. Cha, J. W. Kim, J. E. Jang, K. W. Min, S. H. Cho, M. J. Yoon, J. S. Lee, C. K. Lee, J. H. Yoo, J. M. Kim, J. E. Jung, Y. W. Jin, Y. J. Park, and J. B. You, Applied Physics Letters 80 (2002) 4045-4047.

[39]   Y. H. Lee, Y. T. Jang, D. H. Kim, J. H. Ahn, and B. K. Ju, Advanced Materials 13 (2001) 479-+.

[40]   I. T. Han, H. J. Kim, Y. J. Park, N. Lee, J. E. Jang, J. W. Kim, J. E. Jung, and J. M. Kim, Applied Physics Letters 81 (2002) 2070-2072.

[41]   E. S. Steigerwalt, G. A. Deluga, D. E. Cliffel, and C. M. Lukehart, Journal of Physical Chemistry B 105 (2001) 8097-8101.

[42]   G. L. Che, B. B. Lakshmi, E. R. Fisher, and C. R. Martin, Nature 393 (1998) 346-349.

[43]   C. A. Bessel, K. Laubernds, N. M. Rodriguez, and R. T. K. Baker, Journal of Physical Chemistry B 105 (2001) 1115-1118.

[44]   L. S. Schadler, S. C. Giannaris, and P. M. Ajayan, Applied Physics Letters 73 (1998) 3842-3844.

[45]   P. Calvert, Nature 399 (1999) 210-211.

[46]   K. Takehira, T. Ohi, T. Shishido, T. Kawabata, and K. Takaki, Applied Catalysis a-General 283 (2005) 137-145.

[47]   G. Z. Yue, Q. Qiu, B. Gao, Y. Cheng, J. Zhang, H. Shimoda, S. Chang, J. P. Lu, and O. Zhou, Applied Physics Letters 81 (2002) 355-357.

[48]   A. G. Rinzler, J. H. Hafner, P. Nikolaev, L. Lou, S. G. Kim, D. Tomanek, P. Nordlander, D. T. Colbert, and R. E. Smalley, Science 269 (1995) 1550-1553.

[49]   W. B. Choi, D. S. Chung, J. H. Kang, H. Y. Kim, Y. W. Jin, I. T. Han, Y. H. Lee, J. E. Jung, N. S. Lee, G. S. Park, and J. M. Kim, Applied Physics Letters 75 (1999) 3129-3131.

[50]   P. G. Collins, K. Bradley, M. Ishigami, and A. Zettl, Science 287 (2000) 1801-1804.

[51]   J. Kong, N. R. Franklin, C. W. Zhou, M. G. Chapline, S. Peng, K. J. Cho, and H. J. Dai, Science 287 (2000) 622-625.

[52]   M. Hughes, G. Z. Chen, M. S. P. Shaffer, D. J. Fray, and A. H. Windle, Chemistry of Materials 14 (2002) 1610-1613.

[53]   C. M. Niu, E. K. Sichel, R. Hoch, D. Moy, and H. Tennent, Applied Physics Letters 70 (1997) 1480-1482.

[54]   E. Frackowiak, K. Metenier, V. Bertagna, and F. Beguin, Applied Physics Letters 77 (2000) 2421-2423.

[55]   K. H. An, W. S. Kim, Y. S. Park, Y. C. Choi, S. M. Lee, D. C. Chung, D. J. Bae, S. C. Lim, and Y. H. Lee, Advanced Materials 13 (2001) 497-+.

[56]   R. H. Baughman, A. A. Zakhidov, and W. A. de Heer, Science 297 (2002) 787-792.

[57]   S. Musso, G. Fanchini, and A. Tagliaferro, Diamond and Related Materials 14 (2005) 784-789.

Chapter 2

[1] K. DasChowdhury, J. B. Howard, and J. B. VanderSande, Journal of Materials Research 11 (1996) 341-347.

[2] H. Richter, K. Hernadi, R. Caudano, A. Fonseca, H. N. Migeon, J. B. Nagy, S. Schneider, J. Vandooren, and P. J. VanTiggelen, Carbon 34 (1996) 427-429.

[3] P. M. Ajayan, Chemical Reviews 99 (1999) 1787-1799.

[4] N. Hatta and K. Murata, Chemical Physics Letters 217 (1994) 398-402.

[5] S. Subramoney, Advanced Materials 10 (1998) 1157-1158.

[6] R. T. K. Baker and P. S. Harris, in Chemistry and Physics of Carbon, Vol. 14 (P. L. Walker Jr. and P. A. Thrower, eds.), Marcel Dekker, New York, 1978, p. 83-85.

[7] T. W. Ebbesen and P. M. Ajayan, Nature 358 (1992) 220-222.

[8] D. T. Colbert, J. Zhang, S. M. McClure, P. Nikolaev, Z. Chen, J. H. Hafner, D. W. Owens, P. G. Kotula, C. B. Carter, J. H. Weaver, A. G. Rinzler, and R. E. Smalley, Science 266 (1994) 1218-1222.

[9] S. Amelinckx, X. B. Zhang, D. Bernaerts, X. F. Zhang, V. Ivanov, and J. B. Nagy, Science 265 (1994) 635-639.

[10] J. L. Figueiredo, C. A. Bernardo, J. J. Chludzinski, and R. T. K. Baker, Journal of Catalysis 110 (1988) 127-138.

[11] R. T. K. Baker, M. A. Barber, P. S. Harris, F. S. Feates, and R. J. Waite, Journal of Catalysis 26 (1972) 51-53.

[12] G. G. Kuvshinov, Y. I. Mogilnykh, D. G. Kuvshinov, V. I. Zaikovskii, and L. B. Avdeeva, Carbon 36 (1998) 87-97.

[13] J. Guinot, M. Audier, M. Coulon, and L. Bonnetain, Carbon 19 (1981) 95-98.

[14] C. Park, E. S. Engel, A. Crowe, T. R. Gilbert, and N. M. Rodriguez, Langmuir 16 (2000) 8050-8056.

[15] V. I. Zaikovskii, V. V. Chesnokov, and R. A. Buyanov, Kinetics and Catalysis 40 (1999) 552-555.

[16] Y. H. Hu and E. Ruckenstein, Journal of Catalysis 184 (1999) 298-302.

[17] M. A. Ermakova, D. Y. Ermakov, G. G. Kuvshinov, and L. M. Plyasova, Journal of Catalysis 187 (1999) 77-84.

[18] A. Kock, P. K. Debokx, E. Boellaard, W. Klop, and J. W. Geus, Journal of Catalysis 96 (1985) 468-480.

[19] T. J. Zhang and M. D. Amiridis, Applied Catalysis A-General 167 (1998) 161-172.

[20] C. Park and M. A. Keane, Solid State Ionics 141 (2001) 191-195.

[21] C. Park and M. A. Keane, Langmuir 17 (2001) 8386-8396.

[22] C. Park and M. A. Keane, Journal of Colloid and Interface Science 250 (2002) 37-48.

[23] K. Otsuka, H. Ogihara, and S. Takenaka, Carbon 41 (2003) 223-233.

[24] P. Wang, E. Tanabe, K. Ito, J. Jia, H. Morioka, T. Shishido, and K. Takehira, Applied Catalysis A-General 231 (2002) 35-44.

[25] M. L. Toebes, J. H. Bitter, A. J. van Dillen, and K. P. de Jong, Catalysis Today 76 (2002) 33-42.

[26] M. A. Ermakova and D. Y. Ermakov, Catalysis Today 77 (2002) 225-235.

[27]   C. Park, N. M. Rodriguez, and R. T. K. Baker, Journal of Catalysis 169 (1997) 212-227.

[28]   W. T. Owens, N. M. Rodriguez, and R. T. K. Baker, Journal of Physical Chemistry 96 (1992) 5048-5053.

[29]   M. S. Kim, N. M. Rodriguez, and R. T. K. Baker, Journal of Catalysis 134 (1992) 253-268.

[30]   K. Tomishige, Y. G. Chen, and K. Fujimoto, Journal of Catalysis 181 (1999) 91-103.

[31]   I. Willems, Z. Konya, J. F. Colomer, G. Van Tendeloo, N. Nagaraju, A. Fonseca, and J. B. Nagy, Chemical Physics Letters 317 (2000) 71-76.

[32]   M. Nath, B. C. Satishkumar, A. Govindaraj, C. P. Vinod, and C. N. R. Rao, Chemical Physics Letters 322 (2000) 333-340.

[33]   V. V. Chesnokov, V. I. Zaikovskii, R. A. Buyanov, V. V. Molchanov, and L. M. Plyasova, Kinetics and Catalysis 35 (1994) 130-135.

[34]   P. E. Nolan, D. C. Lynch, and A. H. Cutler, Carbon 32 (1994) 477-483.

[35]   T. koyama, Carbon 10 (1972) 757-758.

[36]   M. Endo, Y. A. Kim, T. Takeda, S. H. Hong, T. Matusita, T. Hayashi, and M. S. Dresselhaus, Carbon 39 (2001) 2003-2010.

[37]   M. Endo, K. Takeuchi, S. Igarashi, K. Kobori, M. Shiraishi, and H. W. Kroto, Journal of Physics and Chemistry of Solids 54 (1993) 1841-1848.

[38]   Y. Lu, Z. P. Zhu, W. Z. Wu, and Z. Y. Liu, Carbon 41 (2003) 194-198.

[39]   M. W. Shao, Q. Li, J. Wu, B. Xie, S. Y. Zhang, and Y. T. Qian, Carbon 40 (2002) 2961-2963.

[40]   K. Hernadi, A. Fonseca, J. B. Nagy, A. Siska, and I. Kiricsi, Applied Catalysis A-General 199 (2000) 245-255.

[41]   C. Menini, C. Park, E. J. Shin, G. Tavoularis, and M. A. Keane, Catalysis Today 62 (2000) 355-366.

[42]   C. Menini, C. Park, R. Brydson, and M. A. Keane, Journal of Physical Chemistry B 104 (2000) 4281-4284.

[43]   P. Albers, K. Seibold, G. Prescher, and H. Muller, Applied Catalysis A-General 176 (1999) 135-146.

[44]   D. W. McKee and C. L. Spiro, Carbon 23 (1985) 437-444.

[45]   G. Tavoularis and M. A. Keane, Journal of Molecular Catalysis a-Chemical 142 (1999) 187-199.

[46]   C. Park, C. Menini, J. L. Valverde, and M. A. Keane, Journal of Catalysis 211 (2002) 451-463.

[47]   P. E. Anderson and N. M. Rodriguez, Chemistry of Materials 12 (2000) 823-830.

[48]   C. Pham-Huu, N. Keller, L. J. Charbonniere, R. Ziessel, and M. J. Ledoux, Journal of chemical society and chemical communicaion (2000) 1871.

[49]   R. T. Yang and J. P. Chen, Journal of Catalysis 115 (1989) 52-64.

[50]   J. Rosrup-Nielsen and D. L. Trimm, Journal of Catalysis 48 (1977) 155-157.

[51]   I. Alstrup, Journal of Catalysis 109 (1988) 241-251.

[52]   M. P. Manning, J. E. Garmirian, and R. C. Reid, Industrial & Engineering Chemistry Process Design and Development 21 (1982) 404-409.

[53] V. V. Chesnokov, V. I. Zaikovskii, and R. A. Buyanov, Journal of Molecular Catalysis a-Chemical 158 (2000) 267-270.

[54] A. Chambers and R. T. K. Baker, Journal of Catalysis 158 (1996) 356-360.

[55] N. Krishnankutty, N. M. Rodriguez, and R. T. K. Baker, Journal of Catalysis 158 (1996) 217-227.

[56] L. B. Avdeeva, D. I. Kochubey, and S. K. Shaikhutdinov, Applied Catalysis A-General 177 (1999) 43-51.

[57] M. A. Ermakova, D. Y. Ermakov, A. L. Chuvilin, and G. G. Kuvshinov, Journal of Catalysis 201 (2001) 183-197.

[58] C. F. Cullis, ACTA Crystallographica 12 (1959) 382-383.

[59] C. L. Pieck, E. L. Jablonski, R. J. Verderone, and J. M. Parera, Applied Catalysis 56 (1989) 1-8.

[60] A. Stanislaus and B. H. Cooper, Catalysis Reviews-Science and Engineering 38 (1996) 159-159.

[61] G. Tavoularis and M. A. Keane, Journal of Chemical Technology and Biotechnology 74 (1999) 60-70.

[62] A. Chambers and R. T. K. Baker, Journal of Physical Chemistry B 101 (1997) 1621-1630.

[63] A. Y. Stakheev and L. M. Kustov, Applied Catalysis A-General 188 (1999) 3-35.

[64] S. Iijima, Nature 354 (1991) 56-58.

[65] C. Park and R. T. K. Baker, Journal of Physical Chemistry B 102 (1998) 5168-5177.

[66] T. E. Muller, D. G. Reid, W. K. Hsu, J. P. Hare, H. W. Kroto, and D. R. M. Walton, Carbon 35 (1997) 951-966.

[67] S. Takenaka, H. Ogihara, and K. Otsuka, Journal of Catalysis 208 (2002) 54-63.

[68] J. W. Snoeck, G. F. Froment, and M. Fowles, Journal of Catalysis 169 (1997) 240-249.

[69] M. A. Keane, Canadian Journal of Chemistry-Revue Canadienne De Chimie 72 (1994) 372-381.

[70] P. L. Walker Jr., M. Shelef, and P. E. Anderson, in Chemistry and Physics of Carbon, Vol. 1 (P. L. Walker Jr. and P. A. Thrower, eds.), Marcel Dekker, New York, 1968, p. 287-288.

[71] D. W. McKee, in Chemistry and Physics of Carbon, Vol. 16 (P. L. Walker Jr. and P. A. Thrower, eds.), Marcel Dekker, New York, 1981, p. 1-2.

[72] K. P. De Jong and J. W. Geus, Catalysis Reviews-Science and Engineering 42 (2000) 481-510.

[73] J. Zheng, T. C. Ekstrom, S. K. Gordeev, and M. Jacob, Journal of Materials Chemistry 10 (2000) 1039-1041.

[74] F. J. Salzano and S. Aronson, J. Chem. Phys. 45 (1966) 2221-2222.

[75] G. L. Che, B. B. Lakshmi, E. R. Fisher, and C. R. Martin, Nature 393 (1998) 346-349.

[76] Z. X. Jin, G. Q. Xu, and S. H. Goh, Carbon 38 (2000) 1135-1139.

[77] R. S. Lee, H. J. Kim, J. E. Fischer, A. Thess, and R. E. Smalley, Nature 388 (1997) 255-257.

[78]   C. Park, P. M. Patterson, and M. A. Keane, Curr. Topics Colloid. Interf. Sci 5 (2002) 93-94.

Chapter 3

[1] J. L. Figueiredo, C. A. Bernardo, J. J. Chludzinski, and R. T. K. Baker, Journal of Catalysis 110 (1988) 127-138.

[2] J. R. Nielsen and D. L. Trimm, Journal of Catalysis 48 (1977) 155-165.

[3] R. L. Vander Wal, T. M. Ticich, and V. E. Curtis, Carbon 39 (2001) 2277-2289.

[4] M. A. Ermakova, D. Y. Ermakov, L. M. Plyasova, and G. G. Kuvshinov, Catalysis Letters 62 (1999) 93-97.

[5] M. A. Ermakova, D. Y. Ermakov, and G. G. Kuvshinov, Applied Catalysis a-General 201 (2000) 61-70.

[6] M. A. Ermakova and D. Y. Ermakov, Catalysis Today 77 (2002) 225-235.

[7] C. Park and M. A. Keane, Journal of Catalysis 221 (2004) 386-399.

[8] X. Z. Jiang, S. A. Stevenson, and J. A. Dumesic, Journal of Catalysis 91 (1985) 11-24.

[9] C. Park, N. M. Rodriguez, and R. T. K. Baker, Journal of Catalysis 169 (1997) 212-227.

[10] P. Chen, H. B. Zhang, G. D. Lin, Q. Hong, and K. R. Tsai, Carbon 35 (1997) 1495-1501.

[11] H. Yan, Q. W. Li, J. Zhang, and Z. F. Liu, Chemical Physics Letters 380 (2003) 347-351.

[12] M. A. Ermakova, D. Y. Ermakov, G. G. Kuvshinov, and L. M. Plyasova, Journal of Catalysis 187 (1999) 77-84.

[13] Y. H. Hu and E. Ruckenstein, Journal of Catalysis 184 (1999) 298-302.

[14] C. Park and R. T. K. Baker, Journal of Physical Chemistry B 102 (1998) 5168-5177.

[15] V. I. Zaikovskii, V. V. Chesnokov, and R. A. Buyanov, Kinetics and Catalysis 40 (1999) 552-555.

[16] I. Willems, Z. Konya, J. F. Colomer, G. Van Tendeloo, N. Nagaraju, A. Fonseca, and J. B. Nagy, Chemical Physics Letters 317 (2000) 71-76.

[17] N. Krishnankutty, C. Park, N. M. Rodriguez, and R. T. K. Baker, Catalysis Today 37 (1997) 295-307.

[18] T. Nemes, A. Chambers, and R. T. K. Baker, Journal of Physical Chemistry B 102 (1998) 6323-6330.

[19] A. Chambers, N. M. Rodriguez, and R. T. K. Baker, Journal of Physical Chemistry 99 (1995) 10581-10589.

[20] C. Park, E. S. Engel, A. Crowe, T. R. Gilbert, and N. M. Rodriguez, Langmuir 16 (2000) 8050-8056.

[21] W. D. Zhang, Y. Wen, W. C. Tjiu, G. Q. Xu, and L. M. Gan, Applied Physics a-Materials Science & Processing 74 (2002) 419-422.

[22] V. V. Chesnokov, V. I. Zaikovskii, R. A. Buyanov, V. V. Molchanov, and L. M. Plyasova, Kinetics and Catalysis 35 (1994) 130-135.

[23] X. Y. Liu, B. C. Huang, and N. J. Coville, Carbon 40 (2002) 2791-2799.

[24] Z. J. Liu, R. C. Che, Z. D. Xu, and L. M. Peng, Synthetic Metals 128 (2002) 191-195.

[25] T. Koyama, Carbon 10 (1972) 757-758.

[26]   M. Endo, Y. A. Kim, T. Takeda, S. H. Hong, T. Matusita, T. Hayashi, and M. S. Dresselhaus, Carbon 39 (2001) 2003-2010.

[27]   M. Endo, K. Takeuchi, S. Igarashi, K. Kobori, M. Shiraishi, and H. W. Kroto, Journal of Physics and Chemistry of Solids 54 (1993) 1841-1848.

[28]   M. W. Shao, Q. Li, J. Wu, B. Xie, S. Y. Zhang, and Y. T. Qian, Carbon 40 (2002) 2961-2963.

[29]   R. Sen, A. Govindaraj, and C. N. R. Rao, Chemistry of Materials 9 (1997) 2078-2081.

[30]   Nikhil Das, Ajay Dalai, Jafar S. Soltan Mohammadzadeh, and J. Adjaye, Carbon 44 (2006) 2236-2245.

[31]   H. J. Lai, M. C. C. Lin, M. H. Yang, and A. K. Li, Materials Science & Engineering C-Biomimetic and Supramolecular Systems 16 (2001) 23-26.

[32]   M. Jung, K. Y. Eun, J. K. Lee, Y. J. Baik, K. R. Lee, and J. W. Park, Diamond and Related Materials 10 (2001) 1235-1240.

[33]   W. T. Owens, N. M. Rodriguez, and R. T. K. Baker, Journal of Physical Chemistry 96 (1992) 5048-5053.

[34]   Z. X. Yu, D. Chen, B. Totdal, and A. Holmen, Journal of Physical Chemistry B 109 (2005) 6096-6102.

[35]   Q. W. Li, H. Yan, J. Zhang, and Z. F. Liu, Carbon 42 (2004) 829-835.

[36]   L. D. Cherukuri, G. Yuan, and M. A. Keane, Topics in Catalysis 29 (2004) 119-128.

[37]   W. K. Maser, E. Munoz, M. T. Martinez, A. M. Benito, and G. F. de la Fuente, Optical Materials 17 (2001) 331-334.

[38]   E. Munoz, W. K. Maser, A. M. Benito, G. F. de la Fuente, and M. T. Martinez, Synthetic Metals 103 (1999) 2490-2491.

[39]   E. Munoz, W. K. Maser, A. M. Benito, M. T. Martinez, G. F. de la Fuente, Y. Maniette, A. Righi, E. Anglaret, and J. L. Sauvajol, Carbon 38 (2000) 1445-1451.

[40]   T. Y. Lee, J. H. Han, S. H. Choi, J. B. Yoo, C. Y. Park, T. Jung, S. Yu, W. K. Yi, I. T. Han, and J. M. Kim, Diamond and Related Materials 12 (2003) 851-855.

[41]   D. J. Yang, Q. Zhang, S. F. Yoon, J. Ahn, S. G. Wang, Q. Zhou, Q. Wang, and J. Q. Li, Surface & Coatings Technology 167 (2003) 288-291.

[42]   Y. H. Mo, A. K. M. F. Kibria, and K. S. Nahm, Synthetic Metals 122 (2001) 443-447.

[43]   A. Weidenkaff, S. G. Ebbinghaus, P. Mauron, A. Reller, Y. Zhang, and A. Zuttel, Materials Science & Engineering C-Biomimetic and Supramolecular Systems 19 (2002) 119-123.

[44]   C. Park and M. A. Keane, Catalysis Communications 2 (2001) 171-177.

[45]   C. Park and M. A. Keane, Langmuir 17 (2001) 8386-8396.

[46]   C. Park and M. A. Keane, Solid State Ionics 141 (2001) 191-195.

[47]   K. Hernadi, A. Fonseca, J. B. Nagy, A. Siska, and I. Kiricsi, Applied Catalysis a-General 199 (2000) 245-255.

[48]   P. E. Anderson and N. M. Rodriguez, Chemistry of Materials 12 (2000) 823-830.

[49]   J. F. Colomer, C. Stephan, S. Lefrant, G. Van Tendeloo, I. Willems, Z. Konya, A. Fonseca, C. Laurent, and J. B. Nagy, Chemical Physics Letters 317 (2000) 83-89.

[50]   P. Piedigrosso, Z. Konya, J. F. Colomer, A. Fonseca, G. Van Tendeloo, and J. B. Nagy, Physical Chemistry Chemical Physics 2 (2000) 163-170.

[51]   L. B. Avdeeva, D. I. Kochubey, and S. K. Shaikhutdinov, Applied Catalysis a-General 177 (1999) 43-51.

[52]   C. Park and R. T. K. Baker, Journal of Catalysis 179 (1998) 361-374.

[53]   L. B. Avdeeva, O. V. Goncharova, D. I. Kochubey, V. I. Zaikovskii, L. M. Plyasova, B. N. Novgorodov, and S. K. Shaikhutdinov, Applied Catalysis a-General 141 (1996) 117-129.

[54]   R. T. K. Baker, Carbon 27 (1989) 315-323.

[55]   R. T. K. Baker, Journal of Catalysis 63 (1980) 523-525.

[56]   P. E. Nolan, D. C. Lynch, and A. H. Cutler, Carbon 32 (1994) 477-483.

[57]   K. L. Yang and R. T. Yang, Carbon 24 (1986) 687-693.

[58]   A. Chambers and R. T. K. Baker, Journal of Physical Chemistry B 101 (1997) 1621-1630.

[59]   J. A. Dean, McGraw-Hill, 1999 (Table 4.11), p. 329-341.

[60]   C. A. Marques, O. Rogozhnikova, M. Selva, and P. Tundo, Journal of Molecular Catalysis a-Chemical 96 (1995) 301-309.

[61]   C. A. Marques, M. Selva, and P. Tundo, Journal of Organic Chemistry 58 (1993) 5256-5260.

[62]   C. Park, C. Menini, J. L. Valverde, and M. A. Keane, Journal of Catalysis 211 (2002) 451-463.

[63]   G. Tavoularis and M. A. Keane, Journal of Chemical Technology and Biotechnology 74 (1999) 60-70.

[64]   T. Halachev and E. Ruckenstein, Journal of Catalysis 73 (1982) 171-186.

[65]   B. Coq, G. Ferrat, and F. Figueras, Journal of Catalysis 101 (1986) 434-445.

[66]   K. Hernadi, Chemical Physics Letters 363 (2002) 169-174.

[67]   A. K. Aboul-Gheit, S. M. Aboul-Fotouh, S. M. Abdel-Hamid, and N. A. K. Aboul-Gheit, Journal of Molecular Catalysis a-Chemical 245 (2006) 167-177.

[68]   J. T. Miller, N. G. B. Agrawal, G. S. Lane, and F. S. Modica, Journal of Catalysis 163 (1996) 106-116.

[69]   J. Zheng, J. L. Dong, Q. H. Xu, Y. Liu, and A. Z. Yan, Applied Catalysis a-General 126 (1995) 141-152.

[70]   T. Tatsumi, L. X. Dai, and H. Sakashita, Catalysis Letters 27 (1994) 289-295.

[71]   L. X. Dai, H. Sakashita, and T. Tatsumi, Bulletin of the Chemical Society of Japan 67 (1994) 1553-1559.

[72]   D. S. Lafyatis, G. F. Froment, A. Pasauclaerbout, and E. G. Derouane, Journal of Catalysis 147 (1994) 552-566.

[73]   E. G. Derouane, V. Jullienlardot, R. J. Davis, N. Blom, P. E. Hojlundnielsen, J. R. A. Clarke, J. J. Rooney, and K. P. Dejong, Studies in Surface Science and Catalysis 75 (1993) 1031-1042.

[74]   W. J. Han, A. B. Kooh, and R. F. Hicks, Catalysis Letters 18 (1993) 219-225.

[75]   D. J. Ostgard, L. Kustov, K. R. Poeppelmeier, and W. M. H. Sachtler, Journal of Catalysis 133 (1992) 342-357.

[76]   Ivanova, II, A. PasauClaerbout, M. Seirvert, N. Blom, and E. G. Derouane, Journal of Catalysis 158 (1996) 521-536.

[77]   A. Onda, T. Komatsu, and T. Yashima, Journal of Catalysis 201 (2001) 13-21.

[78]   P. H. Desai and J. T. Richardson, Journal of Catalysis 98 (1986) 392-400.

[79]   J. Escobar, J. A. DeLosReyes, T. Viveros, and M. C. Barrera, Ind. Eng. Chem. Res. 45 (2006) 5693-5700.

[80]   F. Zaera, S. N. Tjandra, and T. V. W. Janssens, Langmuir 14 (1998) 1320-1327.

[81]   J. Fung and I. Wang, Journal of Catalysis 130 (1991) 577-587.

[82]   J. Fung and I. Wang, Journal of Catalysis 164 (1996) 166-172.

[83]   M. Yang, K. C. Chou, and G. A. Somorjai, Journal of Physical Chemistry B 107 (2003) 5267-5272.

[84]   M. Yang and G. A. Somorjai, J. Am. Chem. Soc. 126 (2004) 7698-7708.

[85]   L. E. Murillo, N. A. Khan, and J. G. Chen, Surface Science 594 (2005) 27-42.

[86]   J. C. Wasilke, Z. J. A. Komon, X. H. Bu, and G. C. Bazan, Organometallics 23 (2004) 4174-4177.

[87]   M. A. Ermakova, D. Y. Ermakov, A. L. Chuvilin, and G. G. Kuvshinov, Journal of Catalysis 201 (2001) 183-197.

[88]   S. Takenaka, H. Ogihara, I. Yamanaka, and K. Otsuka, Applied Catalysis a-General 217 (2001) 101-110.

[89]   C. Park and M. A. Keane, Chemphyschem 2 (2001) 733-741.

[90]   C. Park and M. A. Keane, Journal of Colloid and Interface Science 250 (2002) 37-48.

[91]   S. Inoue, N. Ichikuni, T. Suzuki, T. Uematsu, and K. Kaneko, Journal of Physical Chemistry B 102 (1998) 4689-4692.

[92]   N. M. Rodriguez, M. S. Kim, and R. T. K. Baker, Journal of Physical Chemistry 98 (1994) 13108-13111.

[93]   M. S. Hoogenraad, R. A. G. M. M. vanLeeuwarden, G. J. B. V. Vriesman, A. Broersma, A. J. vanDillen, and J. W. Geus, Preparation of Catalysts Vi 91 (1995) 263-271.

[94]   M. S. Hoogenraad, M. F. Onwezen, A. J. vanDillen, and J. W. Geus, 11th International Congress on Catalysis - 40th Anniversary, Parts A and B 101 (1996) 1331-1339.

Chapter 4

[1]   P. Chen, H. B. Zhang, G. D. Lin, Q. Hong, and K. R. Tsai, Carbon 35 (1997) 1495-1501.

[2]   H. Yan, Q. W. Li, J. Zhang, and Z. F. Liu, Chemical Physics Letters 380 (2003) 347-351.

[3]   M. A. Ermakova, D. Y. Ermakov, G. G. Kuvshinov, and L. M. Plyasova, Journal of Catalysis 187 (1999) 77-84.

[4]   Y. H. Hu and E. Ruckenstein, Journal of Catalysis 184 (1999) 298-302.

[5]   C. Park and R. T. K. Baker, Journal of Physical Chemistry B 102 (1998) 5168-5177.

[6]   V. I. Zaikovskii, V. V. Chesnokov, and R. A. Buyanov, Kinetics and Catalysis 40 (1999) 552-555.

[7]   I. Willems, Z. Konya, J. F. Colomer, G. Van Tendeloo, N. Nagaraju, A. Fonseca, and J. B. Nagy, Chemical Physics Letters 317 (2000) 71-76.

[8]   N. Krishnankutty, C. Park, N. M. Rodriguez, and R. T. K. Baker, Catalysis Today 37 (1997) 295-307.

[9]   T. Nemes, A. Chambers, and R. T. K. Baker, Journal of Physical Chemistry B 102 (1998) 6323-6330.

[10]   A. Chambers, N. M. Rodriguez, and R. T. K. Baker, Journal of Physical Chemistry 99 (1995) 10581-10589.

[11]   C. Park, N. M. Rodriguez, and R. T. K. Baker, Journal of Catalysis 169 (1997) 212-227.

[12]   C. Park, E. S. Engel, A. Crowe, T. R. Gilbert, and N. M. Rodriguez, Langmuir 16 (2000) 8050-8056.

[13]   W. D. Zhang, Y. Wen, W. C. Tjiu, G. Q. Xu, and L. M. Gan, Applied Physics a-Materials Science & Processing 74 (2002) 419-422.

[14]   V. V. Chesnokov, V. I. Zaikovskii, R. A. Buyanov, V. V. Molchanov, and L. M. Plyasova, Kinetics and Catalysis 35 (1994) 130-135.

[15]   X. Y. Liu, B. C. Huang, and N. J. Coville, Carbon 40 (2002) 2791-2799.

[16]   Z. J. Liu, R. C. Che, Z. D. Xu, and L. M. Peng, Synthetic Metals 128 (2002) 191-195.

[17]   T. Koyama, Carbon 10 (1972) 757-758.

[18]   M. Endo, Y. A. Kim, T. Takeda, S. H. Hong, T. Matusita, T. Hayashi, and M. S. Dresselhaus, Carbon 39 (2001) 2003-2010.

[19]   M. Endo, K. Takeuchi, S. Igarashi, K. Kobori, M. Shiraishi, and H. W. Kroto, Journal of Physics and Chemistry of Solids 54 (1993) 1841-1848.

[20]   M. W. Shao, Q. Li, J. Wu, B. Xie, S. Y. Zhang, and Y. T. Qian, Carbon 40 (2002) 2961-2963.

[21]   R. Sen, A. Govindaraj, and C. N. R. Rao, Chemistry of Materials 9 (1997) 2078-2081.

[22]   Nikhil Das, Ajay Dalai, Jafar S. Soltan Mohammadzadeh, and J. Adjaye, Carbon 44 (2006) 2236-2245.

[23]   H. J. Lai, M. C. C. Lin, M. H. Yang, and A. K. Li, Materials Science & Engineering C-Biomimetic and Supramolecular Systems 16 (2001) 23-26.

[24] R. L. Vander Wal, T. M. Ticich, and V. E. Curtis, Carbon 39 (2001) 2277-2289.
[25] A. Kukovecz, Z. Konya, N. Nagaraju, I. Willems, A. Tamasi, A. Fonseca, J. B. Nagy, and I. Kiricsi, Physical Chemistry Chemical Physics 2 (2000) 3071-3076.
[26] S. Takenaka, M. Ishida, M. Serizawa, E. Tanabe, and K. Otsuka, Journal of Physical Chemistry B 108 (2004) 11464-11472.
[27] M. A. Ermakova and D. Y. Ermakov, Catalysis Today 77 (2002) 225-235.
[28] M. A. Ermakova, D. Y. Ermakov, and G. G. Kuvshinov, Applied Catalysis A: General 201 (2000) 61-70.
[29] M. A. Ermakova, D. Y. Ermakov, L. M. Plyasova, and G. G. Kuvshinov, Catalysis Letters 62 (1999) 93-97.
[30] C. Park and M. A. Keane, Journal of Catalysis 221 (2004) 386-399.
[31] M. L. Toebes, J. H. Bitter, A. J. van Dillen, and K. P. de Jong, Catalysis Today 76 (2002) 33-42.
[32] W. T. Owens, N. M. Rodriguez, and R. T. K. Baker, Journal of Physical Chemistry 96 (1992) 5048-5053.
[33] L. Y. Piao, Y. D. Li, J. L. Chen, L. Chang, and J. Y. S. Lin, Catalysis Today 74 (2002) 145-155.
[34] X. Z. Jiang, S. A. Stevenson, and J. A. Dumesic, Journal of Catalysis 91 (1985) 11-24.
[35] N. M. Rodriguez, Journal of Materials Research 8 (1993) 3233-3250.
[36] C. Park and R. T. K. Baker, Journal of Catalysis 190 (2000) 104-117.
[37] J. R. Rostrupnielsen, Journal of Catalysis 85 (1984) 31-43.
[38] K. P. De Jong and J. W. Geus, Catalysis Reviews-Science and Engineering 42 (2000) 481-510.
[39] R. T. K. Baker, Carbon 27 (1989) 315-323.
[40] C. Park and R. T. K. Baker, Journal of Catalysis 179 (1998) 361-374.
[41] A. J. H. M. Kock, P. K. Debokx, E. Boellaard, W. Klop, and J. W. Geus, Journal of Catalysis 96 (1985) 468-480.
[42] T. J. Zhang and M. D. Amiridis, Applied Catalysis a-General 167 (1998) 161-172.
[43] C. Park and M. A. Keane, Solid State Ionics 141 (2001) 191-195.
[44] P. E. Anderson and N. M. Rodriguez, Chemistry of Materials 12 (2000) 823-830.
[45] J. F. Colomer, C. Stephan, S. Lefrant, G. Van Tendeloo, I. Willems, Z. Konya, A. Fonseca, C. Laurent, and J. B. Nagy, Chemical Physics Letters 317 (2000) 83-89.
[46] P. Piedigrosso, Z. Konya, J. F. Colomer, A. Fonseca, G. Van Tendeloo, and J. B. Nagy, Physical Chemistry Chemical Physics 2 (2000) 163-170.
[47] K. Hernadi, A. Fonseca, J. B. Nagy, A. Siska, and I. Kiricsi, Applied Catalysis a-General 199 (2000) 245-255.
[48] M. A. Ermakova, D. Y. Ermakov, A. L. Chuvilin, and G. G. Kuvshinov, Journal of Catalysis 201 (2001) 183-197.
[49] L. B. Avdeeva, O. V. Goncharova, D. I. Kochubey, V. I. Zaikovskii, L. M. Plyasova, B. N. Novgorodov, and S. K. Shaikhutdinov, Applied Catalysis a-General 141 (1996) 117-129.

[50]   L. B. Avdeeva, D. I. Kochubey, and S. K. Shaikhutdinov, Applied Catalysis a-General 177 (1999) 43-51.

[51]   Y. Yamada, Y. Hosono, N. Murakoshi, N. Higashi, H. Ichi-oka, T. Miyake, N. Ikenaga, and T. Suzuki, Diamond and Related Materials 15 (2006) 1080-1084.

[52]   S. Takenaka, H. Ogihara, I. Yamanaka, and K. Otsuka, Applied Catalysis A: General 217 (2001) 101-110.

[53]   K. Hernadi, A. Fonseca, J. B. Nagy, D. Bernaerts, J. Riga, and A. Lucas, Synthetic Metals 77 (1996) 31-34.

[54]   S. Y. Lim, A. Shimizu, S. H. Yoon, Y. Korai, and I. Mochida, Carbon 42 (2004) 1279-1283.

[55]   S. J. Tauster, S. C. Fung, R. T. K. Baker, and J. A. Horsley, Science 211 (1981) 1121-1125.

[56]   C. Park and M. A. Keane, Langmuir 17 (2001) 8386-8396.

[57]   B. Coughlan and M. A. Keane, Journal of Colloid and Interface Science 137 (1990) 483-494.

[58]   C. Park and M. A. Keane, Journal of Molecular Catalysis A: Chemical 166 (2001) 303-322.

[59]   D. W. McKee and C. L. Spiro, Carbon 23 (1985) 437-444.

[60]   C. Amorim, G. Yuan, P. M. Patterson, and M. A. Keane, Journal of Catalysis 234 (2005) 268-281.

[61]   B. W. Hoffer, A. D. van Langeveld, J. P. Janssens, R. L. C. Bonne, C. M. Lok, and J. A. Moulijn, Journal of Catalysis 192 (2000) 432-440.

[62]   M. K. van der Lee, A. J. van Dillen, J. W. Geus, K. P. de Jong, and J. H. Bitter, Carbon 44 (2006) 629-637.

[63]   A. de Lucas, A. Garrido, P. Sanchez, A. Romero, and J. L. Valverde, Industrial & Engineering Chemistry Research 44 (2005) 8225-8236.

[64]   T. Mizushima, K. Nishida, H. Ohkita, and N. Kakuta, Bulletin of the Chemical Society of Japan 75 (2002) 2283-2288.

[65]   Y. H. Choi and W. Y. Lee, Catalysis Letters 67 (2000) 155-161.

[66]   C. Louis, Z. X. Cheng, and M. Che, Journal of Physical Chemistry 97 (1993) 5703-5712.

[67]   B. Mile, D. Stirling, M. A. Zammitt, A. Lovell, and M. Webb, Journal of Molecular Catalysis 62 (1990) 179-198.

[68]   G. Sewell, C. Oconnor, and E. Vansteen, Applied Catalysis A: General 125 (1995) 99-112.

[69]   J. Z. Li and G. X. Lu, Applied Catalysis A: General 273 (2004) 163-170.

[70]   A. Onda, T. Komatsu, and T. Yashima, Journal of Catalysis 201 (2001) 13-21.

[71]   D. J. Lensveld, J. G. Mesu, A. J. van Dillen, and K. P. de Jong, Microporous and Mesoporous Materials 44 (2001) 401-407.

[72]   A. Infantes-Molina, J. Merida-Robles, P. Braos-Garcia, E. Rodriguez-Castellon, E. Finocchio, G. Busca, P. Maireles-Torres, and A. Jimenez-Lopez, Journal of Catalysis 225 (2004) 479-488.

[73]   M. P. Gonzalez-Marcos, J. Gutierrez-Ortiz, C. Gonzalez-Ortizde Elguea, and J. R. Gonzalez-Velasco, Journal of Molecular Catalysis A: Chemical 120 (1997) 185-196.

[74]   K. V. Murthy, P. M. Patterson, G. Jacobs, B. H. Davis, and M. A. Keane, Journal of Catalysis 223 (2004) 74-85.

[75]   A. Lewandowska, S. Monteverdi, M. Bettahar, and M. Ziolek, Journal of Molecular Catalysis A: Chemical 188 (2002) 85-95.

[76]   A. M. Diskin, R. H. Cunningham, and R. M. Z. Ormerod, Catalysis Today 46 (1998) 147-154.

[77]   H. S. Roh, K. W. Jun, W. S. Dong, J. S. Chang, S. E. Park, and Y. I. Joe, Journal of Molecular Catalysis A: Chemical 181 (2002) 137-142.

[78]   H. Y. Zhang, X. M. Xue, D. Y. Wang, Y. Y. He, and S. Q. Peng, Materials Chemistry and Physics 58 (1999) 1-5.

[79]   A. C. Dillon, K. M. Jones, T. A. Bekkedahl, C. H. Kiang, D. S. Bethune, and M. J. Heben, Nature 386 (1997) 377-379.

[80]   J. Juan-Juan, M. C. Roman-Martinez, and M. J. Illan-Gomez, Applied Catalysis A: General 264 (2004) 169-174.

[81]   P. Salagre, J. L. G. Fierro, F. Medina, and J. E. Sueiras, Journal of Molecular Catalysis A: Chemical 106 (1996) 125-134.

[82]   B. Scheffer, P. Molhoek, and J. A. Moulijn, Applied Catalysis 46 (1989) 11-30.

[83]   J. Matos, J. L. Brito, and J. Laine, Applied Catalysis A: General 152 (1997) 27-42.

[84]   G. L. Zhou, Y. Jiang, H. M. Xie, and F. L. Qiu, Chemical Engineering Journal 109 (2005) 141-145.

[85]   A. M. G. Pedrosa, M. J. B. Souza, D. M. A. Melo, A. G. Souza, and A. S. Araujo, Journal of Thermal Analysis and Calorimetry 79 (2005) 439-443.

[86]   M. Afzal, G. Yasmeen, M. Saleem, P. K. Butt, A. K. Khattak, and J. Afzal, Journal of Thermal Analysis and Calorimetry 62 (2000) 721-727.

[87]   H. Dropsch and M. Baerns, Applied Catalysis A: General 158 (1997) 163-183.

[88]   K. Morikawa, T. Shirasaki, and M. Okada, Advanced Catalysis 97 (1969)

[89]   P. Canizares, A. de Lucas, F. Dorado, A. Duran, and I. Asencio, Applied Catalysis A: General 169 (1998) 137-150.

[90]   G. Poncelet, M. A. Centeno, and R. Molina, Applied Catalysis A: General 288 (2005) 232-242.

[91]   A. G. Boudjahem, S. Monteverdi, M. Mercy, and M. M. Bettahar, Applied Catalysis A: General 250 (2003) 49-64.

[92]   C. H. Bartholomew and R. B. Pannell, Journal of Catalysis 65 (1980) 390-401.

[93]   K. Otsuka, H. Ogihara, and S. Takenaka, Carbon 41 (2003) 223-233.

[94]   Z. X. Yu, D. Chen, B. Totdal, and A. Holmen, Journal of Physical Chemistry B 109 (2005) 6096-6102.

[95]   D. R. Rainer and D. W. Goodman, Journal of Molecular Catalysis a-Chemical 131 (1998) 259-283.

[96]   D. R. Rainer, C. Xu, and D. W. Goodman, Journal of Molecular Catalysis a-Chemical 119 (1997) 307-325.

[97]   I. Alstrup, Journal of Catalysis 109 (1988) 241-251.

[98]   P. Albers, K. Seibold, G. Prescher, and H. Muller, Applied Catalysis a-General 176 (1999) 135-146.

[99]   L. D. Cherukuri, G. Yuan, and M. A. Keane, Topics in Catalysis 29 (2004) 119-128.

[100] F. C. Schouten and E. W. Kaleveld, Surface Science 63 (1977) 460-474.

[101] F. C. Schouten, O. L. J. Gijzeman, and G. A. Bootsma, Surface Science 87 (1979) 1-12.

[102] V. Vinciguerra, F. Buonocore, G. Panzera, and L. Occhipinti, Nanotechnology 14 (2003) 655-660.

[103] R. T. K. Baker, E. B. Prestridge, and R. L. Garten, Journal of Catalysis 56 (1979) 390-406.

[104] Y. Aray, J. Rodriguez, J. Rivero, and D. Vega, Surface Science 441 (1999) 344-350.

[105] E. I. Ko and R. L. Garten, Journal of Catalysis 68 (1981) 233-236.

[106] D. W. Goodman, Catalysis Today 12 (1992) 189-199.

[107] F. Frusteri, L. Spadaro, F. Arena, and A. Chuvilin, Carbon 40 (2002) 1063-1070.

[108] A. Stanislaus and B. H. Cooper, Catalysis Reviews-Science and Engineering 36 (1994) 75-123.

[109] M. Perez-Cabero, I. Rodriguez-Ramos, and A. Guerrero-Ruiz, Journal of Catalysis 215 (2003) 305-316.

[110] D. Chen, K. O. Christensen, E. Ochoa-Fernandez, Z. X. Yu, B. Totdal, N. Latorre, A. Monzon, and A. Holmen, Journal of Catalysis 229 (2005) 82-96.

[111] K. Takehira, T. Ohi, T. Shishido, T. Kawabata, and K. Takaki, Applied Catalysis A: General 283 (2005) 137-145.

[112] S. Iijima, Nature 354 (1991) 56-58.

[113] M. S. Hoogenraad, M. F. Onwezen, A. J. vanDillen, and J. W. Geus, 11th International Congress on Catalysis - 40th Anniversary, Parts A and B 101 (1996) 1331-1339.

[114] M. S. Hoogenraad, R. A. G. M. M. vanLeeuwarden, G. J. B. V. Vriesman, A. Broersma, A. J. vanDillen, and J. W. Geus, Preparation of Catalysts Vi 91 (1995) 263-271.

[115] S. Inoue, N. Ichikuni, T. Suzuki, T. Uematsu, and K. Kaneko, Journal of Physical Chemistry B 102 (1998) 4689-4692.

[116] N. M. Rodriguez, M. S. Kim, and R. T. K. Baker, Journal of Physical Chemistry 98 (1994) 13108-13111.

[117] P. L. Walker Jr., M. Shelef, and R. A. Anderson, in Chemistry and Physics of Carbon, Vol. 1 (P. L. Walker Jr. , ed.), Marcel Dekker, New York, 1968, p. 287-297.

[118] S. Takenaka, H. Ogihara, and K. Otsuka, Journal of Catalysis 208 (2002) 54-63.

[119] C. Park and M. A. Keane, Journal of Colloid and Interface Science 250 (2002) 37-48.

[120] M. A. Keane, Canadian Journal of Chemistry-Revue Canadienne De Chimie 72 (1994) 372-381.

[121] A. G. Rinzler, J. Liu, H. Dai, P. Nikolaev, C. B. Huffman, F. J. Rodriguez-Macias, P. J. Boul, A. H. Lu, D. Heymann, D. T. Colbert, R. S. Lee, J. E. Fischer, A. M. Rao, P. C. Eklund, and R. E. Smalley, Applied Physics a-Materials Science & Processing 67 (1998) 29-37.

[122] Z. X. Jin, G. Q. Xu, and S. H. Goh, Carbon 38 (2000) 1135-1139.

[123] R. S. Lee, H. J. Kim, J. E. Fischer, A. Thess, and R. E. Smalley, Nature 388 (1997) 255-257.

[124] F. J. Salzano and S. Aronson, The Journal of Chemical Physics 45 (1966) 2221-2227.

[125] S. Y. Brichka, G. P. Prikhod'ko, Y. I. Sementsov, A. V. Brichka, G. I. Dovbeshko, and O. P. Paschuk, Carbon 42 (2004) 2581-2587.

VITA

Date of Birth: 18th October 1978
Place of Birth: Hyderabad, Andhra Pradesh, India

EDUCATION
Bachelor of Technology (B.Tech), Jawaharlal Nehru Technological, University,
Hyderabad, India
Major: Metallurgical Engineering   Oct 1997-Jul 2001

EXPERIENCE
Environmental Engineer Assistant II:
Environmental Public Protection Cabinet   Jul 2005-Present
Division of Water, Frankfort, KY
Environmental Engineer Assistant I:
Environmental Public Protection Cabinet   Jul 2004-Aug 2005
Division of Air Quality, Frankfort, KY
Research Assistant:
University of Kentucky, Lexington, KY   Jul 2002- Present
Teaching Assistant:
University of Kentucky, Lexington, KY   Aug 2001-Jul 2002
Internship:
Nuclear Fuel Complex, Hyderabad, India   May 2001-Jul 2001

PUBLICATIONS AND PRESENTATIONS
Laxmi D.Cherukuri, Guang Yuan, Mark.A.Keane "Catalytic Growth of Structured
Carbon via Decomposition of Chlorobenzene": Invited Lecture at 16th CATSYMP-
2003, Indian Institute of Chemical Technology, Hyderabad, India.

Laxmi D.Cherukuri, Guang Yuan, Mark.A.Keane "Catalytic Growth of Structured
Carbon via Decomposition of Chlorobenzene": Topics in Catalysis Vol. 29, Nos. 3–4,
June 2004.

Laxmi D. Cherukuri "Corrosion wear resistance of Al-Cu-Pd alloy sliding under 3.5%
NaCl solution" was presented at COSMET-2000, Andhra University, Visakhapatnam,
India

AWARDS AND HONORS
- Ranked among the top 5% of Engineering and Medical Common Entrance Test
  (EAMCET) conducted State wide in Andhra Pradesh, India.
- Awarded 2nd best speaker for an oral presentation at COSMET '2000, a
  Metallurgical Conference held at Andhra University, Andhra Pradesh, India.
- Awarded Kentucky Graduate Scholarship by University of Kentucky
- Awarded full scholarship at University of Kentucky (as Teaching and Research
  Assistant)